Final Report

PENETRATION STUDIES OF ICE WITH APPLICATION TO ARCTIC AND SUBARCTIC WARFARE - PHASE II STUDY

Prepared for

SUBMARINE ARCTIC WARFARE AND SCIENTIFIC PROGRAM
NAVAL ORDNANCE LABORATORY, WHITE OAK
SILVER SPRING, MARYLAND

CONTRACT Nonr-2332(00)

STANFORD RESEARCH INSTITUTE

MENLO PARK, CALIFORNIA

*SRI

STANFORD RESEARCH INSTITUTE
MENLO PARK, CALIFORNIA

NAVAL WARFARE RESEARCH CENTER

Copy No. 50

Final Report

May 1967

PENETRATION STUDIES OF ICE WITH APPLICATION TO ARCTIC AND SUBARCTIC WARFARE - PHASE II STUDY

Prepared for:

SUBMARINE ARCTIC WARFARE AND SCIENTIFIC PROGRAM
NAVAL ORDNANCE LABORATORY, WHITE OAK
SILVER SPRING, MARYLAND

CONTRACT Nonr-2332(00)

By: BERNARD ROSS

SRI Project 2167-613

ABSTRACT

Impact tests with freely falling and explosively powered projectiles were performed on laboratory sea ice test slabs made from frozen seawater at Stanford Research Institute, and on Arctic sea ice in situ at Point Barrow, Alaska. In the experiments, particular attention was devoted to studying the mechanisms of penetration and perforation. Ranges of values investigated for the basic parameters were: impact velocity, 8-20 ft/sec and 50-494 ft/sec; projectile weights, 0.75, 9.69, and 41.5 lb; penetrator diameters, 5/8 in., 1-1/4 in., and 6 in.; penetrator profiles, blunt and conical; sea ice thickness, 3-3/8 - 17 in.; sea ice temperature, $+7^{\circ}F$ - $+32^{\circ}F$, and sea ice salinity, 7.2 - 17.1 ppm. All tests were carried out at normal incidence except for one sequence on Arctic sea ice in which the angle of incidence was 17.3° from vertical.

Results of the tests indicate that a cylindrical, blunt-end penetrator was more effective in perforation than a corresponding penetrator with a conical end. The blunt penetrator, impacting at normal incidence, perforated both laboratory sea ice and Arctic sea ice by expelling a cylindrical-conical shear plug from the test specimen. For this behavior, a mathematical model was constructed and a theoretical analysis developed from which the minimum impact velocity for perforation (critical velocity) was obtained. The critical velocity was found to be a function of projectile mass and diameter, and sea ice thickness, shear strength, tensile strength, and elastic modulus. The theory did not consider effects due to cratering.

Sea ice mechanical properties were related to temperature and salinity content by the Assur theory, and a digital computer program was written to represent these strength relationships. In addition, the present theory was programmed so that, for a given projectile and sea

ice cover, critical impact velocity could be determined directly from temperature and salinity content in the range of temperature, +32°F through -10°F (0°C through -23°C), and salinity, 2 ppm through 20 ppm. Agreement between predictions of the theory and a limited number of experimental results was good.

Finally, it was recommended that future investigations in this problem focus on a better theoretical understanding of the mechanics of penetration and the development of projectiles to be used specifically for perforation of Arctic sea ice.

PREFACE

The investigation reported here was sponsored by the U.S. Naval Ordnance Laboratory (White Oak), Silver Spring, Maryland, under ONR Contract, Nonr-2332(00); SRI Project No. ETU-2167-613. The work was conducted between 1 January 1966 and 31 December 1966, and is denoted Phase II Study. Results of the Phase I Study were published in a Stanford Research Institute final report under the same title dated November 1965.

The contract was monitored by Mr. M. M. Kleinerman, NOL. The project leader for the Institute was Dr. Bernard Ross. Other project participants at the Institute were Mr. Gerald Wagner, project technician, and Mr. Vahe Sagherian, computer mathematician. The laboratory notebook for the experimental work is No. 7829.

The author expresses his gratitude and appreciation to Messrs. Kenneth Toovak and Robert Okpeaha of the Arctic Research Laboratory, Point Barrow, Alaska, for their valuable assistance throughout the field test program.

CONTENTS

CONTENTS (Concluded)

ILLUSTRATIONS

ILLUSTRATIONS (Continued)

ILLUSTRATIONS (Continued)

ILLUSTRATIONS (Concluded)

TABLES

SYMBOLS

A	slant area of a right circular conical frustum
a	radius of penetrator
C_0	location of center of gravity: low impact velocity projectile, see Table 2
C_1	length of block: low impact velocity projectile, see Fig. 8
C_2	length of penetrator: low impact velocity projectile, see Fig. 8
C_3	length of high impact velocity projectile, see Table 3 and Fig. 9
D	diameter of penetrator
E	Young's modulus
$F(\varphi,\eta)$	function related to geometry of cylindrical-conical shear plug, see Eq. 10
$\bar{F}(\varphi,\eta)$	minimum value of $F(\varphi,\eta)$ with respect to φ; η fixed
g	acceleration due to gravity
k	dynamic compression modulus
m_1	mass of projectile
m_2	mass of ejected sea ice plug
P	compressive load, Appendix B
P_D	dynamic compressive load, Appendix C
P_S	static compressive load, Appendix C
R	base radius of cylindrical-conical shear plug, see Fig. 40
r,z	cylindrical coordinates in the radial and axial directions, respectively

SYMBOLS (Continued)

S	salinity content
s	base height of cylindrical-conical shear plug, see Fig. 40
T	temperature of sea ice
t	thickness
v_c	critical value of impact velocity (i.e., minimum value required for perforation)
v_e	velocity of projectile at exit from test slab
v_i	velocity of projectile immediately prior to impact
v_2	velocity of projectile and sea ice plug immediately after impact
z_c	length of cylindrical shear yield surface at critical impact velocity, see Fig. 40
z_T	depth in sea ice at which characteristic ice temperature was recorded
α	compression ratio
η	dimensionless ratio, see Eq. 9
θ	arbitrary angle of rotation in cross-sectional plane
ν	Poisson's ratio
ξ	instantaneous displacement of penetrator
σ_H	horizontal tensile strength of laboratory sea ice
σ_V	vertical tensile strength of laboratory sea ice
σ_z	compressive bearing stress
σ_φ	tensile rupture stress normal to slant area of cylindrical-conical shear plug
$\tau(\xi,\dot{\xi})$	shear yield stress function

SYMBOLS (Concluded)

τ_o	critical value of shear yield stress
τ_φ	shear stress acting parallel to slant area of cylindrical-conical shear plug at incipient perforation
φ	vertex angle of cylindrical-conical plug, see Fig. 40

INTRODUCTION

The strategic significance of the Far North was brought into focus during the early post-World War II era with the development of nuclear arsenals and intercontinental ballistic missiles. These events generated a large amount of scientific enquiry into the feasibility and promise of countermeasure techniques and resulted in the installation of extensive warning and defense systems throughout the Arctic. With the advent of long range transits and tactical under-ice operations by nuclear-powered submarines in the period 1957-1961, attention has been redirected to the importance of the polar regions from a tactical viewpoint. In particular, the study of arctic submarine warfare tactics has initiated a concomitant effort in the development of effective countermeans for search-and-destroy operations. Thus, high resolution integrated electronic systems have been proposed and investigated for the purpose of locating and tracking alien submarines under the Arctic ice cover. If an attack on these underwater craft by means of air-sea missiles (aerial torpedoes) were contemplated, a fundamental knowledge of the penetration*, perforation and fracture behavior of many types of Arctic sea ice would be required. In this context, the problem treated here is particularly important.

However, the emphasis of this study is not restricted to objectives with purely military connotations. Specifically, the following problem areas are all concerned directly with the perforation characteristics of the polar sea ice cover:

- Airdrop of instrumentation packages (e.g., hydrophones) in remote ice-covered regions of the Arctic to study phenomena characteristic of the underlying ocean
- Mineral exploration of the Arctic Ocean and its floor

---

* Penetration is defined here as the embedding of a projectile in a sea ice cover whereas perforation implies piercing through a sea ice cover by the projectile.

- Communication of cargo and operations of search-and-rescue between aircraft and submarines
- Realization of an aeromarine vehicle that can maneuver through an ice cover
- Breakup of ice jams in ports and harbors using airdropped explosives
- Employment of sonobuoys as on-ice sensors, a problem in which penetration but not perforation is desired.

Although abundant literature exists concerning research in ice and snow physics as well as engineering problems posed by the Arctic environment[1-3]*, and even though the penetration of frozen ground by projectiles and piles has been investigated in the past[4,5], little previous attention has been directed to the mechanics of sea ice penetration by impact. The perforation of floating ice slabs by inert projectiles was studied first by Ross[6] in 1965 and the results and experience obtained in that work are fundamental to the present investigation.

The problem treated in both Ref. 6 and this report considers a projectile of specified shape, dimensions, and weight that is released with known initial velocity from a particular height, and determines the impact velocity required to perforate a sea ice cover of measured thickness, temperature, and salinity. Implicit in this problem is an explanation of how the physical properties of the sea ice cover can be determined with reasonable accuracy from a low-flying surveillance aircraft.

Finally, a knowledge of shock environment and the deceleration loads experienced by the projectile or sonobuoy on impact with sea ice are of prime importance in designing the complex electronic packages employed in modern antisubmarine weapon systems. Thus, another objective of this investigation is to develop an analytical technique for the prediction of peak deceleration at impact.

---

* Superscript numbers refer to references collected at the end of this report.

SUMMARY AND CONCLUSIONS

An experimental program was conducted in which circular, fixed-edge sea ice slabs resting on seawater were subjected to the impact of both freely falling and rifle-powered projectiles. Test slabs were manufactured from Pacific Ocean seawater contained in a specially adapted oil drum and all tests were performed in a cold-room at +15°F. In addition, a field test program was carried out during October - November 1966, at the Arctic Research Laboratory, Point Barrow, Alaska. There, young Arctic sea ice cover in situ was subjected to the impact of rifle-powered projectiles and a projectile fired from a Navy 1-pounder gun.

Tests with the freely falling device employed a 9.69-lb projectile fitted with cylindrical penetrators having diameters of 5/8 in. and 1-1/4 in., and blunt and conical end profiles. Impact velocity ranged from 2 ft/sec through 20 ft/sec. The rifle-powered projectiles weighed 0.75 lb and 0.69 lb, were 1-1/4 in. in diameter, and had blunt and conical end profiles. Impact velocity ranged from 61 ft/sec through 494 ft/sec. The Navy 1-pounder projectile weighed 41.5 lb, was 6 in. in diameter, and had a blunt end profile. Impact velocity ranged from 54 ft/sec through 124 ft/sec.

On the basis of tests performed over a fairly wide range of variables, the following results were found applicable to both laboratory sea ice test slabs and Arctic sea ice cover:

- Perforation was obtained by the mechanism of plug formation*; in particular, shear plugs that were cylindrical-conical in outline were produced (Fig. 1).

---

* Possible mechanisms of perforation are illustrated and discussed in Ref. 6.

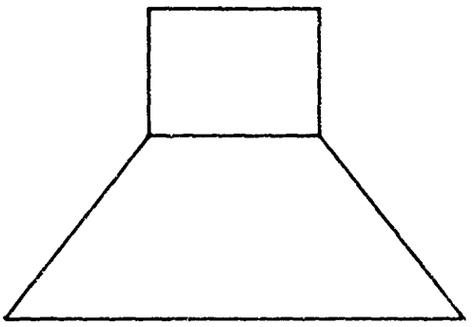

FIG. 1 SKETCH OF CYLINDRICAL-CONICAL SHEAR PLUG

- Perforation at relatively high impact velocities (200 ft/sec - 500 ft/sec) was accompanied by the formation of craters surrounding the point of impact. Cratering was not evident in the low impact velocity range (0 ft/sec - 25 ft/sec), nor in tests with a 6-in. diameter projectile on Arctic sea ice, (50 ft/sec - 125 ft/sec).
- The effects of impact were confined to a small area surrounding the penetrator. Cracks, fissures, and cleavage fractures were not observed, regardless of impact velocity.
- The blunt end penetrator was significantly more effective than the conical penetrator in obtaining perforation at low impact velocities. This advantage was slight at high impact velocities; however, at these velocities, the conical penetrator produced greater amounts of penetration than the blunt penetrator. In the Arctic tests, the presence of snow cover vitiated the blunt penetrator's advantage.
- In tests with the blunt penetrator, complete penetration, or perforation, was obtained whenever the penetration depth was greater than approximately 50% of the ice thickness. However, in similar tests with the conical penetrator, penetration depths up to 80% ice thickness were realized without perforation. Thus, at equivalent impact velocities, an advantage in penetration capability was not necessarily indicative of better perforation performance.

- For both conical and blunt penetrator end profiles, the relationship between penetration depth and impact velocity was approximately linear.

Tests were conducted on Arctic sea ice in which the projectile impacted at approximately 17° incline to the vertical direction. Qualitative results were similar to those obtained at normal incidence; however, at equivalent impact velocities, lesser penetration depths were produced at inclined incidence than at normal incidence.

Using the experimental results as a guideline, a theory was developed for the perforation of a sea ice cover subjected to the impact of a cylindrical blunt-end penetrator at normal incidence. Effects due to cratering were not considered in formulating the theory. The minimum impact velocity (critical value) for perforation was found to depend on the following variables:

- Penetrator mass and diameter
- Sea ice thickness, tensile strength, shear strength, and elastic modulus
- An empirical factor related to plug geometry.

Moreover, the sea ice mechanical strength properties could be related to temperature and salinity content through the Assur theory governing sea ice strength. For this purpose, a computer program was written (Algol 60) to obtain sea ice tensile strength as a function of temperature (0°C through -23°C) and salinity (2 ppm - 20 ppm), and, also, to yield critical impact velocity as a function of the independent variables when values of these variables corresponded to those of the tests, agreement between theory and experiment was good.

For example, in tests on laboratory sea ice with projectile weights of 0.75 lb and 9.69 lb and blunt penetrator diameters of 5/8 in. and 1-1/4 in., theoretical values of critical velocity were lower than experimental critical values and higher than values of maximum impact velocity for which perforation did not occur in ten test series out of twelve. For the remaining two test series, the theory was in error by 7.9% and 11.7%. In tests on Arctic sea ice with projectile weights of 0.75 lb

and 41.5 lb and blunt penetrator diameters of 1-1/4 in. and 6 in., theoretical values of critical velocity were lower than experimental critical values and higher than values of maximum impact energy for which perforation did not occur in six test series out of eight. For the remaining two test series, the theory was in error by 17.9% and 14.4%.

An analysis was developed to determine the peak deceleration force and maximum penetration experienced by a projectile upon impact at normal incidence with a sea ice cover. These quantities were found to depend on:

- Projectile mass and diameter
- Impact velocity
- Sea ice elastic modulus and Poisson's ratio
- Yield load for the penetration of a rigid, cylindrical, flat (blunt nose projectile), or conical (conical nose projectile) indenter in sea ice.

Finally, an outline was made of recommended future research concerning experimental, theoretical, and developmental aspects of the ice perforation problem.

BACKGROUND

To clarify the penetration and fracture behavior of Arctic ice under impact loading, it is necessary first to examine the physical structure and mechanical strength properties of sea ice. With this background, an explanation of experimental results can be based on physical understanding; then, a foundation for formulating theory can be developed, and improved means for perforating a sea ice cover conceived and studied.

The behavior and mechanical properties of sea ice are vastly different from those of freshwater ice. Specifically, when freshwater ice is subjected to rapid loading it behaves as a brittle material whereas sea ice under the same loading exhibits extreme ductility. These results were observed in impact tests on floating ice slabs in which perforation was obtained by breakup due to radial cleavage fracture for freshwater ice and expulsion of a cylindrical shear plug for sea ice.[6] The reasons for this behavior can be related to the structure of sea ice.

Normal seawater contains approximately 35 ppm of soluble salts (e.g., NaCL, $MgCl_2$, Na_2SO_4, $CaCl_2$, KCl, $NaHCO_3$). During the freezing process, salt ions are rejected from the ice crystal lattice resulting in almost pure solid ice and a melt containing the precipitated salts. Although a portion of the salt is absorbed by the underlying seawater, much of the precipitate-rich liquid phase is contained throughout the sea ice cover in the form of brine inclusions. The quantity of brine trapped by the growing ice crystals is a highly variable function of freezing rate.[7] When frozen seawater is considered as a polyphase system of solid H_2O, brine, and precipitated salts, phase equilibrium studies show that certain temperatures (e.g., $-8.2^{\circ}C$, $-22.9^{\circ}C$, $-54.0^{\circ}C$) are critical. These values correspond to points at which particular solid salt phases begin to appear and are important because they delineate regions where the physical properties of the sea ice can differ significantly. In this regard, Assur[8] has stated that the mechanical strength of sea ice depends

on both the brine content and its distribution through the ice thickness and on the precipitation hardening effect contributed by the solid salts. The latter effect is greatest at ice temperatures below -23°C.

Quantitatively, the volume fraction of sea ice occupied by brine or air, denoted the brine content, can be calculated from the salinity, temperature, and density of the sea ice, and a knowledge of the low temperature equilibrium phase relationships for seawater. Initially, the brine content distribution with depth in the sea ice cover is a function of the freezing rate. It changes, subsequently, because of downward brine cell drainage and migration due to gravity, overburden pressure, and temperature gradient.

It is known that the physical structure of sea ice consists of macroscopic crystals with a complex internal structure of pure ice platelets and large numbers of brine cells.[7] Assur,[8] Weeks[9], and others have proposed physical models for sea ice that are represented typically by Fig. 2. With the aid of this model and a knowledge of the physical structure of sea ice, it is possible to explain the experimental results that were obtained in tests on both laboratory sea ice and Arctic sea ice. For instance, the presence of numerous liquid-filled brine inclusions, which under rapid loading conditions produce negligible resistance to shear forces, and the porous nature of sea ice, which results in the strong attenuation of propagating stress waves, combine in effect to render sea ice weak in shear and of exceptional toughness in resisting crack propagation and cleavage fracture.

As an example, previous tests on laboratory sea ice[6] demonstrated clearly the superiority of a blunt end penetrator over a conical one in perforation whereas the opposite behavior was true for tests on fresh ice. Specifically, upon impact, the blunt penetrator with its attendant high shear stress concentration around the penetrator rim readily expelled a plug out of the sea ice; however, the conical penetrator was ineffective in producing fracture by splitting the ductile sea ice. Moreover, the effects of impact loading on sea ice were confined locally to the point of contact, but with fresh ice the propagation of cracks and fissures was complete to outer boundaries of the test slab.

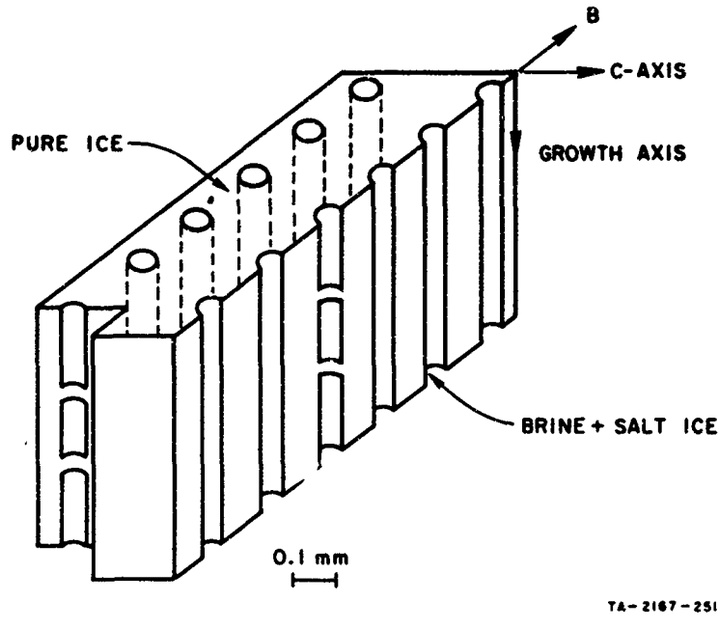

FIG. 2 PHYSICAL MODEL OF SEA ICE SHOWING INTERRUPTED AND CONTINUOUS BRINE INCLUSIONS, FROM REF. 8

Results of the Phase I study* were qualified by the particular physical structure and high salinity contents of the test slabs. This occurred because the sea ice was manufactured in a shallow closed container so that all of the rejected salts accumulated in a relatively large skeleton layer on the slab's bottom. Skeleton ice is essentially mush and has negligible strength; thus, the perforation of these sea ice slabs resulted in the expulsion of nearly cylindrical shear plugs.

Experience obtained in the Phase I study indicated that the sea ice perforation problem could not be attacked experimentally in the usual manner employed for penetration problems. That is, it was not possible to vary individual parameters selectively while holding others constant

---

* The most important results of this investigation are described in Appendix A.

to establish empirical relationships between characteristic nondimensional groups. This was so because it was virtually impossible to manufacture laboratory sea ice test slabs having identical or even consistent physical and mechanical properties. As a result, in this investigation, dimensional analysis and modeling laws have not been employed; instead, a theory was developed that is applicable in a range of typical, realistic values for the important projectile and sea ice variables.

In the present experiments, test slabs were manufactured in a semi-closed system where an underlying seawater to sea ice volume ratio of 3 through 8 was maintained. The resulting sea ice slabs exhibited low values of salinity and relatively narrow skeleton layers. Perforation of these test slabs at normal incidence with a blunt end penetrator produced shear plugs that were cylindrical-conical in outline.

Because these plugs were significantly different in geometry from those obtained in the previous study, a new and more sophisticated theoretical approach was taken and an innovation in the experimental program was carried out. In this regard, tests were performed with styrofoam slabs having uniform properties in order to gain a better understanding of the perforation process by excluding material effects related to the inhomogeneity and anisotropy of sea ice. In some respects, styrofoam is quite similar to sea ice, both substances being porous media with zero shear strength inclusions and having similar mechanical strength properties. One important difference is in their respective densities; however, this property is of minor consequence in the present problem because the masses of the plugs expelled from these materials are extremely small in comparison to the projectile mass.

The styrofoam tests were of great value because they produced shear plug configurations and perforation hole geometries that remained intact and permanent, unlike sea ice in this respect,* and could be studied in

---

* Although the laboratory sea ice plugs always disintegrated after expulsion leaving just the cylindrical-conical perforation hole outline for plug identification purposes, tests on Arctic ice with a large diameter projectile produced an intact plug specimen similar to those observed in styrofoam.

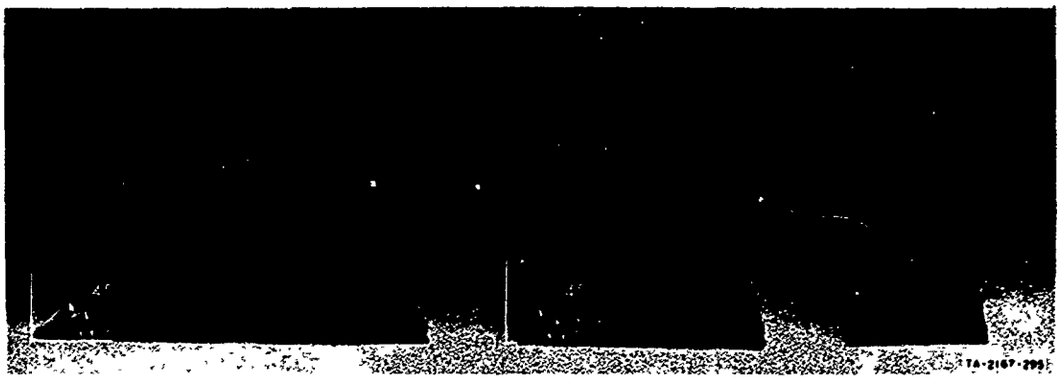

FIG. 3 CROSS-SECTION VIEWS SHOWING REGIONS OF PLASTIC DEFORMATION IN STYROFOAM CYLINDRICAL-CONICAL SHEAR PLUGS AT DIFFERENT RATIOS OF STYROFOAM THICKNESS TO PENETRATOR DIAMETER (t/D): LOW IMPACT VELOCITY TESTS (a) t/D = 1.6, (b) t/D = 1.6, (c) t/D = 3.2

detail after testing. In addition, the internal plastic stress distributions resulting from impact were outlined clearly in cross-section cuts through the shear plugs (Fig. 3). As a result of observations made in these tests, a theory was developed that appears to provide useful results for both laboratory sea ice and Arctic sea ice. This theory showed that critical impact velocity depended on the following basic parameters:

- Projectile mass and diameter
- Sea ice thickness, shear strength, tensile strength, and elastic modulus.

By introducing Assur's theory governing the composition and strength of sea ice[8], the present analysis was recast so that critical impact velocity was a function of

- Projectile mass and diameter
- Sea ice thickness, temperature, and salinity.

There is a good possibility that an airborne computer could be developed for surveillance aircraft to employ these requisite variables

as inputs and obtain theoretical values of impact velocity for perforation. For example, projectile mass, diameter, and profile shape are known a priori. Sea ice thickness can be determined probably by radio echo sounding techniques.[15,16]* The characteristic temperature of sea ice could be obtained by finding first sea ice surface temperature utilizing the aircraft external ambient temperature, the atmospheric lapse rate, and/or local meteorological conditions. Then, knowing the ice thickness, the bottom surface temperature (e.g., the sea ice-seawater equilibrium value, +28°F (-1.5°C), and assuming the typical bilinear variation of sea ice temperature with depth (see Ref. 17 and present test results), the characteristic sea ice temperature can be determined by interpolative calculation. Finally, a measure of the sea ice salinity content can be realized from a knowledge of local geography and seasonal ice conditions. For example, Assur[8] reports typical salinities for different types of ice as follows:**

2 ppm - perennial sea ice (Polar ice)

5 ppm - normal one-season sea ice in the middle of winter (annual ice)

10 ppm - first formation of young sea ice

20 ppm - salt ice produced by flooding.

In addition to providing values of critical impact velocity, the theory is valuable because it shows how individual changes in the independent variables affect the dependent variable. Thus, an example is

---

* Evans and de Q. Robin[16] report that present-day radio echo sounding techniques are capable of determining sea ice thicknesses in the range 40 m ± 5 m. These authors do not provide any information about experience with lesser thickness ice sheets (e.g., 1 m - 4 m). However, even if this capability is not available presently, there is always expectation that future technological development will fulfill this need. A progress report on radio echo sounding appeared in the Polar Record, January 1967.

** Annual sea ice is less than one year in age, greyish white in color, averages 1 ft through 9 ft in thickness, and ranges in salinity content from 4 ppm through 15 ppm. Polar sea ice is often several years in age, pale blue in color, averages 9 ft through 12 ft in thickness, and ranges in salinity content from trace quantities through 2 ppm.

worked out in the present report for a standard size ordnance projectile and the bounded ranges of each sea ice parameter are determined for perforation of typical Arctic ice cover thicknesses.

TEST SPECIMENS, EQUIPMENT, AND PROCEDURE

Laboratory Test Specimens

All laboratory sea ice test specimens employed in the investigation were manufactured from Pacific Ocean seawater having an average salinity content of 30 ppm. The specimens were circular slabs, 22-1/2 in. in diameter, and varied from 3 in. to 16 in. in thickness. Typical salinity contents and temperatures for the sea ice slabs were between 6 ppm through 15 ppm and +5°F (-15°C) through +23°F (-5°C), respectively. These data were recorded for each test slab and are summarized in the section entitled "Test Results". Density was not determined for every test slab; however, a characteristic value obtained by weighing a sea ice core and measuring an equivalent volume of displaced kerosene yielded a value of 0.918 gm/cc. The crystallographic structure of the sea ice was not investigated, nor was the air content or porosity determined.

A typical sea ice test slab was manufactured over a 3 - 7 day period, depending on thickness desired, by freezing seawater contained in a 55 gal commercial oil drum that was placed in a forced-air cold storage freezer locker operating at -4°F (-20°C).

The test specimens exhibited top and bottom surfaces which were both flat and parallel. In particular, top surfaces were free of any surface cracks and humps caused by constraining the ice slab in the drum during freezing. Moreover, the outer edge surfaces of the sea ice slabs adhered firmly to the surrounding drum resulting in "built-in" or "fixed" edge support conditions.

The styrofoam test slabs were cut from Dow expanded polystyrene boards having commercial designations Styrofoam FR and Styrofoam BB for specimen thicknesses of 1, 1-1/2, 2, 3, 4, and 10 in. The densities and mechanical properties supplied by the manufacturer for these materials and a comparison with typical values for Arctic sea ice are listed in Table 1.

TABLE 1

DENSITY AND MECHANICAL PROPERTIES OF STYROFOAM AND TYPICAL ARCTIC SEA ICE

Type	Density (lb/ft^3)	Compressive Strength (psi)	Tensile Strength (psi)	Shear Strength (psi)	Flexural Strength (psi)	Compressive Modulus (psi)	Bending Modulus (psi)
Styrofoam FR*	1.9	30	70	35	60	1000	2200
Styrofoam BB*	1.8	18	55	30	40	800	1300
Typical Arctic Sea Ice**	56.0-60.0	200-1500	20-300	20-250	10-250	6.0×10^4-10.0×10^5	2×10^5-3.5×10^5

* Data from manufacturer.

** Data from Refs. 10 through 14.

Test Equipment

The basic equipment of the test facility consisted of the oil drum, a thermocouple array, a guide rail assembly and a rifle assembly for the low and high impact velocity tests, respectively, and associated electronic instruments. Projectiles with various end profiles were also required. Photos of the test setups and of the projectiles employed in each are shown in Figs. 4 through 7.

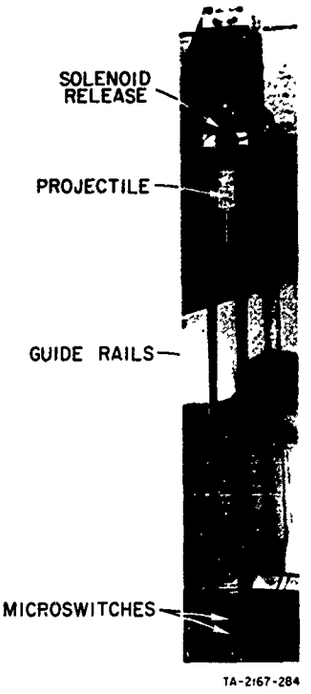

FIG. 4 LOW IMPACT VELOCITY TEST APPARATUS

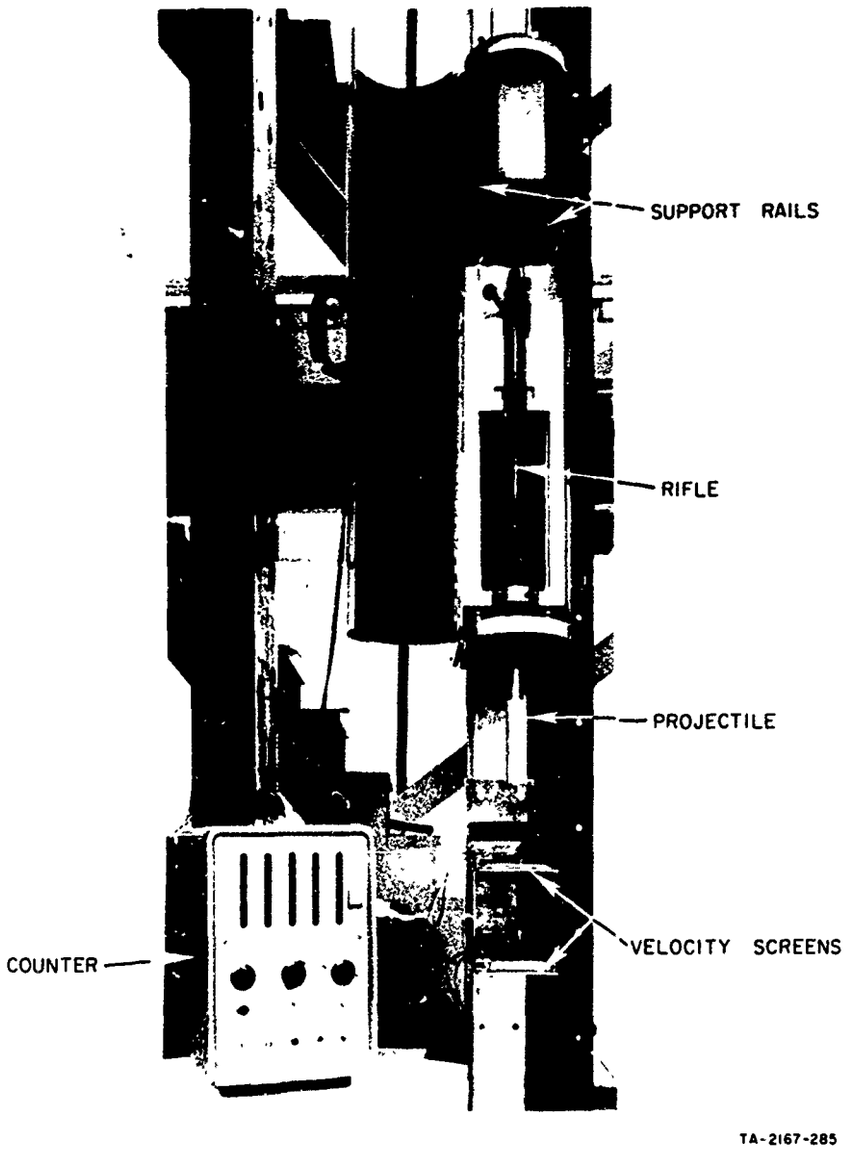

FIG. 5 HIGH IMPACT VELOCITY TEST APPARATUS

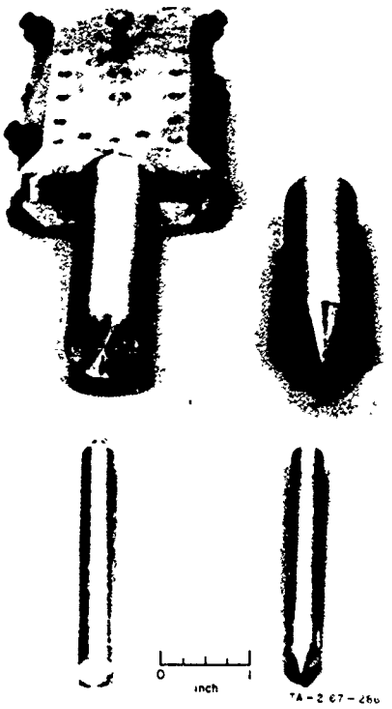

FIG. 6 LOW IMPACT VELOCITY PROJECTILE AND VARIOUS PENETRATORS

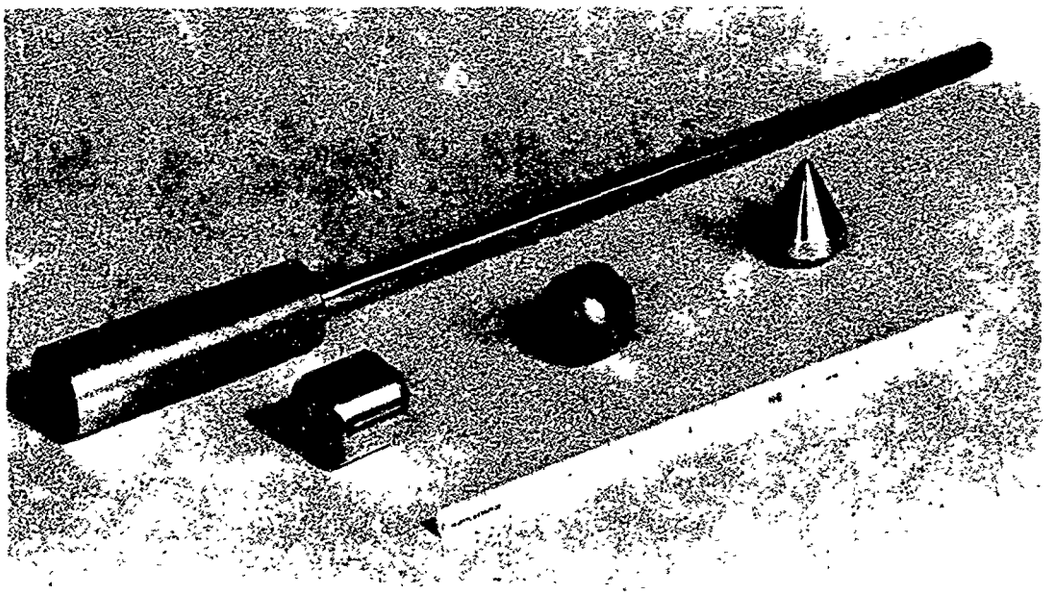

TA-2167-287

FIG. 7 HIGH IMPACT VELOCITY PROJECTILE AND VARIOUS PENETRATOR TIPS

The oil drum in which the sea ice slabs were manufactured incorporated certain features designed to promote realistic freezing conditions. For example, to ensure unidirectional freezing of the ice slab from its top surface, the drum was insulated on both bottom and outer surfaces by rock wool with a heavy tarpaulin protective wrap. In addition, a 300-watt heating tape controlled by a Powerstat transformer was embedded in the insulation to prevent heat loss through the drum walls. The Powerstat output was set to maintain an underlying sea ice-seawater equilibrium temperature of 27°F - 28°F (-1.5°C). With the drum heating system, control of the rate of freezing and resulting slab thicknesses and the faster melting-out of a slab after testing could be achieved readily.

Another feature of the drum was an inner circumferential liner of waterproof neoprene rubber padding 1 in. thick and extending to a depth of 10 in. from the drum's top edge. The liner allowed the sea ice slab to form under very much lower radial stresses than would be present within the confines of the "rigid" drum wall. As a result, surface cracks, fissures, and humps were eliminated completely.

A pressure relief valve was installed at the bottom of the drum to enable the release of accumulated hydrostatic pressure during the ice formation process. The inside bottom surface of the drum was protected against the projectiles by a 2-in. layer of sponge rubber and a 1/4-in. circular plate of aluminum.

Finally, the drum was mounted on a movable dolly to facilitate pre-positioning of the sea ice slab with respect to the projectile.

The thermocouple array was utilized to measure the vertical temperature distribution through the sea ice thickness. Thermocouples were spot-welded iron-constantan junctions and were attached to a vertical plastic rod that was frozen into the sea ice slab. The thermocouple outputs were read on a temperature-compensated Honeywell-Brown recorder.

The guide rails employed for the low velocity free-fall drop tests were 1-1/4-in. OD commercial steel pipes supported and maintained 3-1/2 in. apart by spacer blocks.

The projectile mass comprised two side plates of brass and a middle slab of lead. Four Teflon roller bearings were mounted on the projectile's edges to provide free sliding motion in the guide rails. The various penetrators that could be screwed into the projectile's base were made of aluminum. Table 2 summarizes data concerning the geometries and weights of the projectile mass and penetrators.

TABLE 2

DIMENSIONS AND WEIGHTS: LOW IMPACT VELOCITY PROJECTILE

Penetrator Profile	D (in.)	C_o (in.)	m_1 (slugs)	$m_1 g$ (lb.)
Blunt	5/8	3.03	0.283	9.125
Blunt	1-1/4	3.31	0.301	9.688
Conical	5/8	3.03	0.283	9.125
Conical	1-1/4	3.30	0.300	9.650

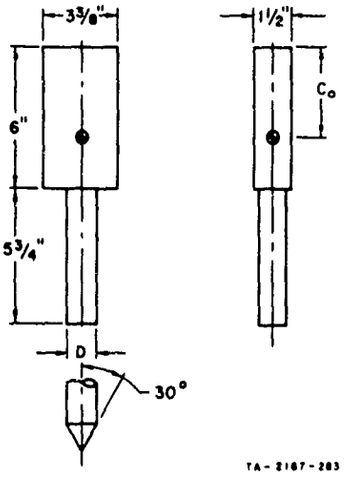

The projectile was released by a solenoid-actuated trip. Impact velocity was read with an electronic counter that measured the elapsed time between two consecutive signals furnished as the lower and upper edges of the projectile body passed across the wiper arm of a single microswitch. With this scheme, the fixed projectile body length (6 in.) was the distance interval for the velocity calculations, thereby eliminating difficulties associated with switch spacing and unlike switch response times. To ascertain when the penetrator's impact end emerged from the ice slab bottom (ice-water interface), a signal was captured with a miniature magnetic head from a magnetized pinpoint embedded in the projectile's side. The magnetic head's pickup position with respect to the projectile was determined by the thickness of the ice slab. The signal was recorded on one beam of a dual-beam oscilloscope and provided a cutoff pip for identification purposes.

The other beam of the oscilloscope portrayed the resisting force-time history experienced by the projectile during the perforation process. These records were obtained as output traces of a piezoelectric accelerometer mounted in the impact end of the penetrator. The accelerometer signal was amplified and filtered before its input to the oscilloscope. An external scope trigger signal was obtained from a microswitch tripped by the projectile just prior to impact. The impact velocity measuring microswitch, the magnetic head, and the scope trigger microswitch were all attached to a machinist's magnetic holder that could be positioned easily on the guide rails for each particular test slab thickness. The procedure and tests employed to calibrate the accelerometer and its associated electronic equipment are described in Appendix C. A block diagram of the complete instrumentation system is shown in Fig. 8.

The assembly for the high velocity impact tests incorporated a 458 Winchester Magnum rifle that propelled a projectile having interchangeable penetrator heads. The rifle was mounted on a carriage fitted with bronze bushings to two support rails, and recoil was absorbed by motion along the rails against bearing friction forces. The assembly was

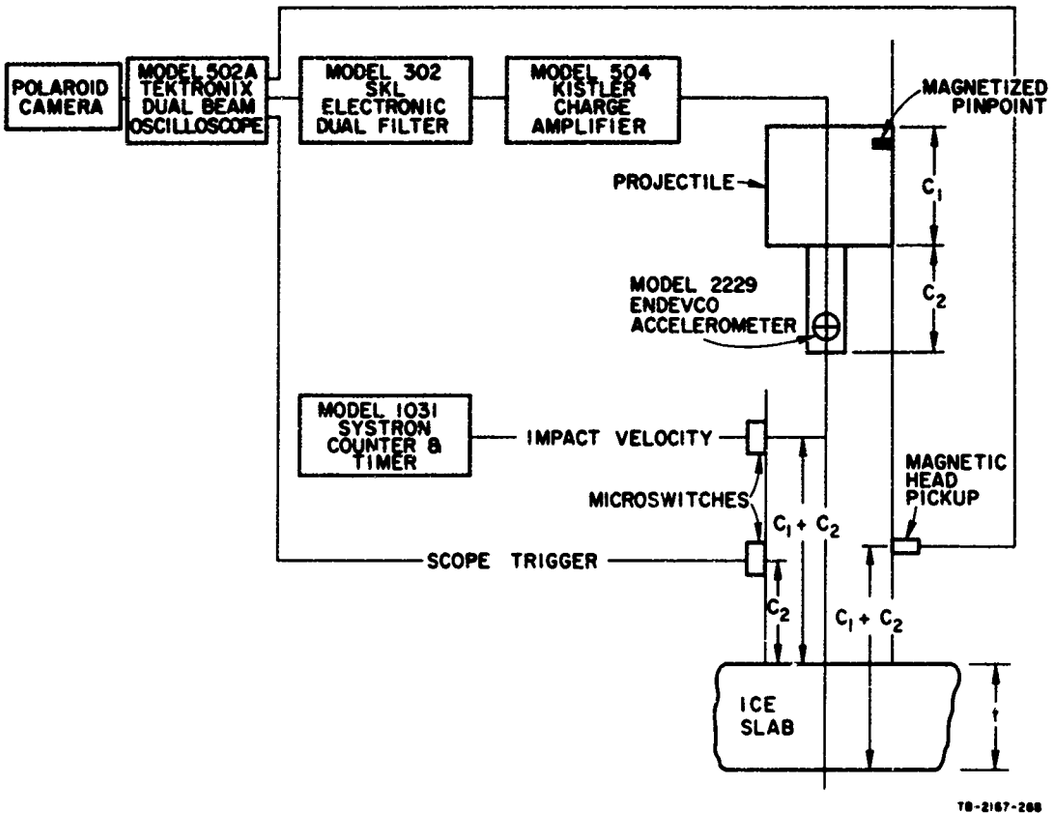

FIG. 8 BLOCK DIAGRAM OF LOW IMPACT VELOCITY INSTRUMENTATION SYSTEM

positioned vertically to fire downwards, and the projectile was held in the rifle prior to firing by a thin rubber sleeve. For safety purposes, the entire assembly was enclosed by steel plate, and the rifle was fired by a remotely-controlled solenoid actuator. Cartridges were hand-loaded with a mixture of smokeless rifle and pistol powders in quantities ranging from 2.5 grains to 45 grains. A schematic drawing of the oil drum, rifle assembly, and instrumentation system is shown in Fig. 9; the dimensions and weights of the projectiles are summarized in Table 3.

TABLE 3

DIMENSIONS AND WEIGHTS:
HIGH IMPACT VELOCITY PROJECTILE

Penetrator Profile	D (in.)	m_1 (slugs)	$m_1 g$ (lb)
Blunt	1.25	0.0233	0.750
Conical	1.25	0.0214	0.688

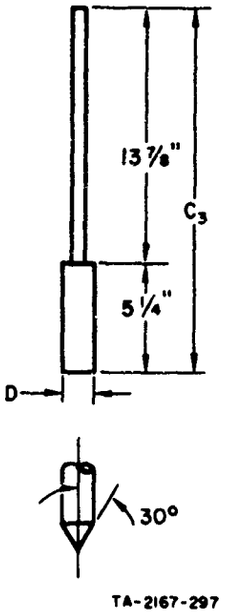

TA-2167-297

Impact velocity was measured by triggering an electronic counter from the outputs of two screen sections placed 6 in. apart with the lower screen within 2 in. of the test slab surface. Each screen section was made up to two thin household aluminum foils, 4 x 4-in. square, separated 3/32 in. apart in a plastic holder. The electronic circuit was a "make" circuit; that is, it was designed to furnish a signal when contact was obtained instantaneously between the two foils in a screen section by the passing projectile. An electronic circuit diagram of the velocity measuring system is shown in Fig. 10.

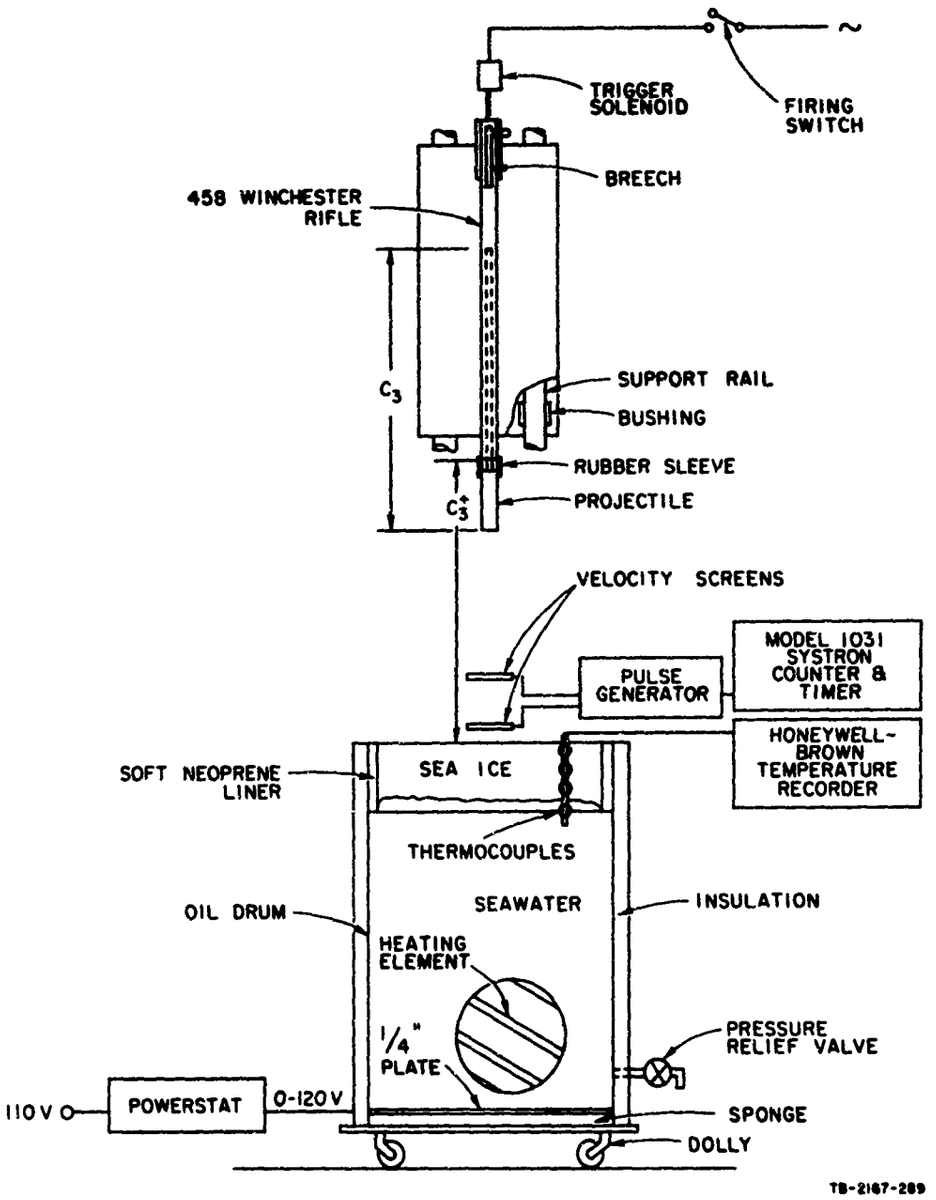

FIG. 9 SCHEMATIC DRAWING OF HIGH IMPACT VELOCITY RIFLE ASSEMBLY AND TEST SLAB MANUFACTURING APPARATUS

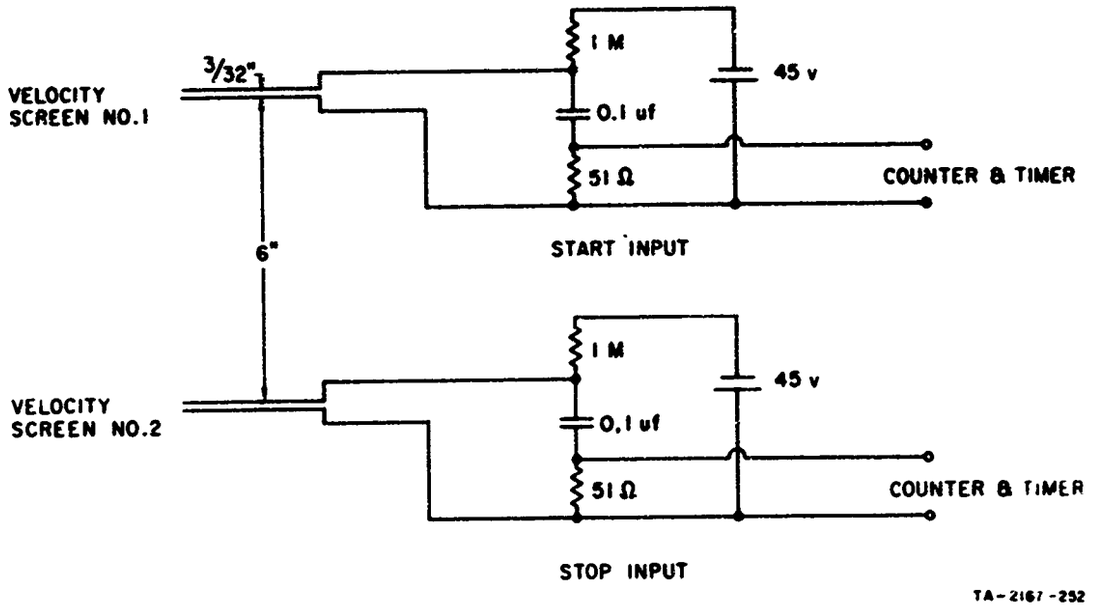

FIG. 10 ELECTRONIC CIRCUIT DIAGRAM FOR VELOCITY MEASURING SYSTEM

A check on the accuracy of the velocity measuring system was obtained by determining simultaneously, over a typical range of impact velocities, the velocities read by the electronic counter and those observed in ultra-high speed motion pictures taken with a 10,000-frame/sec Red Lake Hycam camera. Velocities measured independently by these means agreed within 2-1/2% on the average. These data were plotted in the form of a rifle calibration curve (Fig. 11) correlating impact velocity versus powder charge. The rifle assembly produced impact velocities in the range 50-500 ft/sec with a 0.75-lb blunt projectile.

A hand coring tool was designed and developed during the course of experiments. This device was used to take 1-1/4-in. diameter core samples from the sea ice slab for salinity determination and for boring holes through the ice to obtain thickness profiles. The coring tool

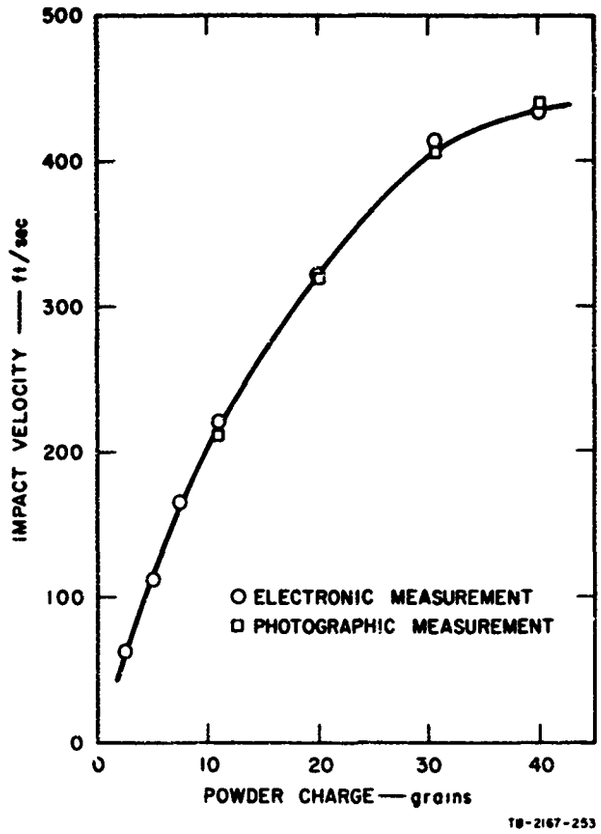

FIG. 11 CALIBRATION CURVE FOR 458 WINCHESTER RIFLE AND HIGH IMPACT VELOCITY PROJECTILE (Blunt Profile)

(Fig. 12) consisted of a 5-in. long, 1/8-in. wall thickness, brass tube with a sawtooth, serrated cutting edge. An electric hand drill was used to turn the corer with a 3/16-in. diameter steel drill rod connected through an endplate and a driving dog to the base plate of the corer. By removing a holding nut, the rod and endplate could be displaced to eject the sea ice core sample contained in the tube.

Finally, modifications to the test equipment that were required in the Arctic tests are described in the chapter entitled "Experimental Observations-Field Tests".

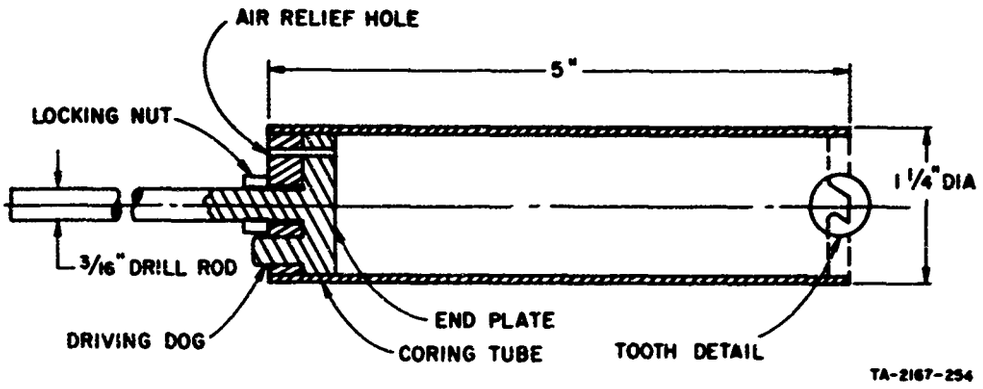

FIG. 12 STANFORD RESEARCH INSTITUTE — CORING TOOL

Test Procedure

The test procedure was similar for all tests with minor exceptions in the experiments on styrofoam slabs. For a typical sea ice test, the slab thickness and temperature profile were monitored daily. A slab was deemed ready for testing when its thickness reached the value required for a scheduled experiment. The remaining sea ice parameters, i.e., salinity content and characteristic temperature, were recorded as secondary variables; that is, these quantities were not chosen a priori as conditions for conducting an experiment. Salinity content was determined from sample cores by titration for total halides (Mohr procedure). Usually, two full cores through the thickness were taken from the test slab, one to yield an average salinity content, the other partitioned in sections to provide a 3-part salinity profile. In addition, a salinity determination of the seawater was made before freezing each sea ice slab.

Prior to testing, the drum pressure relief valve was opened to ensure that the underlying seawater was at atmospheric pressure. Next, the temperature profile across the slab was established by reading the outputs of the thermocouple array; then, the freezer temperature, underlying seawater temperature, and all dial position settings on the electronic instruments were recorded.

Both the low and high impact velocity tests were conducted in the following manner. Starting at modest impact velocities, the free-fall and rifle-powered projectile impact velocities were increased in finite increments by augmenting the drop height and powder charge, respectively.

This procedure was continued until perforation occurred; then, higher and lower impact velocities were attempted to bracket the threshold value of impact velocity. For each test, the penetration or perforation process was observed and data concerning penetration depth, failure surfaces, and crater profiles were noted. The various tests were characterized by different penetrator diameters and end profiles. Only tests at normal incidence were attempted in the laboratory.

The styrofoam test slabs were floated in the same drums employed to manufacture the sea ice test specimens. About 1/2-in. radial clearance between the slab and the drum's rubber lining was allowed. Thus, whereas the sea ice slabs were "fixed" or "built-in" around their periphery, the styrofoam slabs were "free".

Finally, the minor changes in test procedure that were necessary in conducting the Arctic tests are described in the chapter entitled "Experimental Observations-Field Tests".

TEST RESULTS

Impact-penetration experiments were conducted on test slabs of laboratory sea ice and styrofoam and, in field tests, on Arctic sea ice. The numerical data obtained are given in Appendix D. The most important data are summarized in Tables 4, 5, and 6, 7 for laboratory sea ice and Arctic sea ice, respectively.

Classification of the sea ice with regard to temperature and salinity ranges tested is shown by the bounded areas in Fig. 13. Temperature and salinity profiles through thickness for the laboratory sea ice are plotted in Figs. 14 and 15, respectively; similar information for the Arctic sea ice is contained in Figs. 16 and 17. Figures 18 and 19 are collections of photographs portraying the cellular structure of the Arctic sea ice as a function of ice thickness.

Results of high impact velocity tests on laboratory sea ice and Arctic sea ice in which penetration but not perforation occurred are plotted in Figs. 20 and 21. These plots show penetration depth versus impact velocity for penetrators of 1-1/4-in. diameter with blunt and conical end profiles. Figure 22 displays results obtained in tests on Arctic sea ice with a 6-in. diameter projectile. In this figure, the relationship between penetration depth and impact velocity is plotted for a sequence of shots up to and including perforation at the critical impact velocity.

Perforation results are given in Figs. 23 through 26. Figures 23 and 24 plot experimental data points relating critical impact velocity and/or maximum impact velocity to the slab thickness-penetrator diameter ratio for laboratory sea ice and Arctic sea ice, respectively. Figure 25 is a plot of critical impact velocity versus thickness for styrofoam in which theoretical perforation threshold boundaries are included with the experimental data points. Figure 26 shows the relationship between shear peretration depth and slab thickness for styrofoam. These plots all refer to tests conducted with blunt end penetrators at normal incidence.

Photographs of typical plugs produced in the perforation of styrofoam test slabs are shown in Figs. 27 and 28. Crater profiles and perforation geometries produced in high impact velocity tests on laboratory sea ice are shown in Figs. 29 and 30. Figure 29 portrays the relationship between crater cross-section area and impact velocity and Fig. 30 indicates the relative performances of the conical and blunt profiles in the penetration and perforation of an 11-1/2-in. thick sea ice test slab.

Oscillograms showing the typical deceleration response obtained in low velocity impact tests on laboratory sea ice and styrofoam are found in Fig. 31; a comparison of experimental and theoretical values of peak deceleration loads is given in Appendix B.

Table 4

SUMMARY OF EXPERIMENTAL RESULTS:
LABORATORY SEA ICE TEST SLABS, BLUNT PENETRATOR

Date	Test Slab	Ice Thickness (in.)	Freezer Temp. (°F)	Surface Temp. (°F)	Sea Ice Temp. (°F)	Sea Water Temp. (°F)	z_T* (in.)	Salinity (ppm)	Type of Test	Penetrator Diameter (in.)	v_i† (ft/sec)	$\frac{1}{2} m_i v_i^2$** (ft-lb)	t/D ‡	Perforation
5/16/66	A	6-3/4	0	-	16.7	35.5	3	12.0	Drop	1-1/4	13.7	34.0	5.4	No
5/20/66	B	5	- 4	-	22.1	35.0	3	10.2	Drop	5/8	14.7	32.8	8.0	Yes
5/24/66	C	4-1/4	5	-	19.4	29.5	3	15.0	Drop	1-1/4	11.3	19.2	3.4	Yes
6/09/66	D	4-1/8	10	-	24.5	25.8	3	-	Drop	1-1/4	-	-	3.3	-
7/22/66	E	3-3/8	7	15.5	19.4	27.0	3/4	15.6	Drop	1-1/4	8.6	11.1	2.7	Yes
8/25/66	G	10	16	4.0	14.5	28.0	2	10.6	Rifle	1-1/4	237.0	655.0	8.0	No
9/07/66	H	9-1/4	- 7	0	7.8	27.5	2	7.2	Rifle	1-1/4	414.0	2000.0	7.4	Yes
9/13/66	I	11-1/4	16	5.0	19.0	37.0	2	8.2	Rifle	1-1/4	411.0	1970.0	9.0	Yes
9/13/66	J	15-1/2	-13	5.0	19.0	27.5	2	9.3	Rifle	1-1/4	402.0	1880.0	12.4	No
9/22/66	K	8-1/2	- 6	3.5	10.0	27.5	1	12.2	Rifle	1-1/4	324.0	1225.0	6.8	Yes
9/23/66	L	10-1/2	6	10.0	14.0	27.5	1	12.2	Rifle	1-1/4	370.0	1590.0	8.4	Yes
10/07/66	N	15-3/4	- 6	4.0	7.0	25.0	2	13.8	Rifle	1-1/4	430.0	2150.0	12.6	No
10/09/66	O	9-1/4	- 9	0	6.0	26.0	2	6.5	Rifle	1-1/4	252.0	741.0	7.4	No

* z_T = Depth at which characteristic sea ice temperature was recorded.
† v_i = Impact velocity. For a test in which perforation did not occur, v_i is the maximum value experienced by the test slab.
** m_i = Projectile mass.
‡ t/D = Ratio, sea ice thickness to penetrator diameter.

Table 5

SUMMARY OF EXPERIMENTAL RESULTS:
LABORATORY SEA ICE TEST SLABS, CONICAL PENETRATOR

Date	Test Slab	Ice Thickness (in.)	Freezer Temp. (°F)	Surface Temp. (°F)	Sea Ice Temp. (°F)	Sea Water Temp. (°F)	Salinity z_T* (in.)	Salinity (ppm)	Type of Test	Penetrator Diameter (in.)	v_i† (ft/sec)	$\frac{1}{2} m_i v_i^2$** (ft-lb)	t/D‡	Perforation
5/1[illegible]/66	A	6-3/4	0	-	16.7	35.5	3	12.0	Drop	1-1/4	14.6	32.1	5.4	No
5/20/66	B	5	- 4	-	22.1	35.0	3	10.2	Drop	5/8	13.8	26.9	8.0	Yes
5/24/66	C	4-1/4	5	-	19.4	29.5	3	15.0	Drop	1-1/4	10.5	16.6	3.4	No
7/23/66	F	2-3/4	11	22.0	22.0	28.0	3/4	-	Drop	5/8	6.3	5.62	4.4	Yes
7/23/66	F	2-3/4	11	22.0	22.0	28.0	3/4	-	Drop	1-1/4	7.7	8.90	2.2	Yes
9/13/66	I	11-1/4	16	5.0	19.0	37.0	2	8.2	Rifle	1-1/4	428.0	1960.0	9.0	Yes
9/13/66	J	15-1/2	-13	5.0	19.0	27.5	2	9.3	Rifle	1-1/4	436.0	2035.0	12.4	No
9/28/66	M	9-3/4	- 3	1.5	11.5	28.5	2	17.1	Rifle	1-1/4	305.00	995.0	7.8	Yes

* z_T = Depth at which characteristic sea ice temperature was recorded.

\+ v_i = Impact velocity. For a test in which perforation did not occur, v_i is the maximum value experienced by the test slab.

** m_i = Projectile mass.

‡ t/D = Ratio, sea ice thickness to penetrator diameter.

TABLE 6

SUMMARY OF EXPERIMENTAL RESULTS: ARCTIC SEA ICE TEST SERIES, BLUNT PENETRATOR

Date	Test Series	Ice Thickness (in.)	Air Temp. (°F)	Surface Temp. (°F)	Sea Ice Temp.& (°F)	Sea Water Temp. (°F)	z_c* (in.)	Salinity (ppm)	Type of Test	Penetrator Diameter (in.)	v_i† (ft/sec)	$\frac{1}{2} m_i v_i^2$** (ft-lb)	t/D‡	Perforation
10/27/66	A	8	+18	+10	+15.5	31.0	--	12.1	Rifle	1-1/4	262.0	798.0	6.4	No
10/28/66	B	10-3/4	+ 9.5	+14.5	+14.5	30.0	9-1/8	13.8	Rifle	1-1/4	494.0	2840.0	8.6	Yes
10/29/66	C	9-3/4	+ 8	+ 8.5	+14.0	30.5	8-1/8	12.4	Rifle	1-1/4	444.0	2295.0	7.8	Yes
11/02/66#	D1	11-3/8	- 4	+16.0	+26.0	35.0	--	14.0	Rifle	1-1/4	380.0	1820.0	9.1	No
11/02/66	D2	11-3/8	- 4	+16.0	+26.0	35.0	--	14.0	Rifle	1-1/4	417.0	2190.0	9.1	No
11/04/66	E	11-1/4	0	+18.0	+24.5	33.0	--	14.0	Rifle	1-1/4	433.0	2360.0	9.0	No
11/05/66	F	13	+17	+18.0	+24.0	30.0	--	10.3	Rifle	1-1/4	409.0	2110.0	10.4	No
11/17/66	G	15-3/4	+18	+31.5	+32.0	32.0	--	--	Navy 1Pdr	6	--	--	12.6	No
11/19/66	H	16	+12	+11.0	+17.0	28.0	14	10.6	Navy 1Pdr	6	124.0	9890.0	12.8	Yes
11/21/66	I	16-1/4	+ 4	+10.0	+16.5	28.0	--	10.6	Navy 1Pdr	6	100.0	6440.0	13.0	No
11/22/66	J	17	- 8	+ 7.5	+15.5	28.0	--	9.4	Navy 1Pdr	6	96.5	5990.0	13.6	No

\# Test Series D1 was carried out at 17.3° inclined incidence to vertical. All other series were carried out at normal incidence.

& Sea ice temperature recorded at depth of approximately 1/4 the thickness.

* z_c = Length of cylindrical shear yield surface at critical impact velocity.

† v_i = Impact velocity. For a test in which perforation did not occur, v_i is the maximum value experienced by the sea ice.

** m_i = Projectile mass.

‡ t/D = Ratio, ice thickness to penetrator diameter.

TABLE 7

SUMMARY OF EXPERIMENTAL RESULTS: ARCTIC SEA ICE TEST SERIES, CONICAL PENETRATOR

Date	Test Series#	Ice Thickness (in.)	Air Temp. (°F)	Surface Temp. (°F)	Sea Ice Temp.& (°F)	Sea Water Temp. (°F)	z_c* (in.)	Salinity (ppm)	Type of Test	Penetrator Diameter (in.)	v_1† (ft/sec)	$\frac{1}{2} m_1 v_1^2$** (ft-lb)	t/D‡	Perforation
11/02/66	D1	11-3/8	- 4	+16.0	+26.0	35.0	--	14.0	Rifle	1-1/4	308.0	1195.0	9.1	No
11/04/66	E	11-1/4	0	+18.0	+24.5	33.0	--	14.0	Rifle	1-1/4	469.0	2770.0	9.0	No
11/05/66	F	13	+17	+18.0	+24.0	30.0	--	10.3	Rifle	1-1/4	406.0	2080.0	10.4	No

\# All tests at normal incidence.

& Sea ice temperature recorded at depth of approximately 1/4 the thickness.

* z_c = Length of cylindrical shear yield surface at critical impact velocity.

† v_1 = Impact velocity. For a test in which perforation did not occur, v_1 is the maximum value experienced by the sea ice.

** m_1 = Projectile mass.

‡ t/D = Ratio, ice thickness to penetrator diameter.

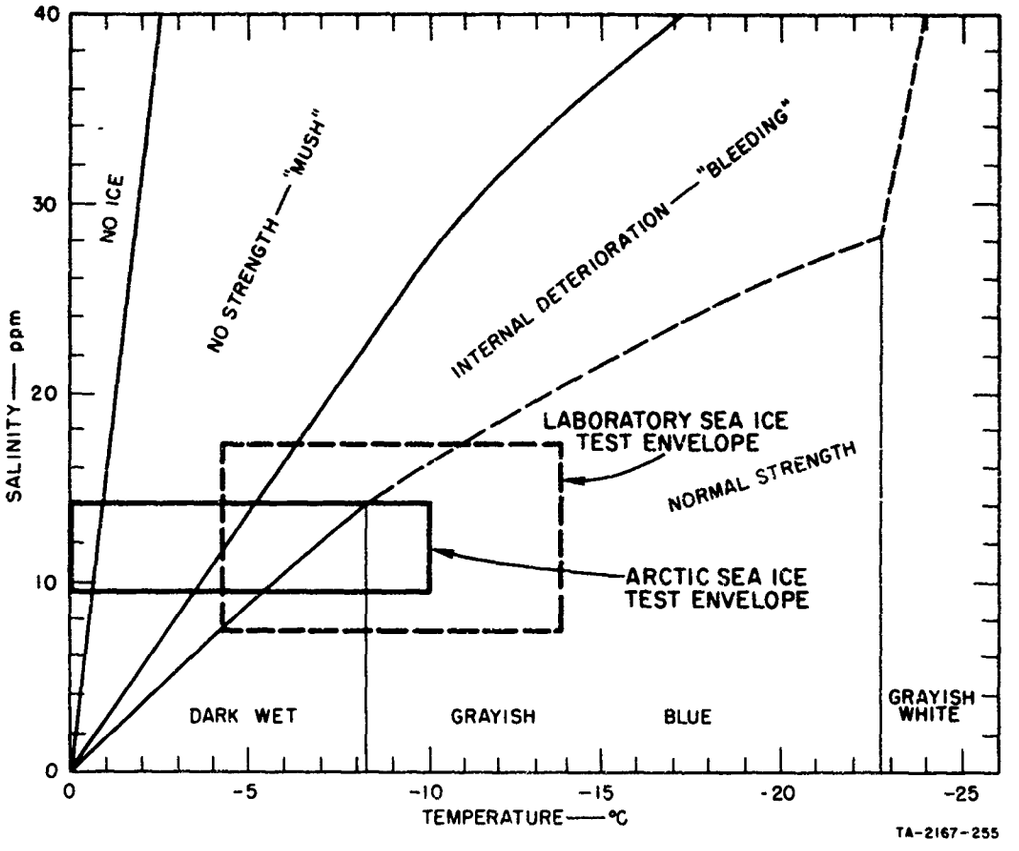

FIG. 13 STRENGTH CONDITIONS OF SEA ICE FOR VARIOUS TEMPERATURE AND SALINITY RANGES, FROM REF. 8

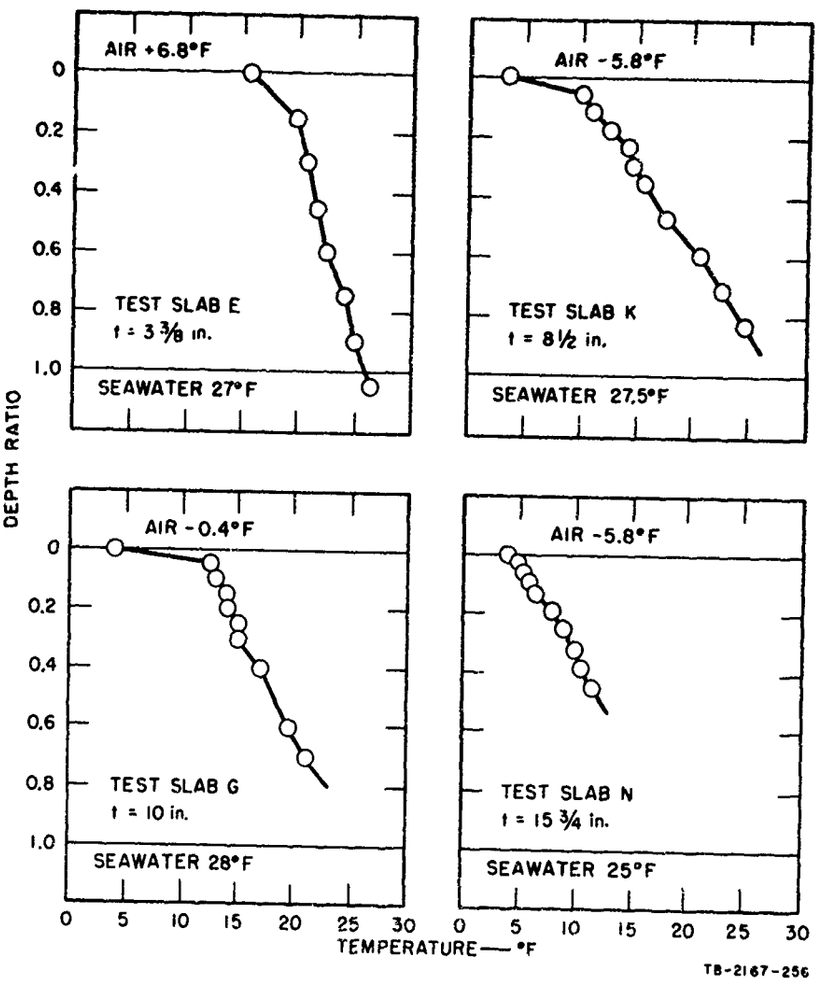

FIG. 14 TYPICAL TEMPERATURE PROFILES: LABORATORY SEA ICE

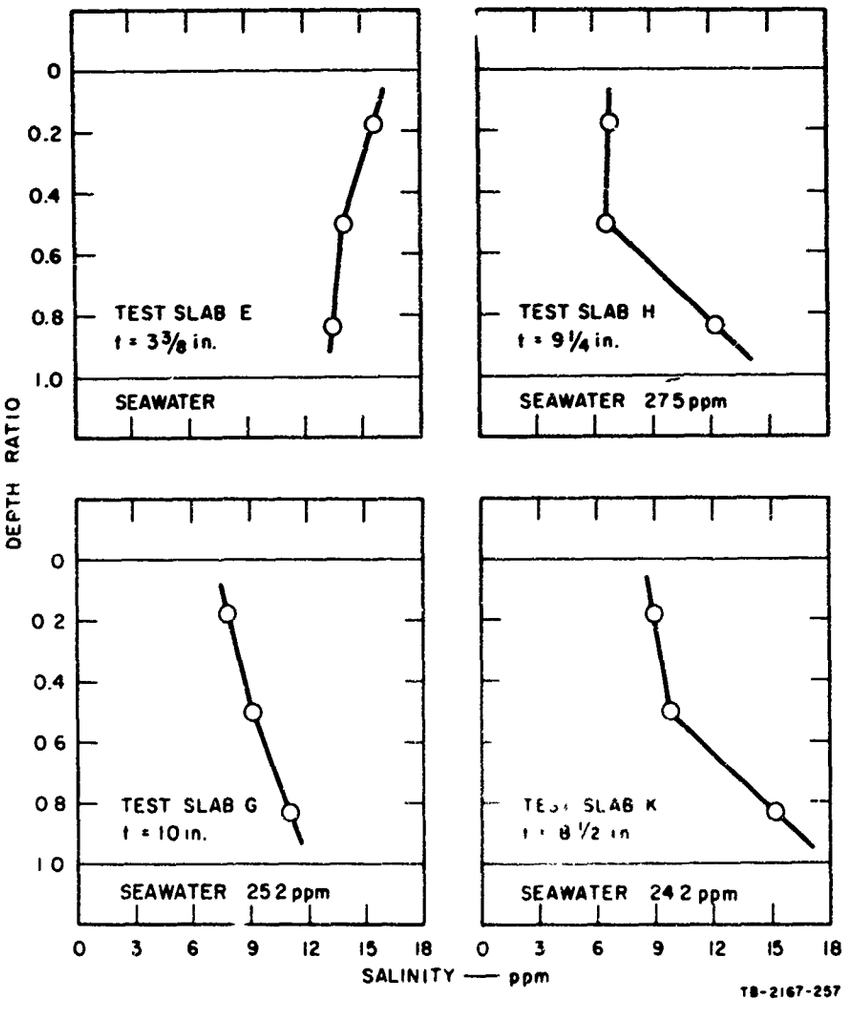

FIG. 15 TYPICAL SALINITY PROFILES: LABORATORY SEA ICE

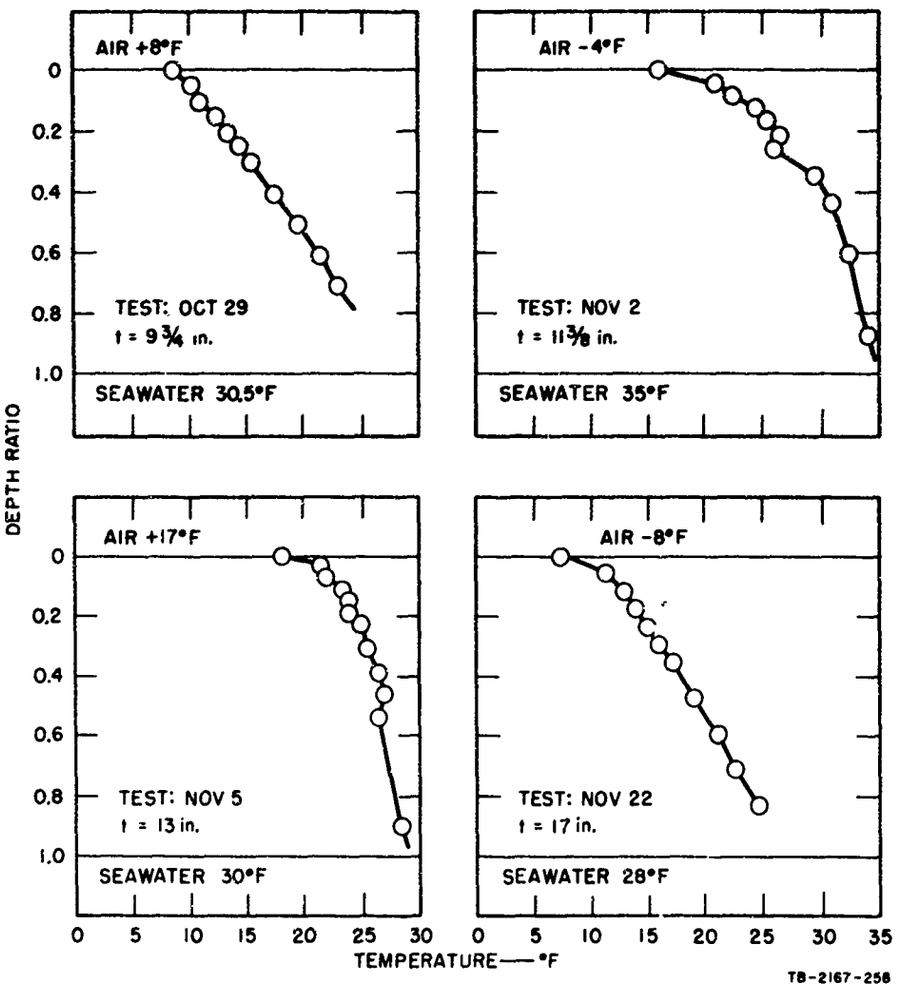

FIG. 16 TYPICAL TEMPERATURE PROFILES: ARCTIC SEA ICE

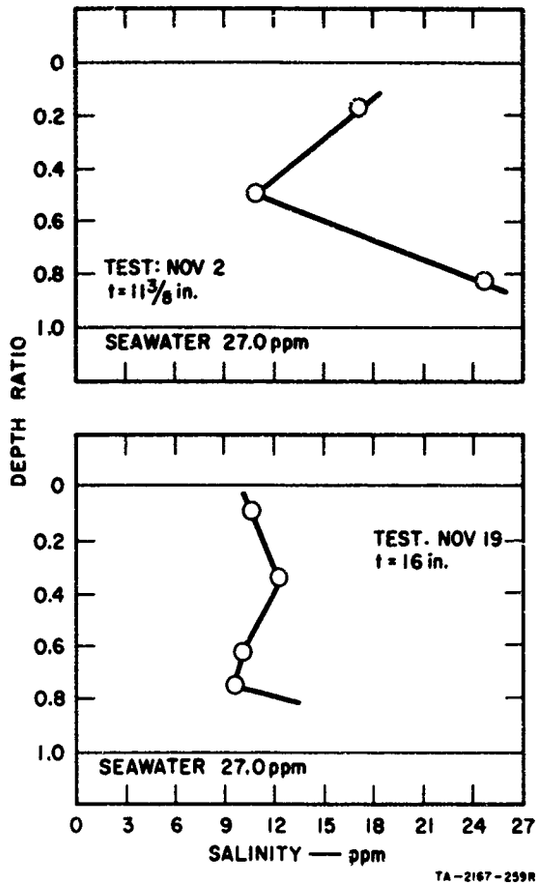

FIG. 17 TYPICAL SALINITY PROFILES: ARCTIC SEA ICE

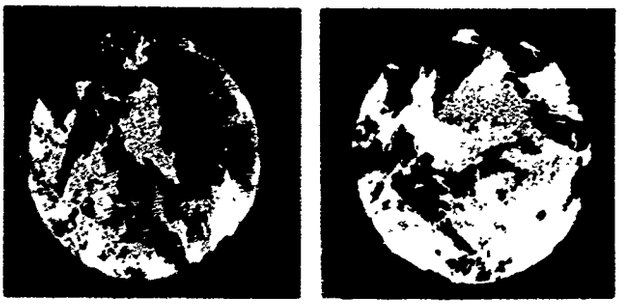

DEPTH = 0.5 in. θ = 0°

DEPTH = 0.5 in. θ = 60°

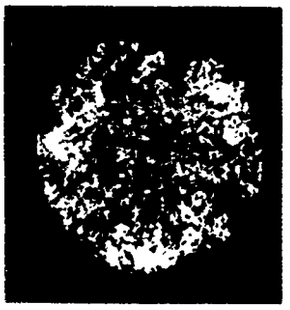

DEPTH = 5.5 in.

DEPTH = 10 in.

DEPTH = 13.5 in.

TC-2167-230

FIG. 18 THIN DIAMETRAL CROSS SECTIONS OF A VERTICAL SEA ICE CORE PHOTOGRAPHED IN POLARIZED LIGHT

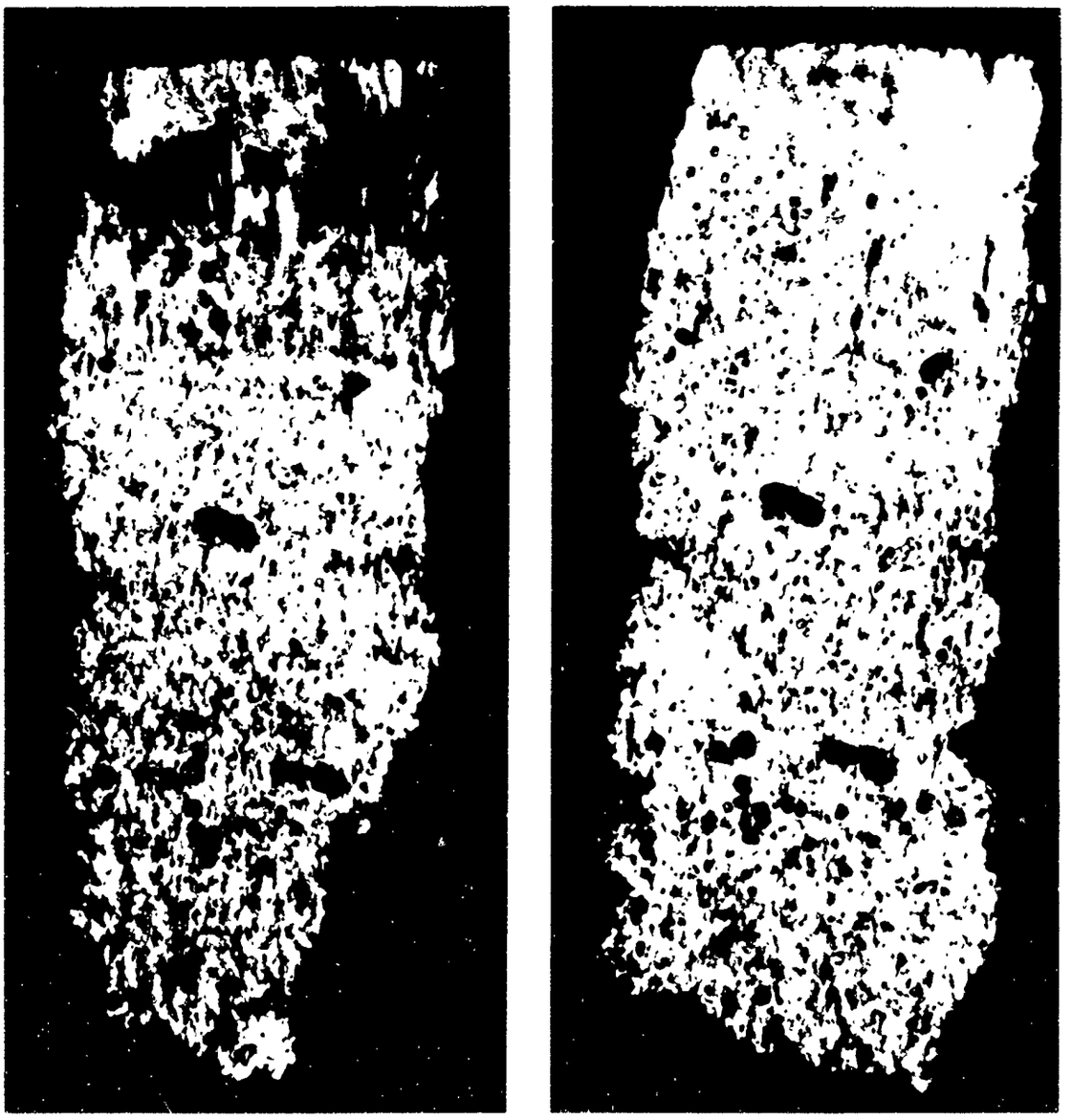

$\theta = 0°$ $\theta = 60°$

TA-2167-231

FIG 19 THIN LONGITUDINAL CROSS SECTIONS OF A VERTICAL SEA ICE CORE PHOTOGRAPHED IN POLARIZED LIGHT

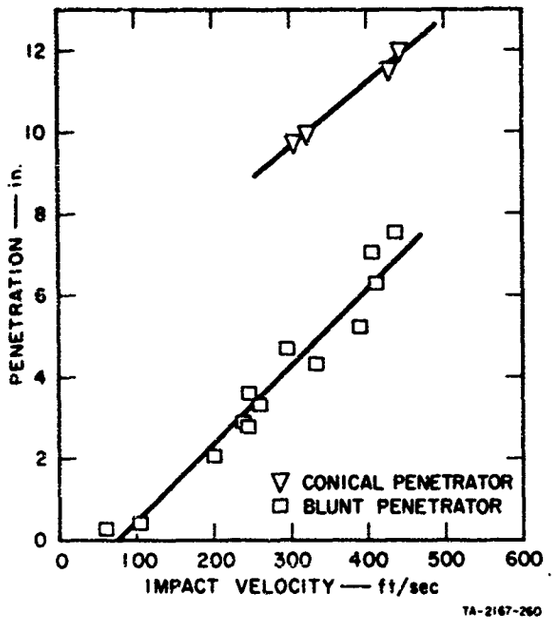

FIG. 20 PLOT OF PENETRATION DEPTH vs IMPACT VELOCITY FOR TESTS ON LABORATORY SEA ICE: 1-1/4-in. DIAMETER PROJECTILE

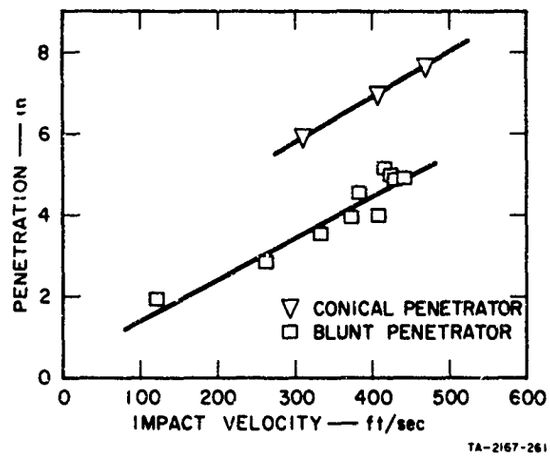

FIG. 21 PLOT OF PENETRATION DEPTH vs IMPACT VELOCITY FOR TESTS ON ARCTIC SEA ICE: 1-1/4-in. DIAMETER PROJECTILE

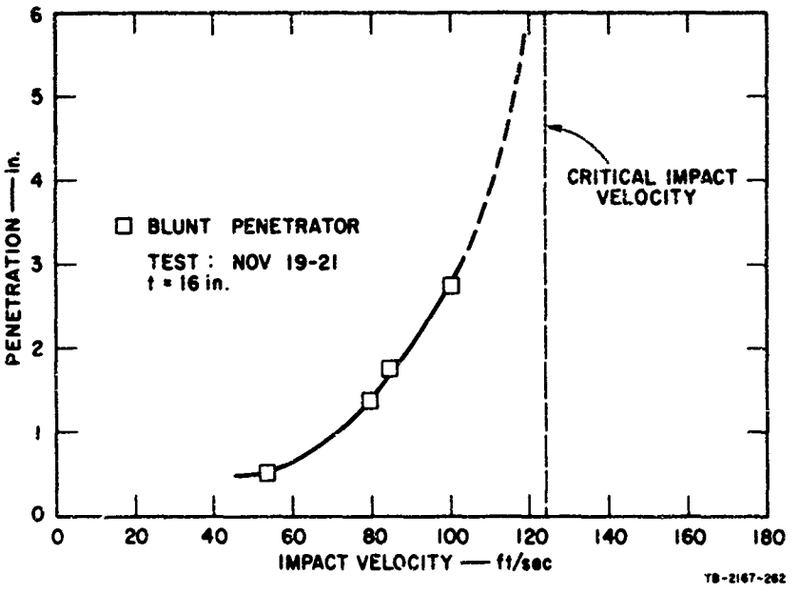

FIG. 22 PLOT OF PENETRATION DEPTH vs IMPACT VELOCITY FOR TEST SEQUENCE ON ARCTIC SEA ICE: 6-in. DIAMETER PROJECTILE

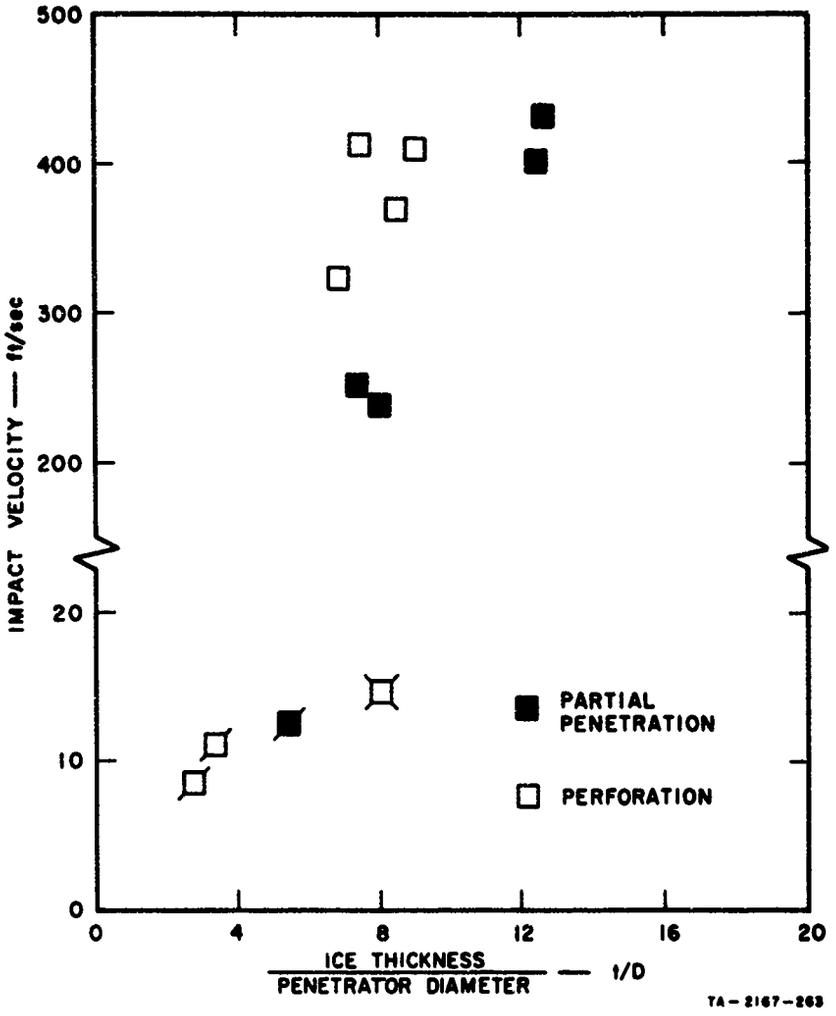

FIG. 23 PLOT OF IMPACT VELOCITY vs THICKNESS-DIAMETER RATIO FOR LABORATORY SEA ICE: BLUNT PENETRATOR

- D = 1-1/4 in., m_1 = 0.75 lb
- D = 1-1/4 in., m_1 = 9.688 lb
- D = 5/8 in., m_1 = 9.125 lb

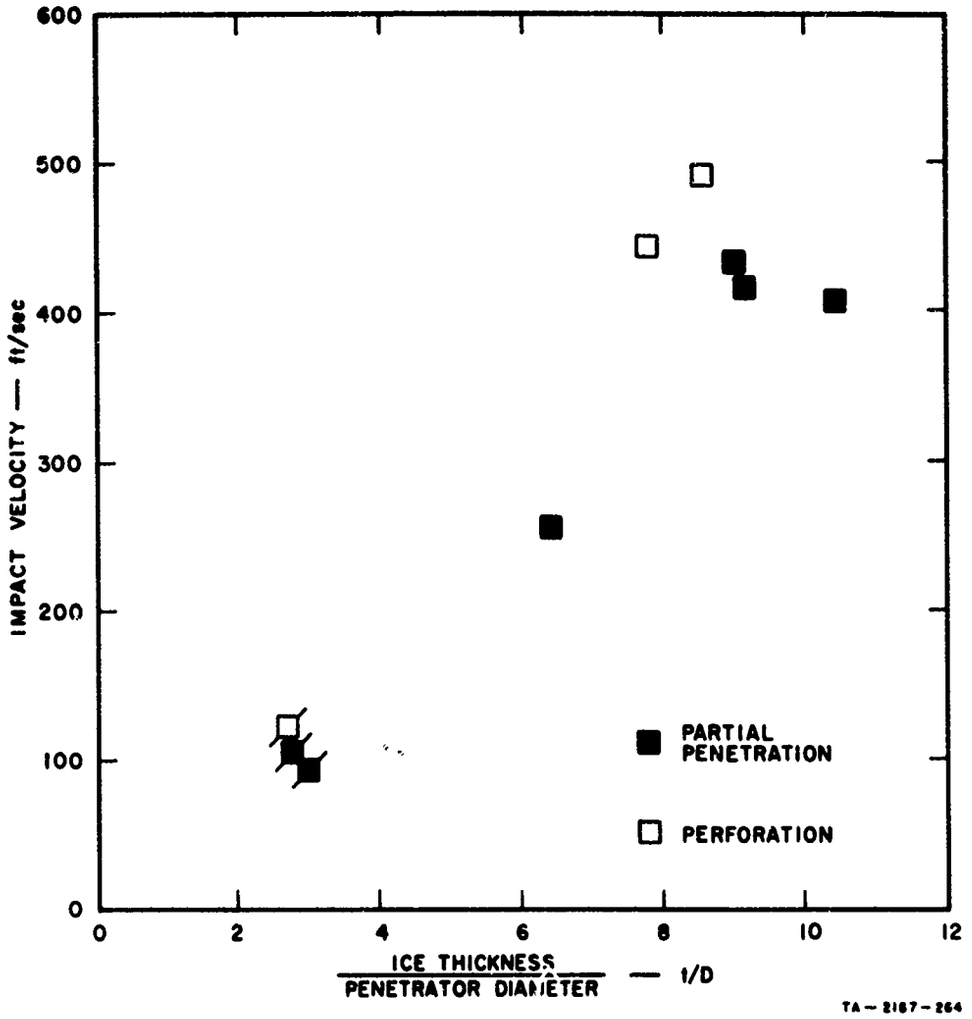

FIG. 24 PLOT OF IMPACT VELOCITY vs THICKNESS-DIAMETER RATIO FOR ARCTIC SEA ICE: BLUNT PENETRATOR

- D = 1-1/4 in., m_1 = 0.75 lb
- D = 6 in., m_1 = 41.5 lb

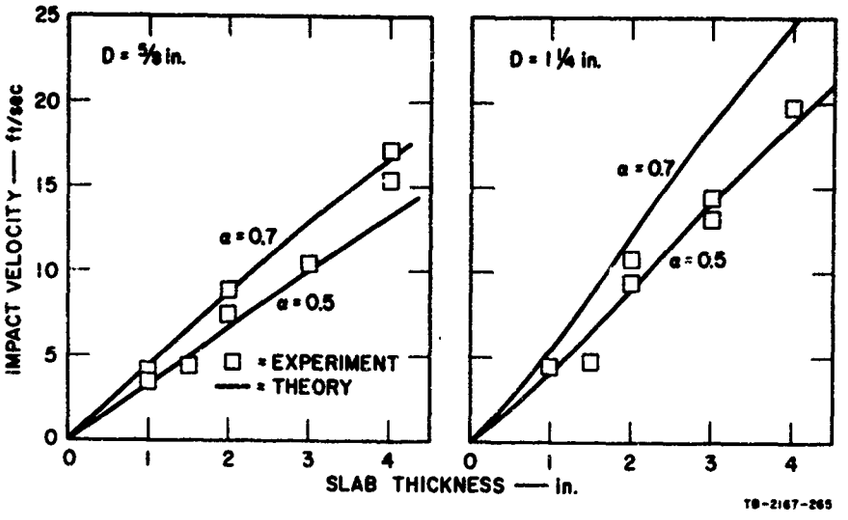

FIG. 25 PLOTS OF CRITICAL IMPACT VELOCITY vs THICKNESS FOR TESTS ON STYROFOAM: BLUNT PENETRATOR

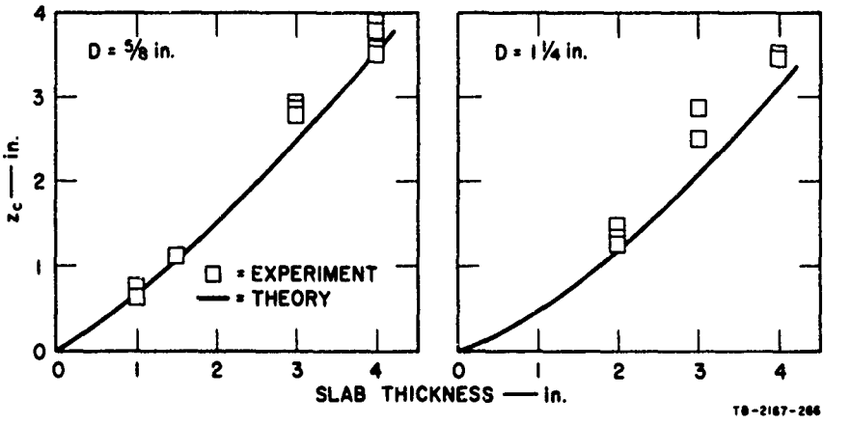

FIG. 26 PLOTS OF SHEAR PENETRATION DEPTH, z_c, vs THICKNESS FOR TESTS ON STYROFOAM: BLUNT PENETRATOR

FIG. 27 PHOTO SHOWING CYLINDRICAL-CONICAL SHEAR PLUGS OBTAINED IN PERFORATION OF STYROFOAM SLABS BY A BLUNT PENETRATOR; $1.5 < t/D < 3$: (a) $t/D = 1.6$, $D = 1\text{-}1/4$ in.; (b) $t/D = 1.6$, $D = 1\text{-}1/4$ in.; (c) $t/D = 2.4$, $D = 5/8$ in.

FIG. 28 PHOTO SHOWING CONICAL-OGIVAL PLUGS OBTAINED IN PERFORATION OF STYROFOAM SLABS BY A BLUNT PENETRATOR; $t/D > 3$: (a) $t/D = 8$, $D = 1\text{-}1\ 4$ in.; (b) $t/D = 8$, $D = 1\text{-}1/4$ in.; (c) $t/D = 3.2$, $D = 1\text{-}1/4$ in.

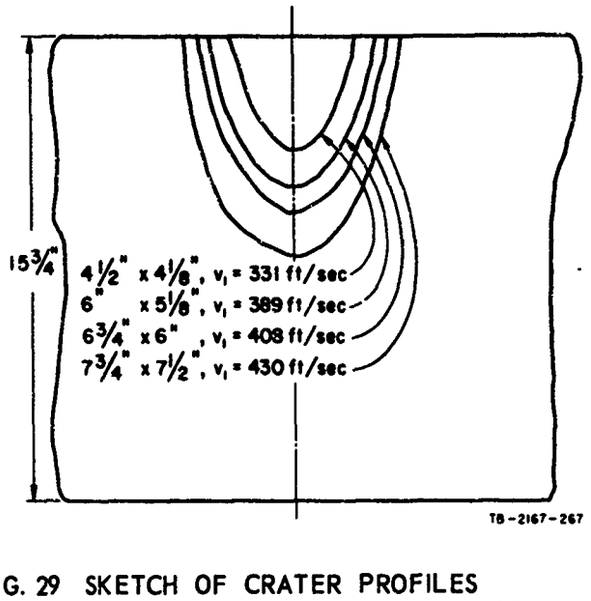

FIG. 29 SKETCH OF CRATER PROFILES PRODUCED IN TESTS ON LABORATORY SEA ICE AT DIFFERENT IMPACT VELOCITIES: 1-1/4-in. DIAMETER BLUNT PENETRATOR

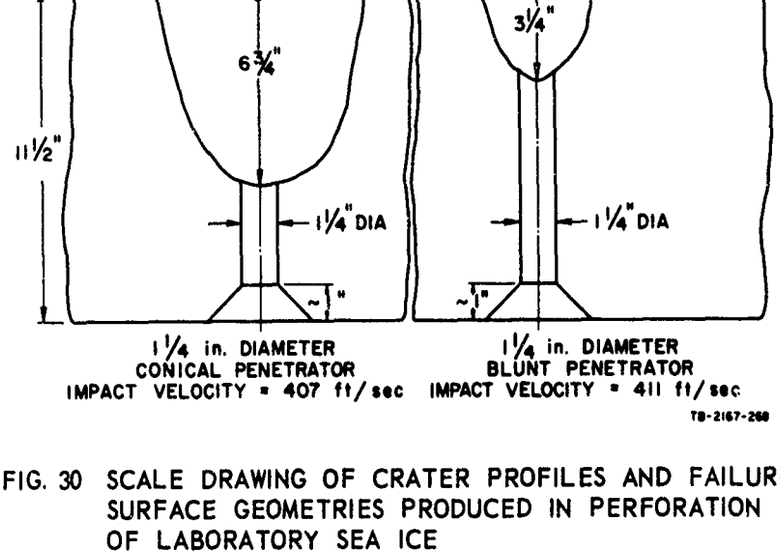

FIG. 30 SCALE DRAWING OF CRATER PROFILES AND FAILURE SURFACE GEOMETRIES PRODUCED IN PERFORATION OF LABORATORY SEA ICE

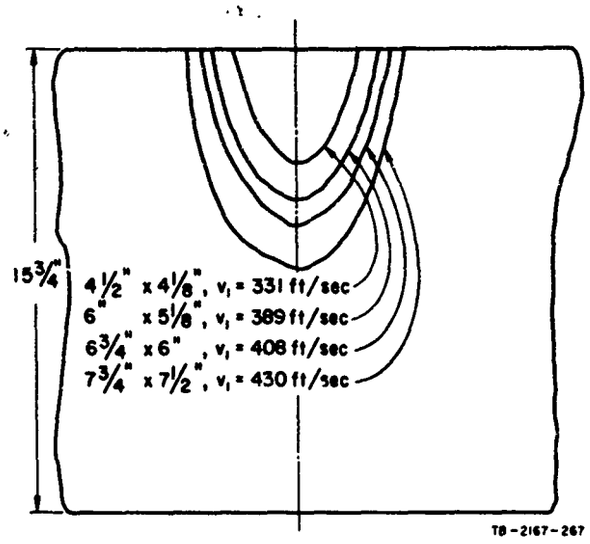

FIG. 29 SKETCH OF CRATER PROFILES PRODUCED IN TESTS ON LABORATORY SEA ICE AT DIFFERENT IMPACT VELOCITIES: 1-1/4-in. DIAMETER BLUNT PENETRATOR

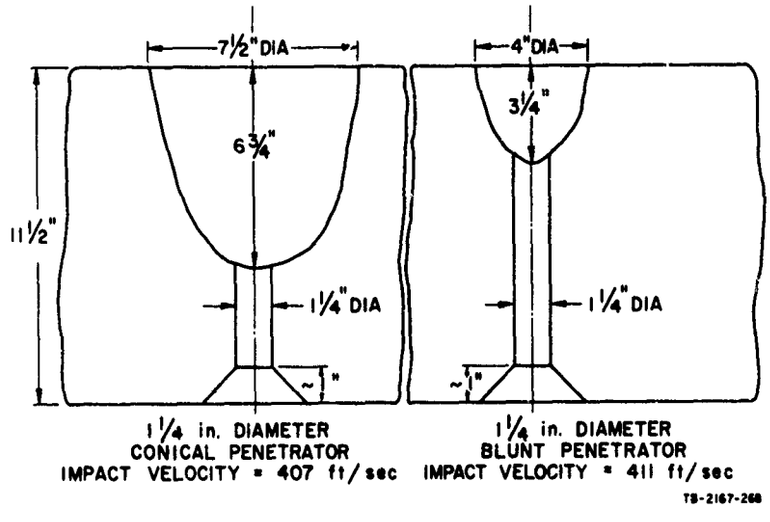

FIG. 30 SCALE DRAWING OF CRATER PROFILES AND FAILURE SURFACE GEOMETRIES PRODUCED IN PERFORATION OF LABORATORY SEA ICE

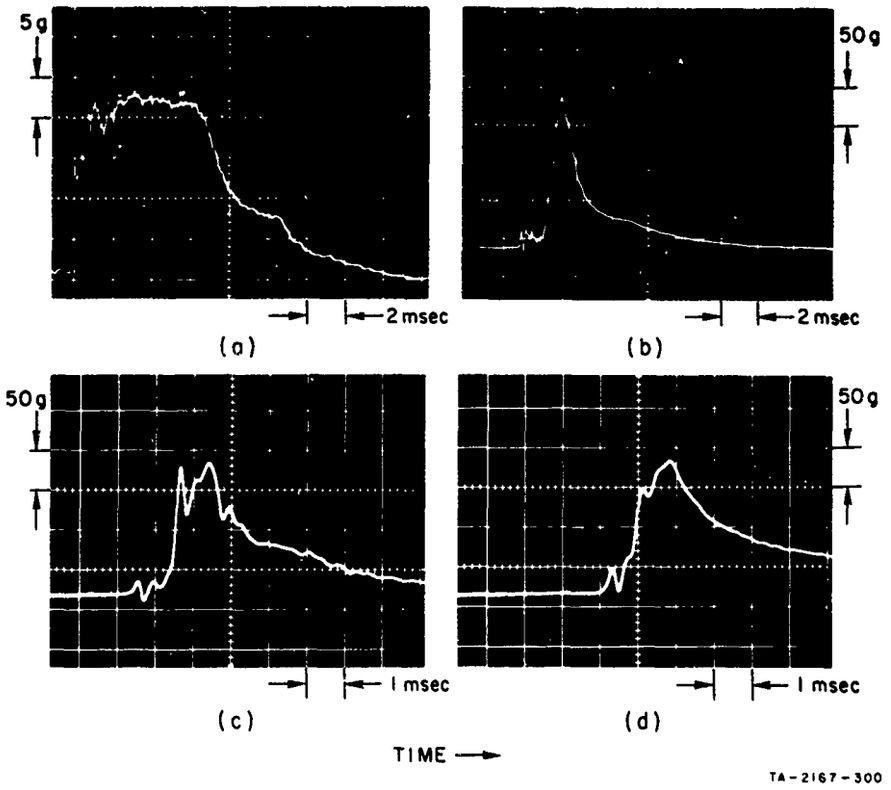

FIG. 31 OSCILLOGRAMS SHOWING DECELERATION vs. TIME RESPONSE OBTAINED IN LOW IMPACT VELOCITY TESTS; 1-1/4-in. DIAMETER BLUNT PENETRATOR

(a) Perforation of a 2-in. styrofoam slab
(b) Perforation of a 4-in. sea ice slab manufactured in a closed container[6]
(c) Perforation of a 3-3/8-in. laboratory sea ice slab
(d) Penetration of a 3-3/8-in. laboratory sea ice slab

EXPERIMENTAL OBSERVATIONS - LABORATORY TESTS

Low Impact Velocity Tests on Laboratory Sea Ice

Low impact velocity tests were carried out on sea ice test slabs that ranged in thickness from 2-3/4 in. through 6-3/4 in. (Tables 4 and 5). Slabs thinner than 2-3/4 in. could not be tested because the sea ice formed below this thickness (frazil ice) was too mushy to withstand impact loading. The upper thickness was the maximum that could be perforated successfully with the available kinetic energy of the freely falling projectile. Thus, for the 5/8-in. and 1-1/4-in. diameter penetrators employed, the range of slab thickness, penetrator diameter ratios (t/D) investigated was $2.20 \leq t/D \leq 10.8$.

The laboratory sea ice had both the characteristic greyish white appearance of Annual sea ice and its ductility. Typical ice temperatures and salinity contents were 16.7°F through 24.5°F (-8.4°C through -4.2°C) and 7.2 ppm through 17.1 ppm, respectively. The relatively high temperature of the sea ice was a consequence of both the ice manufacturing process and the thinness of the test slabs. For example, the temperature of the underlying seawater was +28°F (-1.5°C),* and the bulk of seawater was approximately 7 to 10 times larger than the sea ice test slab. Because the freezer temperature was -4°F (-20°C) and the sea ice temperature gradient was high only in the narrow region of the top surface, it was expected that the test slab average temperatures would be close to the seawater temperature. These observations were corroborated in the previous experiments[6] where 4-in. test slabs exhibited subzero temperatures when they were manufactured in a shallow closed container.

Typical temperature profiles measured in the present tests** and portrayed in Fig. 14 show that the greatest temperature drop across the

---

* The seawater temperature was higher in a few tests because of external heating.

** Sea ice temperatures were not recorded below 8-in. depth because of the limited number of thermocouples in the fixed array.

sea ice thickness occurred in a relatively shallow surface layer, after which a low gradient rise to the sea ice seawater equilibrium temperature took place. This phenomenon explained qualitatively the shape of the salinity profiles in Fig. 15 that were determined for the same test slab.*

The results of tests conducted with both conical and blunt end penetrators indicated that the visible effects of impact were confined to the immediate area of contact. When perforation did not occur, penetration was accompanied by plastic deformation in the adjacent ice. Because of the very local nature of impact effects, it was possible to perform many tests on each sea ice slab. Unfortunately, since the slabs were fixed in the drum, it was difficult to inspect the bottom surface of the sea ice after a test. Impact of the penetrator did not produce surface cracks or fissures, or fracture along cleavage planes. For every instance in which perforation occurred, a plug was sheared out of the sea ice. Measurements taken after ejection of the plug showed that the resulting hole in the ice slab was clean and circular at the top surface; however, at the bottom surface the hole was enlarged considerably although still circular in outline. This change in perforation area did not occur gradually through the slab thickness; instead, the hole was of nearly constant diameter from the upper surface to approximately 6/10 to 8/10 the slab thickness at which point the diameter of the hole increased uniformly to its final value on the slab's bottom surface. Thus, the material removed as a result of perforation occupied a volume of cylindrical-conical frustum shape. It was not possible to recover shear plugs from the sea ice

---

* During initial freezing, the surface ice is exposed to relatively cold air and the local freezing rate is much higher than in layers that accrete to the bottom surface as the ice cover increases in thickness. The rapid freezing rate causes an increased number of brine inclusions to be trapped in the growing sea ice crystals instead of being precipitated into the melt. Thus, sea ice can evidence a relatively high salinity content in its surface layers (for example, test slabs E and H). As the ice grows in thickness, the freezing rate tends to some equilibrium value that is a function of thermal budget considerations. Then, variations in salinity content with age become important. Specifically, brine drainage due to gravity, and brine migration along the temperature gradient in the direction of higher temperature result in an accumulation of brine cells in the lower ice layers (for example, test slabs G, H, and K). In sum, physical considerations show that a young sea ice cover can exhibit increased salinity in its top and bottom layers.

slabs because they were pulverized with the remnants melting in the seawater or disappearing beneath the ice.

However, in the tests on styrofoam, the shear plugs were recovered intact and for comparable slab thickness-penetrator diameter ratios these plugs were also cylindrical-conical in shape (Fig. 27) indicating that hole and plug outlines (Fig. 34) were nearly alike. This mechanism of perforation was identified as cylindrical-conical shear plug perforation.

The threshold value of impact velocity or velocity at incipient perforation (critical value) was determined within close limits by adjusting the free-fall height of the projectile until complete penetration occurred. To define threshold perforation, passage of the projectile through the test slab was classified into three categories. These categories are shown schematically in Fig. 32 and referenced in the tables of experimental data (Appendix D). Generally, the threshold value of impact velocity recorded corresponded to the condition denoted hilt penetration (H).

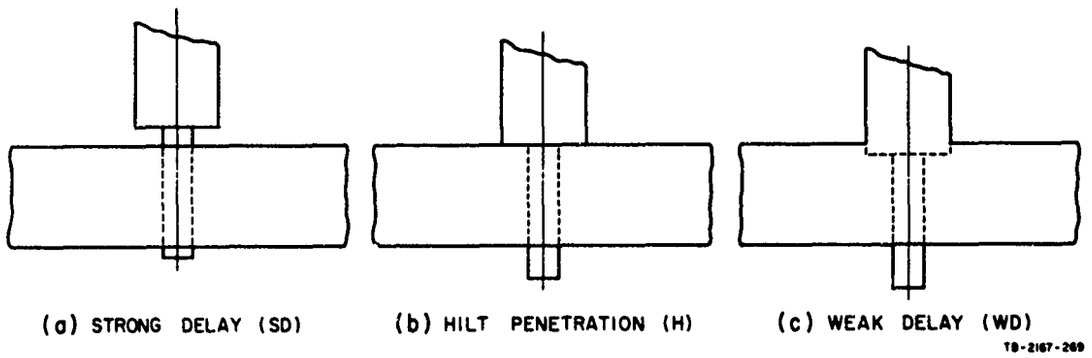

FIG. 32 CLASSIFICATION OF THRESHOLD VALUES AT INCIPIENT PERFORATION

The test results obtained from the initial penetration study[6] established the superiority of the blunt end penetrator over the conical penetrator; in particular, for identical test conditions at incipient perforation, impact of the conical penetrator produced limited penetration while the blunt penetrator perforated the sea ice slab. These same results were observed in the present low impact velocity experiments with sea ice test specimens having lower salinity contents. Thus, only a few tests were conducted with the conical penetrator.

Finally, in none of the low impact velocity tests was cratering on the top surface nor spalling on the bottom surface observed. In addition, the relative scale of projectile, test slab, and tank dimensions was such that impact loads produced negligible motion of the test slab either in vertical translation or bending.

High Impact Velocity Tests on Laboratory Sea Ice

High impact velocity tests were carried out on sea ice test slabs that ranged in thickness from 8-1/2 in. through 15-3/4 in. (Tables 4 and 5). These thicknesses represented minimum and maximum limits with respect to effective performance of the rifle-powered projectile. Only the 1-1/4-in. diameter projectile was employed in these tests; thus, the range of slab thickness, penetrator diameter ratios (t/D) investigated was $6.80 \leq t/D \leq 12.62$.

The quality of the test specimen sea ice was comparable to that reported for the low impact velocity tests. Characteristic ice temperatures and salinity contents were 7.0°F through 19.0°F (-13.9°C through -7.2°C) and 7.2 ppm through 17.1 ppm, respectively. The relatively lower sea ice temperatures in comparison to values of the low impact velocity test series was a consequence of the larger test slab thicknesses.

Because of their longer formation times, the thicker sea ice slabs employed in high impact velocity tests did not evidence the relatively large temperature gradient characteristic of the surface layer (e.g., test slab N, Fig. 14). Also, these slabs did not show an appreciable increase in salinity even though they occupied a much greater volume in the sea ice seawater confined system.

The results of tests conducted with both conical and blunt end penetrators showed that the visible effects of impact covered a significantly larger surface area of the test slab than that associated with the low impact velocity tests. The penetrators caused cratering in the slab material in all tests, whether penetration or perforation occurred. In the formation of these craters, the conical penetrator disrupted a much larger volume of sea ice than the blunt penetrator. These results were expected because, for the two profile shapes, the compressive shock wave

generated by the conical penetrator on impact has the significantly greater divergence. However, the impact forces produced by both penetrators did not create extended radial surface cracks or fissures, or fracture along cleavage planes. Also, the crater debris was not ejected to any measurable degree. This material consisted of finely pulverized ice and coarse snow. The growth of crater volume with impact velocity is shown in Fig. 29. An analysis of cratering phenomena was beyond the scope of this investigation.

After the cratering process, the mechanism of perforation was identical to that observed in the low impact velocity tests on sea ice and styrofoam. That is, the material expelled from the test slab occupied a cylindrical-conical frustum volume and was probably a cylindrical-conical shear plug. The overall perforation process at high velocity impact consisted of three distinct stages: cratering, boring due to cylindrical shear, and tear-out due to tensile rupture (Fig. 30). Similar results were reported by Livingston[18] for the penetration of frozen ground by free-falling bombs. This author indicated that cratering alone occurred below a well-defined characteristic impact velocity and that cratering and tunneling (Livingston's terminology) were observed at higher velocities. This same behavior was observed in the tests on thick sea ice slabs at velocities below the value for incipient perforation.

Crater volumes became larger with increased impact velocity. More importantly, at a particular impact velocity, even though the conical penetrator yielded a significantly greater depth of penetration, this did not result in an advantage over the blunt penetrator in perforating the slab. In effect, the conical penetrator attempted to crater its way through the slab whereas the blunt penetrator produced a combination of cratering and tunneling in perforation. The limited comparative data obtained in experiments with these two penetrators indicated that the blunt penetrator was slightly more effective than the conical penetrator in perforation of the sea ice at high impact velocity.

Due to the extended damage produced by cratering effects, it was not possible to conduct more than four tests per slab. Thus, it was beyond the scope of these experiments to establish the critical impact

velocity with precision. At best, the series of four shots was designed so that, for incremental increases in powder charge and resulting impact velocities, three shots would produce increasing depths of penetration and the fourth shot would achieve perforation.* It is estimated conservatively that in obtaining the critical impact velocity this procedure was accurate to within 10-20%.

Finally, in none of the high impact velocity tests was spalling apparent. Again, the relative scale of projectile, test slab, and tank were such that, upon impact, no significant motion of the slab took place.

Tests on Styrofoam

Low impact velocity tests were conducted on type FR styrofoam slabs of 1-in., 1-1/2-in., 2-in., 3-in., and 4-in., thickness, and high impact velocity tests were conducted on a type BB styrofoam slab, 10-in. thick (Table D3). All of the slabs were 22 in. in diameter and were "freely" supported around their outer circumference.

The 1-in. slab fractured into pie-shaped segments when subjected to central impact forces produced by both the 5/8-in. and 1-1/4-in. diameter blunt penetrators. The segments were outlined by nearly straight radial cleavage cracks emanating from the point of impact. Between adjacent segments, the fracture surfaces were perpendicular to both top and bottom surfaces of the test slab. Failure of this type occurred at well defined impact velocities (i.e., critical values); at lower impact velocities, only slight shear penetration was noted. Radial cleavage cracks and resulting slab fracture were also observed in tests on the 1-1/2-in. slab with the 1-1/4-in. blunt penetrator. A small number of tests with conical penetrators indicated that cleavage fracture occurred at corresponding or slightly smaller values of impact velocity than those obtained

* In contrast with the low impact velocity tests, relative degrees of perforation (strong delay, hilt, etc.) could not be established in these tests.

with the blunt penetrator. In general, the cleavage mode of failure* was restricted to slab thickness, penetrator diameter, t/D, ratios less than 2. In this range, the slabs could be considered as thin plates and, for the loading rates characteristic of this problem, material behavior assumed to be in the elastic range.

Problems concerning the elastic response of thin plates subject to impact loads have been treated in Refs. 19 and 20; however, a more recent investigation has been carried out by Dr. A. Florence of Stanford Research Institute.[21] Briefly, these analyses show that radial cleavage cracks can develop in impact-loaded thin plates as a result of tensile hoop stresses caused by circumferential bending moments. From a knowledge of allowable stresses and the dynamic response of the plates due to impact, critical velocity and crack geometry can be determined.

Test results obtained with the 5/8-in. and 1-1/4-in. blunt penetrators on styrofoam slabs having thicknesses of 1-1/2 in., 2 in., and 3 in. ($1.5 \leq t/D \leq 3.5$) were markedly different than those for lesser t/D ratios. Instead of slab fracture due to bending stresses, localized perforation occurred and the mechanism of failure was due to the formation of a cylindrical-conical shear plug. The plug configuration and failure surface characteristic of this process are shown in Figs. 27 and 34, respectively. Closer inspection revealed that the bottom surface of the plugs often contained fissures caused by bending stresses. These effects can be seen in Fig. 3. In addition, cylindrical surfaces over which shear failure was realized showed scratches and striations and the dull or fibrous appearance typical of shear fractures in which large plastic deformations have taken place. However, the slant surfaces of the conical frustum showed the granular or crystalline bright appearance common to cleavage fractures (tensile rupture) that occur along tensile stress axes at small plastic strains.[22]

---

* A schematic representation of a typical cleavage fracture geometry and a classification of these results on a chart with abcissa representing slab thickness-penetrator diameter ratio, t/D, are shown in Fig. 33.

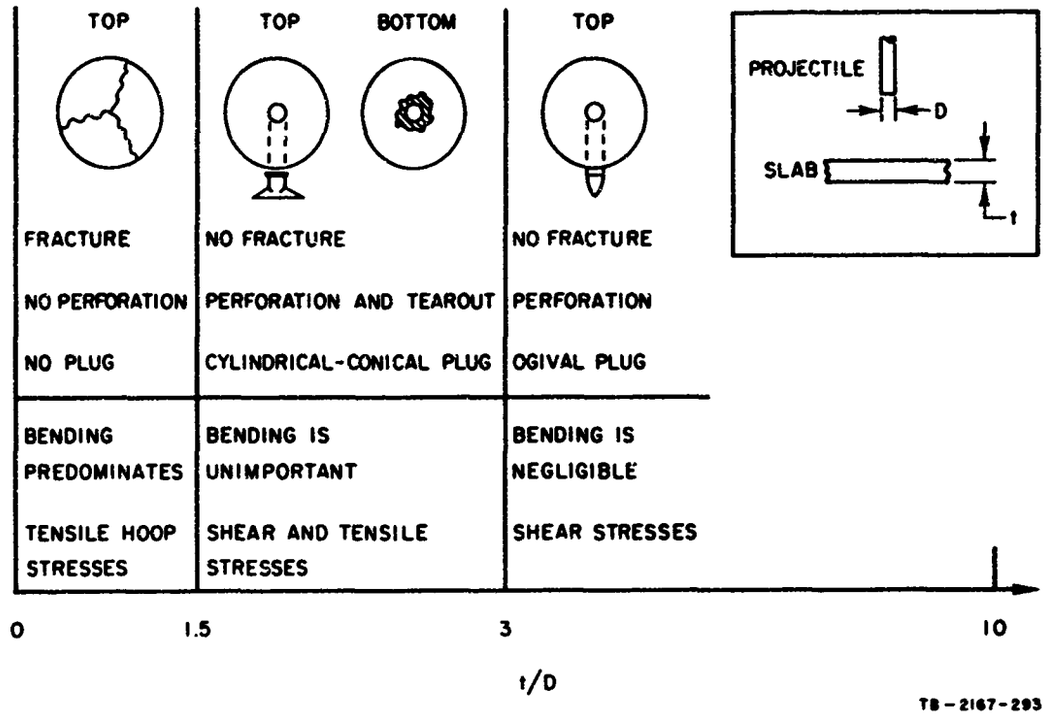

FIG. 33 CLASSIFICATION OF FRACTURE AND PERFORATION BEHAVIOR OBSERVED IN IMPACT TESTS ON STYROFOAM SLABS

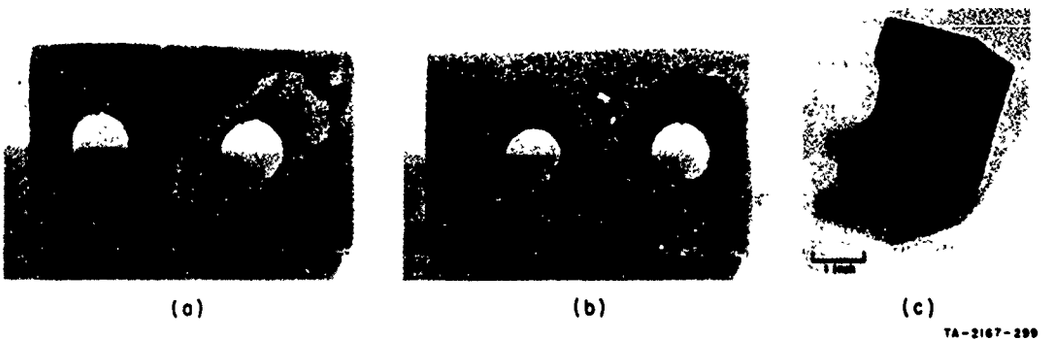

FIG. 34 PHOTO SHOWING OUTLINE OF CYLINDRICAL-CONICAL SHEAR PLUG HOLE OBTAINED IN PERFORATION OF A 2-in. STYROFOAM SLAB BY A 1-1/4-in. DIAMETER, BLUNT END PENETRATOR: (a) Top view, (b) Bottom view, (c) Cross-section view

Impact tests carried out over a similar range of t/D ratios with conical penetrators demonstrated quantitatively that, when compared to blunt penetrators and under similar conditions, these penetrators required greater impact energies to effect perforation in test slabs of equal thickness. Although this result was expected for the porous styrofoam material and was shown to be true for higher salinity sea ice,[6] it is interesting to note that identical behavior was reported in Ref. 23 for the perforation of steel plates by steel rods. The authors reported that, for the perforation of 1-in. plates by 1/2-in. blunt and conical rods, 11% greater impact energy was required by the conical rods. In the present conical penetrator impact tests, cylindrical-conical shear plugs were not obtained; instead, failure resulted from slab breakup or tunneling.

The experimental results observed with the 5/8-in. and 1-1/4-in. blunt penetrators on test slabs of 3-in., 4-in., and 10-in. thickness were also quite different from those characteristic of smaller t/D ratios. In this case, t/D values were greater than 3, and the type of plug produced in the perforation process was intermediate in shape to conical-ogival extremes. For example, plugs (a) and (b) (Fig. 28)* were obtained from the high impact velocity (160 ft/sec) tests on the 10-in. slab. These plugs were permanently deformed to approximately 2/10 of their original length. Some of the plugs had curled-up tips (e.g., plug (b)); this feature resulted probably from the hydrodynamic forces exerted on the plug during high speed expulsion from the slab's bottom surface. The compressed plugs comprized material that was essentially in a "locked" condition, and they were impervious to thumbnail or similar indentation.

---

* For tests on sea ice in a range of t/D values between 3 and 13, well-outlined cylindrical-conical hole geometries were obtained during perforation. Thus, it is unlikely that conical-ogival plugs were produced and, in this case, the behavior of sea ice did not correspond to that of styrofoam over the same range of t/D values. However, this does not preclude the possibility that conical-ogival plugs could be obtained in sea ice at t/D ratios greater than those explored in the present experiments.

Plug (c) resulted from low impact velocity tests (20 ft/sec) on a 4-in. styrofoam FR slab. This plug shows some evidence of conical frustum tear-out and bottom surface fissures.

Although it appears that both this type of perforation and the plugs obtained were far removed from the process which produced cylindrical-conical shear plugs, further examination revealed that such was not the case. For example, cross-section views of plugs (a) and (b) in Fig. 3 indicate clearly that nearly ogival volumes of material have undergone permanent deformation during perforation of a 2-in. slab. In contrast, plug (c) obtained in the perforation of a 4-in. slab experienced permanent deformation throughout its volume. Based on this evidence, it appears that a transitional phase can exist over a limited range of slab-penetrator t/D ratios in which different zones of plastic deformation are produced within the shear plugs. When the thickness-diameter ratio is greater than 3, the shape of this interior yield surface corresponds to the plug obtained and resembles closely the theoretical slip line field for static, punch indentation problems[24] (Fig. 35).

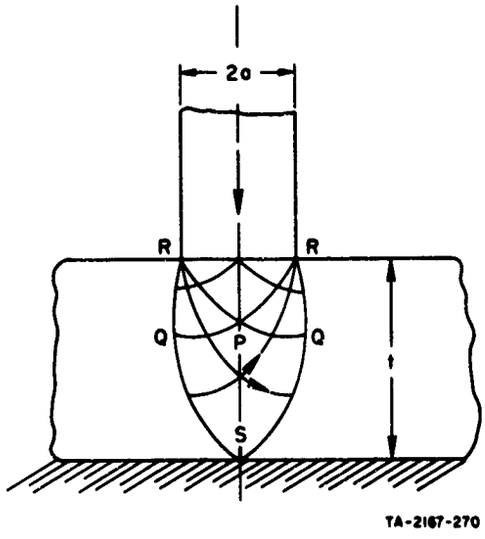

FIG. 35 SLIP LINE FIELD AT YIELD POINT FOR INDENTATION OF A SLAB RESTING ON A PLANE FOUNDATION, FROM REF. 23

Finally, neither cratering nor spalling was observed in the high impact velocity tests performed on the 10-in. test slab. A limited number of tests with conical penetrators indicated, again, that a blunt penetrator was most efficient in the perforation of slabs having t/D ratios greater than 3.

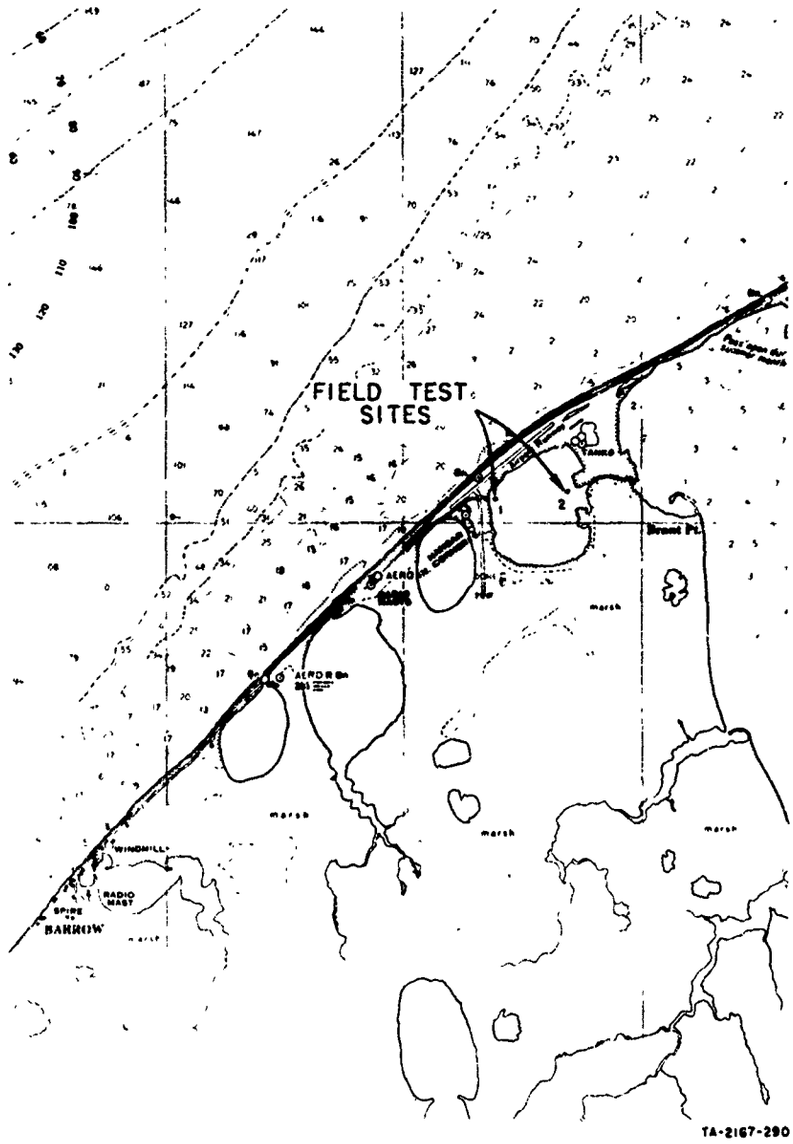

FIG. 36 MAP SHOWING LOCATION OF FIELD TEST SITES, POINT BARROW, ALASKA

EXPERIMENTAL OBSERVATIONS - FIELD TESTS

Tests on Arctic Sea Ice With 1-1/4-in. Diameter Projectiles

Field tests were conducted from October 27 through November 5, 1966, at the Arctic Research Laboratory, Point Barrow, Alaska (Tables 6 and 7, and Appendix D). The specific location of the sea ice tested is shown in Fig. 36, Location 1. This body of seawater is known locally as Float Plane Lake and is connected directly to the much larger Elsen lagoon. A string of outer islands separates this lagoon from the Beaufort Sea.

At the test site, the sea ice was exceptionally smooth and level on its top surface and had the typical greyish white appearance of young sea ice. Salinity of the underlying seawater was 27.0 ppm. A seawater sample from the Chukchi Sea indicated a salinity content of 34 ppm; thus, some fresh water runoff was present at the test site. Test specimen sea ice varied in thickness from 8 in. through 13 in. and had characteristic temperatures in the range 8.5°F through 26.0°F (-13.0°C through -3.3°C). The range of sea ice thickness, penetrator diameter ratios (t/D) explored was $6.4 \leq t/D \leq 10.4$. Depth of underlying seawater was generally 4 ft.

The first three test series (October 27, 28, and 29) were carried out on sea ice that had virtually no snow cover. The seawater and sea ice temperatures were approximately 30.5°F and 14.5°F (-0.8°C and -9.7°C), respectively. Between October 29 and November 2, some snowfall and high winds produced an 8-in. to 24-in. snow cover over the test site. Due to the insulation effects of this snow, the seawater and sea ice temperatures rose considerably so that the later tests series, November 2, 4, and 5, were characterized by seawater and sea ice temperatures that averaged 34.0°F and 26.0°F (1.1°C and -3.3°C), respectively. Average sea ice salinities* taken from full-core (SRI-Corer) samples were in

* Salinity was determined by titration for chlorides and use of a standard multiplicative factor to account for total salt content. Core samples were tested usually on the day that they were taken from the sea ice.

the range, 10.3 ppm through 14.0 ppm. A three-part sample through 9 in. of an 11-1/4-in. thick ice sheet indicated salinities of 17.2 ppm, 10.9 ppm, and 24.6 ppm for the top, middle, and bottom sections, respectively. Density of the sea ice was determined by the displacement technique (methanol) and a typical value was 0.905 g/cc.

Typical temperature and salinity profiles are plotted in Figs. 16 and 17, respectively. The temperature profiles obtained for the Arctic sea ice show a fairly linear increase through the thickness with depth, and the proportionately larger increase, noted previously for laboratory sea ice, in the top surface layer. Salinity profiles indicate the characteristic heavy concentration of salts in the upper and lower thirds of the sea ice sheet. The overall salinity contents of the Arctic sea ice were approximately 20% higher than those representative of the laboratory sea ice.

For the field tests, the rifle assembly and velocity measuring system described previously were bolted to a sled-mounted framework constructed from 2-in. O.D. pipe and commercial scaffold swivel clamps. The electronic instruments and control center were located in a heated 6 x 3-ft wanigan on sled runners. Power was supplied by a 1000-ft electrical extension cable from shore. The entire test facility could be moved readily to traverse the sea ice within the test site. A photo of the field test equipment is shown in Fig. 37.

Test procedure for the field tests was similar to the scheme employed in the laboratory experiments. That is, series of tests were conducted at increasing impact velocites until perforation occurred. All except one series were conducted with impact occurring at normal incidence. For series D1 (Table 6) three tests were conducted in which the 1-1/4-in. blunt penetrator impacted the ice sheet at inclined incidence. For this purpose, the entire test rig was raised up along one side so that the rifle bore centerline was inclined 17.3^{0} to the vertical. For comparison, this same series included two tests at normal incidence, one each with the conical and blunt penetrators. In all test series, crater geometries (Fig. 38) and critical impact velocities were recorded.

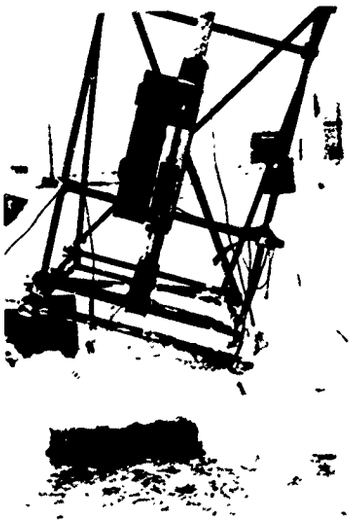

(a)

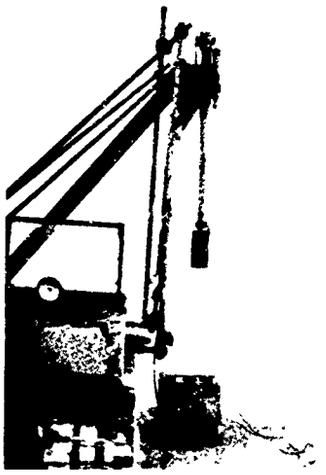

(b)

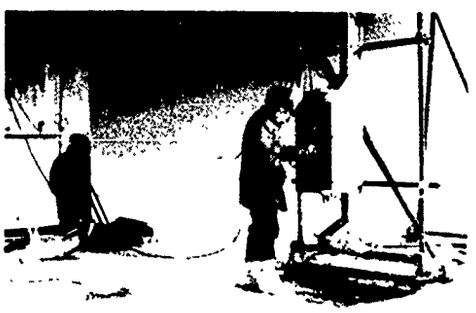

(c)

TA-2167-.91

FIG. 37 PHOTOS OF ARCTIC FIELD TEST EQUIPMENT
(a) Rifle assembly set-up for tests at inclined incidence
(b) Navy 1-pounder gun, 6-in. diameter projectile, and velocity measuring device
(c) Rifle assembly set-up for tests at normal incidence

The behavior of the Arctic sea ice under impact loading was similar to that observed in the testing of laboratory sea ice. For example,

- The surface areas affected by the penetrator were relatively small and localized
- Surface cracks and fissures did not occur
- Penetration and perforation were accompanied by cratering, and this effect was most pronounced for the conical penetrator
- The crater debris was not ejected, and consisted of finely pulverized ice
- Perforation resulted in the characteristic cylindrical-conical shear plug holes whose outlines were especially well-defined.

Tests on Arctic Sea Ice With 6-in. Diameter Projectile

These tests were carried out with a Navy 1-pounder gun from November 17 through November 22 (Table 6 and Appendix D). The first test series took place in the same location as the rifle-powered projectile tests; the remaining tests were performed in the northeast corner of Float Plane Lake (Fig. 36, Location 2) where the snow cover was relatively small and ice and seawater temperatures were not unduly high due to the insulating effects of the snow. Upon removal of the snow cover, the sea ice at the first test site was found to be quite mushy on its top surface and in a short period was covered by 3 to 4 in. of seawater. The sea ice at test site location 2 was smooth and hard on its top surface and typical of young sea ice.

Sea ice tested varied in thickness from 15-3/4 in. through 17 in., and had characteristic temperatures in the range, 7.5°F through 16.0°F (-13.6°C through -8.9°C). The range of sea ice thickness-penetrator diameter ratios (t/D) investigated was $12.6 \leq t/D \leq 13.6$. Average sea ice salinities taken from full-core samples were grouped between 9.4 ppm and 10.6 ppm. A four-part core sample through 15 in. of a 16-in. thick ice sheet indicated salinities of 10.6 ppm, 12.3 ppm, 10.1 ppm, and 9.63 ppm, from the top downwards. Salinity of the underlying seawater was 29.0 ppm. A collection of photomicrographs showing the internal structure of this sea ice as a function of depth is portrayed in Figs. 18 and 19.

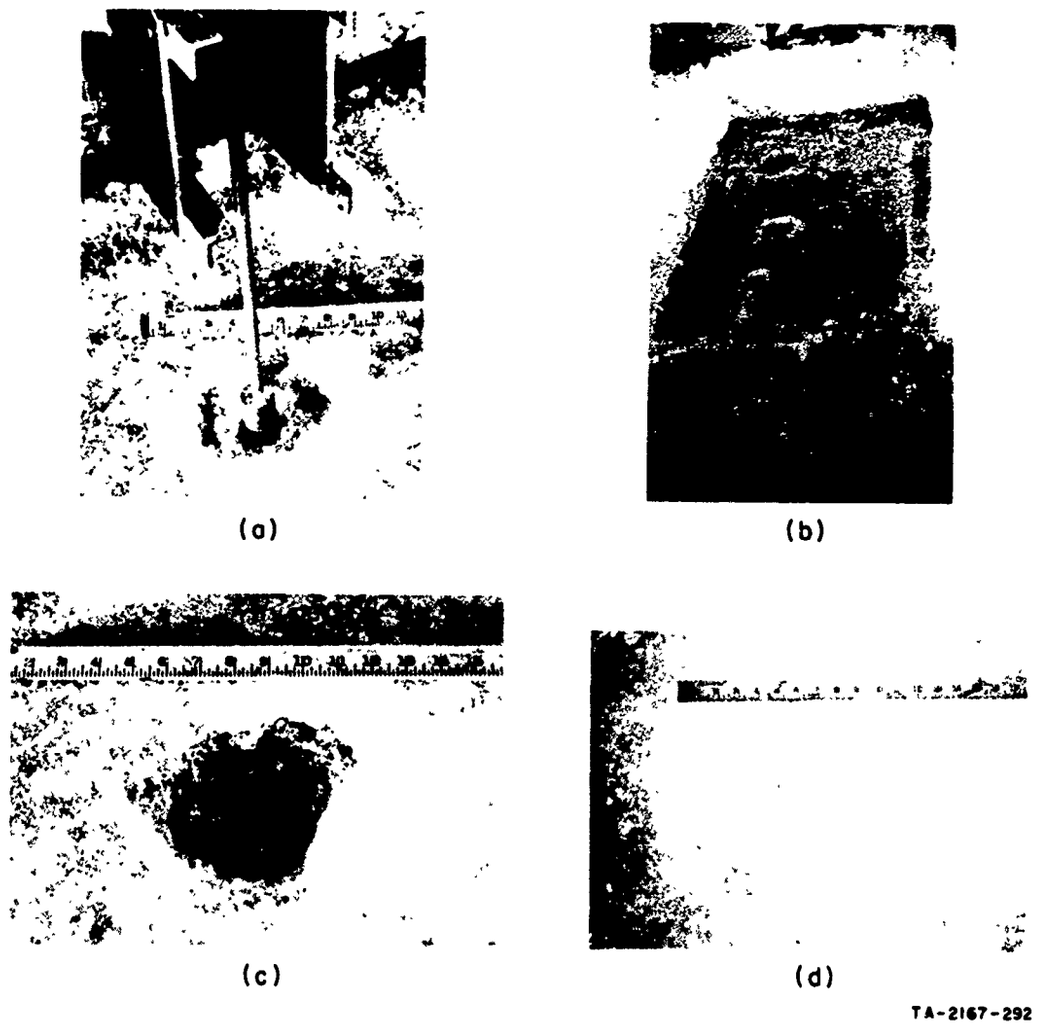

FIG. 38 PHOTOS SHOWING THE EFFECTS OF IMPACT ON ARCTIC SEA ICE
(a) Crater and debris obtained with 1-1/4-in. diameter blunt penetrator, v_1 = 417 ft/sec
(b) Craters produced by 1-1/4-in. diameter blunt and conical penetrators
(c) Close-up of crater in photo (a), debris removed
(d) Results of impact with 6-in. diameter blunt penetrator

Test equipment consisted of the Navy 1-pounder that was mounted on a tracked vehicle (Weasel) and positioned to fire vertically downwards (Fig. 37), velocity screens placed 1-ft apart, and ancillary electronic equipment. The gun was fired by a remotely controlled solenoid actuator, and electrical power for this device and the instruments was supplied by an Onan diesel, 3-kva generator. The projectile used is shown in Fig. 39.

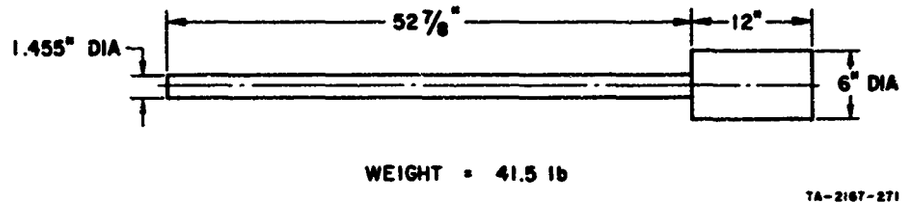

FIG. 39 SKETCH OF PROJECTILE FOR NAVY 1-POUNDER GUN

Test procedure for these experiments was similar to that of the rifle-powered projectile tests; however, experiments were performed only at normal incidence.

The first test series (November 17) was conducted on ice that was soaked thoroughly with seawater and of relatively high characteristic temperature (+32.0°F, 0°C). Under normal impact velocities, a relatively large amount of penetration and/or easy perforation was expected. However, because of the overlying seawater cover, the highly concentrated shear stresses produced upon impact (blunt end penetrator) were dissipated in hydrodynamic turbulence so that contact with the ice produced only small depths of penetration.

The remaining test series on better quality sea ice yielded results comparable in many respects to those obtained with 1-1/4-in. diameter projectiles on both laboratory sea ice and Arctic sea ice. Specifically,

- Surface areas affected by impact were small in comparison to the penetrator diameter
- Surface cracks and fissures did not occur

- Penetration and perforation were not accompanied by cratering
- Perforation resulted in the characteristic cylindrical-conical shear plug and, in this case, the plug outline was exceptionally well-defined.

The absence of cratering suggested strongly that this phenomenon is related to some ratio of impact energy to penetrator diameter. Insufficient data were acquired to verify this conclusion quantitatively. Figure 38(c) shows typical effects of impact and the craterless penetration obtained in these tests.

Because of the relatively large penetrator diameter employed, perforation yielded the first cylindrical-conical shear plug that was completely intact after impact. Unfortunately, because of the ice thickness (17 in.), it was not possible to enlarge the hole further and remove the plug for photographing.

THEORY

An analysis is formulated for the perforation of a porous medium (e.g., styrofoam and sea ice with numerous brine inclusions) by a blunt cylindrical penetrator impacting at normal incidence. It applies to the perforation mechanism that produces a cylindrical-conical shear plug, and it provides the critical impact velocity and energy at incipient perforation. This type of plug was produced in the perforation of styrofoam, laboratory sea ice, and Arctic sea ice with slab thickness, penetrator diameter ratios, t/D, ranging from 1 through 4 for styrofoam and 3 through 13 for sea ice.

The theory assumes that under the relatively short time intervals of impact loading, the material behaves elastically up to yielding and/or fracture.* Furthermore, the laws of conservation of momentum and mechanical energy are assumed to hold for sea ice. Neglected in the analysis are effects due to transient stresses, contact deformations and vibrations of the penetrator, stress wave effects, and spalling.** Also, no attempt is made to include effects of cratering in the theory. In agreement with experimental observations, it is assumed that the impact is plastic (no rebound) and that the test slab is large and remains motionless during shear plug ejection. Moreover, at incipient perforation, the motion of the conical frustum plug with respect to the underlying seawater is negligible; therefore, hydrodynamic drag forces are neglected. Finally, no distinction is made between static and dynamic values of tensile rupture stress and shear yield stress.

To represent a cylindrical-conical shear plug and the forces acting on it a simple mathematical model can be constructed (Fig. 40). The behavior of the slab material upon impact can be described, with reference to Figs. 40 and 41, as follows. Due to the high stress concentration

---

* Pounder[7] states that under these conditions sea ice behaves elastically.

** Spalling and related phenomena were not observed in any tests reported here.

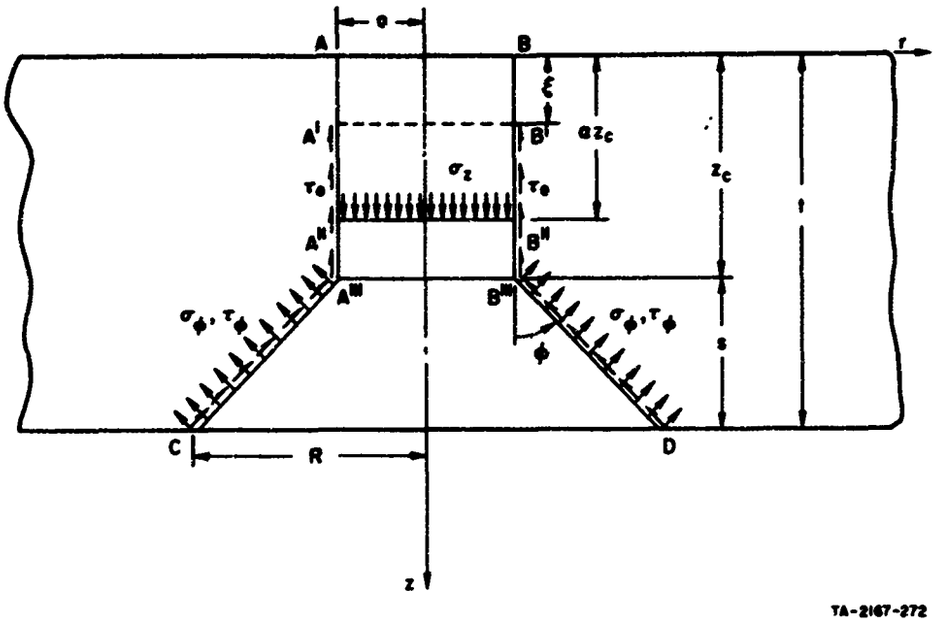

FIG. 40 SKETCH OF MATHEMATICAL MODEL FOR CYLINDRICAL-CONICAL SHEAR PLUG

around the perimeter, AB, of the blunt penetrator, local yielding due to shear stresses takes place. Initial penetration results in the well-defined cylindrical shear yield surface, AA'-BB', over which the shear flow stress, τ_0, acts during a vertical displacement, ξ. Further penetration compresses a cylindrical volume of material along the path, AA'"-BB'". During this process, the material absorbs a portion of the projectile's kinetic energy in overcoming surface tractions due to τ_0, and resisting forces due to compressive normal stresses or bearing stresses, σ_z. For an elastic material, the stress σ_z increases linearly with compression. Eventually, at incipient perforation, the normal force, $\sigma_z \pi a^2$, becomes large enough to tear a cylindrical-conical frustum of material, A"A'"CDB'" B", out of the slab. This occurs when the tensile rupture stress of the material, σ_φ, is attained on the slant surface, A'"C-B'" D. Moreover, once the conical frustum plug has been formed, a certain amount of elastic recovery takes place such that the collapsed

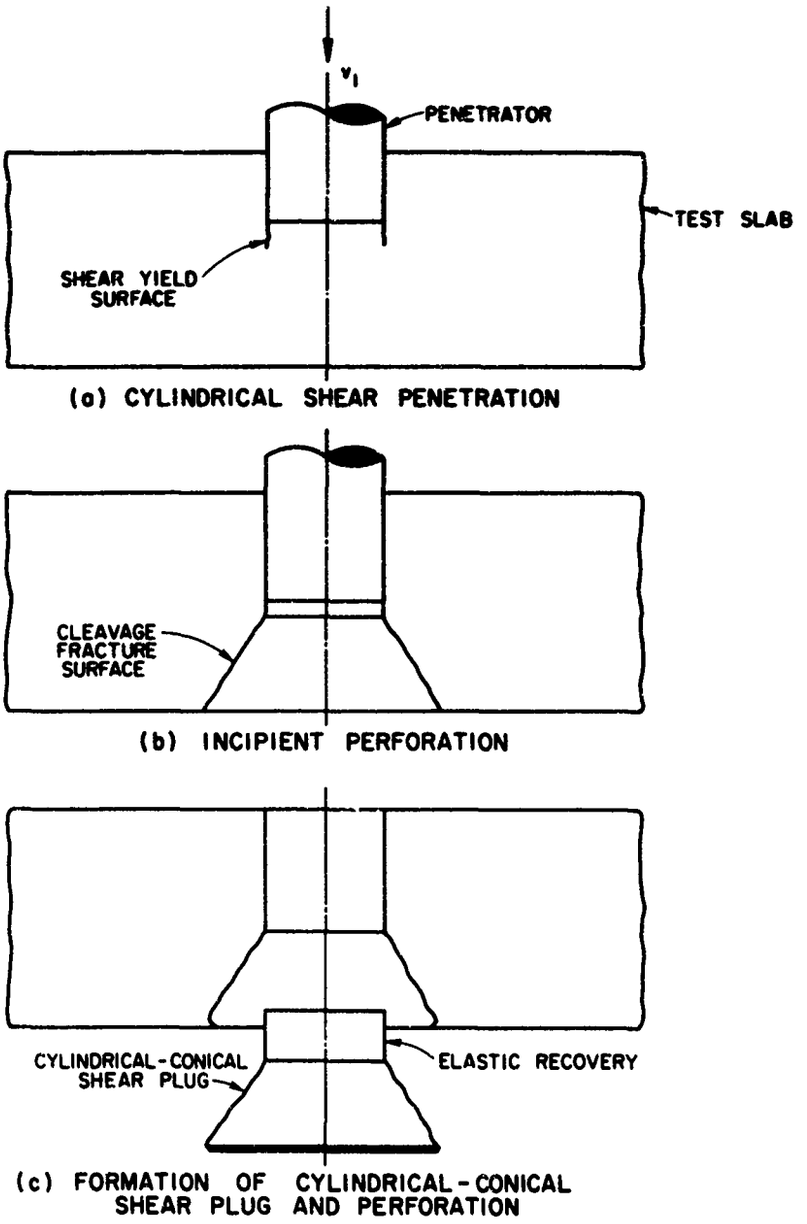

FIG. 41 SKETCH OF PERFORATION PROCESS THAT PRODUCES A CYLINDRICAL-CONICAL SHEAR PLUG

cylindrical portion of the plug expands back along the axis of the plug to some intermediate position.

An equation expressing conservation of mechanical energy is used to relate available kinetic energy at impact to the work done in deformation of the material during cylindrical shear penetration. For the condition of incipient perforation, the final velocity of the projectile is taken to be zero. Thus,*

$$1/2\ m_1 v_1^2 = \int_0^{z_c} \tau_{rz}\,[\xi,\dot{\xi}]\ 2\pi a\ \alpha\ (z_c-\xi)d\xi + \int_0^{\alpha z_c} \sigma_z[\xi,\dot{\xi}]\ \pi a^2 d\xi \qquad (1)$$

where τ_{rz} and σ_z, the shear yield stress and compressive bearing stress, respectively, are in general functions of displacement ξ, and velocity $\dot{\xi}$. Moreover, α is an axial compression ratio that relates the collapsed height of the shear plug to the total shear penetration depth, z_c (Fig. 40). In solving Eq. 1, the dynamic compressive stress, σ_z, is assumed to vary linearly with displacement, ξ, so that

$$\sigma_z = k\xi \qquad (2)$$

where k, the dynamic compression modulus, is a constant. Furthermore, $\tau_{rz}(\xi,\dot{\xi})$ is assumed constant during the shear penetration phase.** Thus,

$$\tau_{rz}(\xi,\dot{\xi}) = \tau_0 \qquad (3)$$

---

* The left-hand member of Eq. 1 is derived in greater detail in Appendix A, Eqs. A1 through A6.

** The assumptions underlying Eqs. 2 and 3 are not restrictive but have been introduced as reasonable estimates of the material behavior during compression due to penetration. Further study into the mechanics of this process was beyond the scope of this investigation. However, if warranted, a more general polynomial relationship between these stresses and displacement can be introduced into the kernels of Eq. 1.

where τ_0 is the shear yield stress in the vertical direction. After integration and rearrangement, Eqs. 1, 2, and 3 yield

$$z_c^2 = \frac{m_1 v_1^2}{\alpha\pi a\,(2\tau_0 + \alpha a k)} \tag{4}$$

At incipient perforation, the cylindrical-conical frustum of material A"A'"CDB'"B" in the mathematical model is assumed to be a rigid plug. The plug is held in the slab by tensile stresses, σ_φ, and shear stresses, τ_φ, that are assumed constant over the slant surface area. Circumferential shear stresses are neglected because of symmetry and the absence of plug rotation about the vertical axis. For the plug, the equation of motion in the vertical direction can be written as

$$\sigma_z \pi a^2 - \sigma_\varphi A \sin\varphi - \tau_\varphi A \cos = m_2 \frac{d^2\xi}{dt^2} \tag{5}$$

where

$$A = \pi(r+a)\,[s^2 + (r-a)^2]^{1/2} \tag{6}$$

Because only one-dimensional motion of the rigid plug in the vertical direction is considered, the gross assumption is made that on the slant surface area of the plug the reaction forces needed for equilibrium are vertical and the complementary horizontal radial forces are identically zero.* Thus,

$$\sigma_\varphi A \cos\varphi - \tau_\varphi A \sin\varphi = 0. \tag{7}$$

---

* For an elastic plug, contact surface deformations of the plug and slab due to surface tractions must be obtained and an equation expressing compatibility of deformations employed to relate, mutually, the contact surface stresses, σ_φ and τ_φ. This problem would be exceptionally difficult to solve and its consideration was not warranted in this investigation.

Combining Eqs. 5, 6, and 7 yields

$$\sigma_z \eta^2 = \sigma_\varphi \frac{(\tan \varphi + 2\eta)(\tan^2 \varphi + 1)}{\tan \varphi} \tag{8}$$

where

$$\eta = \frac{a}{t - z_c} \tag{9}$$

Because the mass of the plug is small compared with the mass of the penetrator, the inertia forces are insignificant with respect to the contact forces, $\sigma_z \pi a^2$. Thus, in Eq. 8, the terms involving $m_2 d^2\xi/dt^2$ have been neglected. Rearranging Eq. 8 results in

$$\sigma_z = \sigma_\varphi F(\varphi, \eta) \tag{10}$$

where

$$F(\varphi, \eta) = \frac{(\tan \varphi + 2\eta)(\tan^2 \varphi + 1)}{\eta^2 \tan \varphi} \tag{11}$$

The mechanical strength properties of sea ice exhibit exceptionally large scatter. Therefore, in lieu of more sophisticated failure criteria, it is assumed simply that perforation occurs when the tensile stress normal to the slant surface area of the plug reaches the tensile rupture (and/or yield) stress of the sea ice.* For a given value of tensile rupture stress, σ_φ, it is expected that a value of conical frustum angle, φ, exists which provides a minimum equilibrium impact force, $\sigma_z \pi a^2$, at incipient perforation. This fact can be demonstrated on physical grounds. As φ approaches $\pi/2$, the slant area becomes infinite; thus, for a given σ_φ the impact force required for perforation approaches an infinite value.

* An alternative failure criterion would be to assume that perforation occurs when the vertical tensile stress on the slant surface area of the plug reaches the tensile rupture (and/or yield) stress of sea ice.

Conversely, as φ approaches 0 the value of σ_φ required to provide equilibrium becomes infinite; however, this is not possible because σ_φ can be no greater than the yield and/or fracture value. Thus, for a given cylindrical-conical shear plug geometry, a value of φ intermediate to the extremes of 0 and $\pi/2$ exists and determines uniquely the values of impact force and velocity for perforation. Inspection of Eq. 10 shows that these values are obtained when $F(\varphi,\eta)$ is a minimum with respect to variations in φ, where η is held constant.

At incipient perforation, substitution of the maximum compressive stress developed during penetration, $\sigma_z = \alpha k z_c$, into Eq. 10 and elimination of z_c between Eqs. 4 and 10 results in the final expression for the critical impact energy; and for given projectile mass, the critical impact velocity, v_c.

$$1/2\ m_1 v_c^2 = \frac{\pi a^4}{2\alpha} k\ \bar{\sigma}_\varphi^2\ (\alpha + 2\ \bar{\tau}_0)\ \bar{F}^2 \tag{12}$$

where

$$\bar{\sigma}_\varphi = \frac{\sigma_\varphi}{ak} \qquad \bar{\tau}_0 = \frac{\tau_0}{ak} \tag{13}$$

and

$$\bar{F} = F(\varphi,\eta) \text{ when } \left.\frac{\partial F}{\partial \varphi}\right|_\eta = 0 \tag{14}$$

For a typical cylindrical-conical shear plug geometry, a plot $\eta^2 F(\varphi,\eta)$ versus φ is shown in Fig. 42. The curves exhibit minima with respect to φ that are given by the locus intersection points.

Equation 12 cannot be solved directly to yield critical impact velocity because the function $\bar{F}$ is not known a priori but is related implicitly to the dependent variable, v_c. However, a calculation procedure can be developed and programmed* on a digital computer to obtain the solution of this equation.

---

* The computer program that was written for this problem is contained in Appendix E.

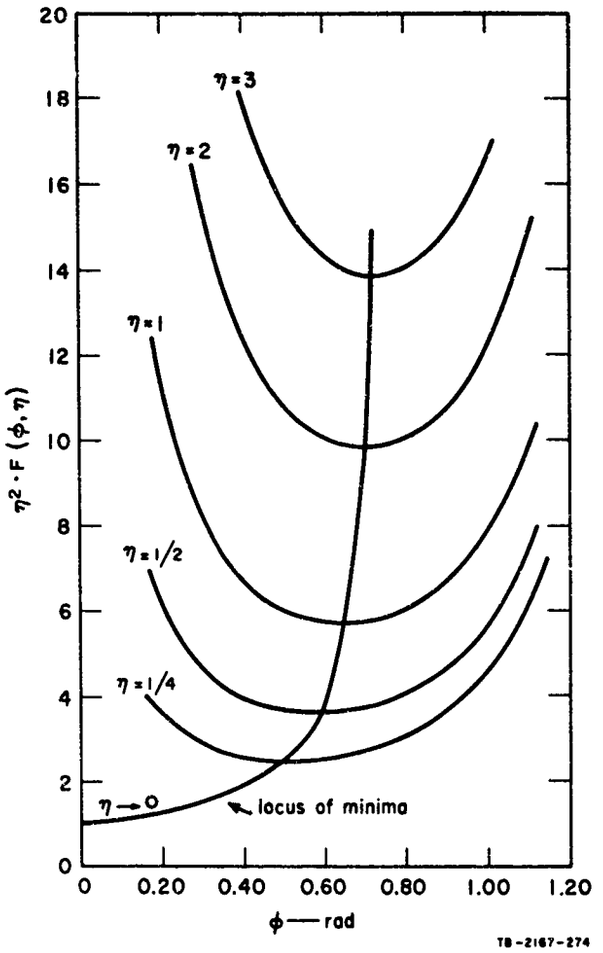

FIG. 42 PLOT OF $\eta^2 F(\phi,\eta)$ vs ϕ SHOWING MINIMA OF $F(\phi,\eta)$ WITH RESPECT TO $\phi;\eta$ FIXED

Subsequently, the values of $\bar{F}$, φ, η, and z_c which describe the geometry of the cylindrical-conical shear plug can be obtained. Briefly, in the problem, quantities: t, a, m_1, τ_0, σ_ω, and k, are provided and the critical impact velocity, v_c, is sought. First, a value of v_c is assumed so that the quantity z_c given by Eq. 4 satisfies the relationship, $0 \leq z_c \leq t$. Then, the value of z_c obtained through Eq. 10 is reconciled

to the first calculated value (Eq. 4) by an iterative process until the two simultaneous equations are satisfied mutually. The value of v_c which fulfills this condition also satisfies Eq. 12, and represents the critical impact velocity.

The theory is complete for test slabs of styrofoam and other porous materials for which the mechanical properties, τ_0, σ_φ, and k, are readily available. The same mechanical properties have been obtained for sea ice by many investigators[10-12,25] using a great variety of testing techniques. In addition, empirical relations have been formulated by researchers in attempts to correlate these data and to represent the mechanical behavior of "typical" sea ice. Unfortunately, these studies do not provide a coherent and fundamental explanation of sea ice strength phenomena, over a wide range of salinities and temperatures, on a rational basis. However, the mechanical properties of sea ice can be related to certain basic physical properties; for example: temperature, salinity, and brine content. Because these latter properties are determined easily and with relatively high accuracy and consistency, there is good reason to develop a theory that yields strength properties from characteristic physical data. This task has been attempted by a few investigators.[8,26-28] Of these, the most comprehensive analysis and the one that explains best the behavior of sea ice under the environmental conditions of the present investigation is the work of Assur.[8] Assur assumes that the mechanical strength of sea ice is related primarily to the relative brine content of the sea ice which can be computed from temperature and salinity, considering the precipitated salts on the basis of phase relations. Secondary factors that influence the strength properties such as density, age, hysteresis phenomena, and some spatial effects due to anisotropy and inhomogeneity can be interpreted through their implicit relationships with sea ice salinity. Assur's theory shows agreement with experimental data obtained from ring tensile tests over a wide range of ice types, temperatures, and salinities. The most important results of Assur's work are shown in Fig. 43. In this plot, the relative tensile strength of sea ice is related to a computed "basic strength" for an idealized brine-free sample of ice in which stress concentration factors exist. Assur reports

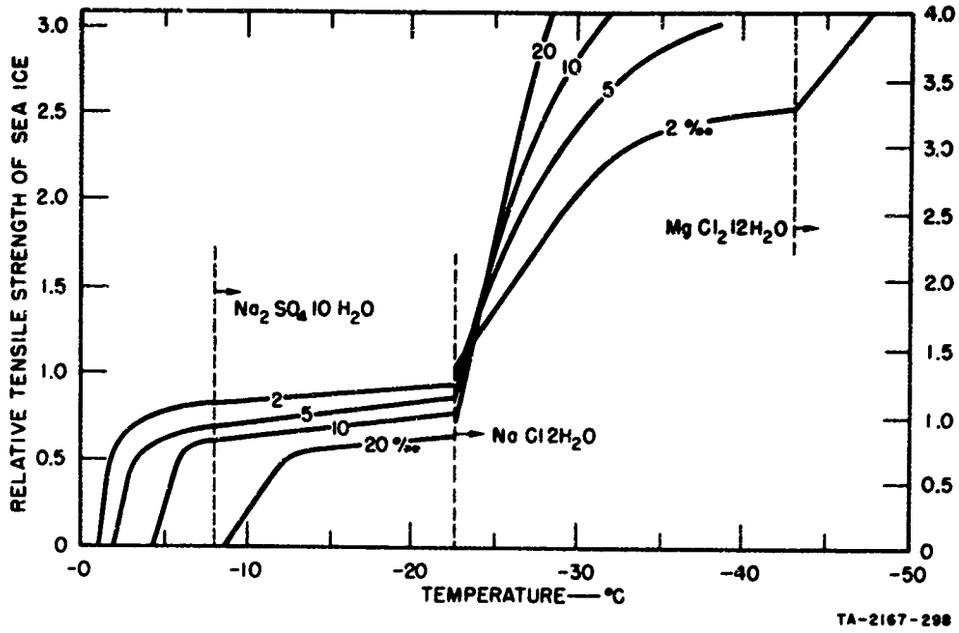

FIG. 43 RELATIVE TENSILE STRENGTH OF SEA ICE AS A FUNCTION OF TEMPERATURE AND SALINITY, FROM REF. 8

"basic strength" values of 202 psi for sea ice at +14°F (-10°C), and 270 psi at subzero temperatures down to -10°F (-23°C).

Assur's general theory has been used in this investigation to provide the tensile strength, σ_{φ}, as a function of sea ice temperature and salinity. The same "basic strength" values computed by Assur were employed in the present theoretical calculations for the Arctic field test program. However, in similar calculations for the laboratory sea ice, the tensile strength data published recently by Dykins[13] for sea ice grown artificially in a confined system were used to establish a "basic strength" value within the appropriate temperature range. Specifically, tensile strengths in the horizontal (67.4 psi) and vertical (152.3 psi) directions obtained by Dykins for sea ice cores at -10°C, and 7.59 and 6.80 ppm salinity contents, respectively, were employed. Then, the relative linear scale on the ordinate of Assur's plot was correlated on an absolute basis to the Dykins "basic strength" value. The horizontal (σ_H) and vertical (σ_V) strengths were combined as component principal stresses to yield resultant tensile rupture stress, normal to the conical frustum slant surface, as a function of the conical half-angle, φ. That is,

$$\sigma_{\varphi} = \sigma_{H} \cos^2 \varphi + \sigma_{V} \sin^2 \varphi \qquad (15)$$

For both Arctic and laboratory sea ice, the Assur theory plot (Fig. 43) was programmed on the Burroughs B5500 digital computer. Assur's curves were fitted in the region of temperatures between 0° through -23°C by third-order polynomial expressions and stored in the computer memory. Next, a subroutine was developed to ascribe the correct "basic strength" values for the tensile strengths of laboratory sea ice and Arctic sea ice. Then, a knowledge of temperature, salinity, and "basic strength" permitted the computer determination of tensile rupture strength, σ_{φ}.

The shear yield strength, τ_0, for both laboratory and Arctic sea ice was assumed to equal 1/2 the tensile strength, this choice corresponding to the Tresca yield condition for unidirectional principal stress. Available data for the shear strength of sea ice[25] support this condition approximately.

Two means were employed to determine the dynamic compression modulus, k. For a low impact velocity test on laboratory sea ice, k was obtained from an oscillographic trace showing projectile deceleration-time history (Fig. 31) during penetration by measuring the initial linear portion of the curve's slope. For the high impact velocity tests on laboratory sea ice and Arctic sea ice, k was assumed proportional to the static elastic compression modulus and was calculated from values given in Tabata.[14]* In this case, k was equal to Young's modulus divided by the ice thickness.

---

* The average value of Young's modulus obtained from the oscillographs was E = 273,000 psi for ice at approximately -8°C (+17.6°F). Tabata's results obtained from flexural tests on small Arctic sea ice beams in a range of stress rates where elastic behavior occurred provide values of Young's moduli, E = 179,000 through 238,000 psi, for a sea ice temperature range, 0°C (+32°F) through -15°C (+5.0°F).

DISCUSSION OF EXPERIMENTAL RESULTS AND COMPARISON WITH THEORY

Laboratory Tests

The experimental results summarized in Table 4 are plotted in Fig. 23. Darkened data points pertain to tests on sea ice in which perforation was not obtained, and they indicate the maximum value of impact velocity sustained by the slab. Undarkened data points indicate critical impact velocity values. These data points represent the results of test series performed on individual slabs having characteristic temperatures and salinities. Because these quantities varied for each test slab, it was not possible to plot a unique theoretical perforation threshold boundary that was a function only of thickness.

In Fig. 23, the experimental data were plotted with respect to slab thickness-penetrator diameter ratio, t/D, for convenience only; therefore, it is not implied that the critical impact velocities are related functionally to this quantity. As expected, for a fixed penetrator diameter (D = 1-1/4 in.), critical impact velocity increases with ice thickness. For the high impact velocity tests, a perforation threshold zone is evident in the plot of experimental results.

The critical impact velocities predicted by the present theory for each of the sea ice slabs tested are compared with experimental values in Table 8. The agreement between theory and experiment for two projectile weights that differed by an order of magnitude (0.75 lb and 9.688 lb) and two penetrator diameters (5/8 in. and 1-1/4 in.) is reasonably good. For example, in the low impact velocity tests ($v_1 < 25.0$ ft/sec), the theoretical value for the 4-1/4-in. thick slab is intermediate to the experimental "no-go" and "go" (perforation) values, and for the 5-in. slab it is close to the perforation value. Theoretical values for the 3-3/8-in. and 6-3/4-in. slabs conform to "necessary" conditions being below the experimental "go" value in the former case and above the "no-go"

Table 8

COMPARISON OF THEORETICAL AND EXPERIMENTAL RESULTS:
LABORATORY SEA ICE TEST SLABS, BLUNT PENETRATOR

Ice Thickness (in.)	Temperature (°F)	Salinity (ppm)	Penetrator Diameter (in.)	Projectile Weight (lb)	Perforation	Experiment v_1* (ft/sec)	Experiment v_c† (ft/sec)	Theory v_c† (ft/sec)	Remarks
3-3/8	19.4	15.6	1-1/4	9.688	Yes	-	8.6	6.56	One shot perforation, free-fall projectile
4-1/4	19.4	15.0	1-1/4	9.688	Yes	9.3	11.3	10.4	Free-fall projectile
5	22.1	10.2	5/8	9.688	Yes	13.4	14.7	16.9	Free-fall projectile
6-3/4	16.7	12.0	1-1/4	9.688	No	13.7	-	24.9	Free-fall projectile
8-1/2	10.0	12.2	1-1/4	0.75	Yes	-	324.0	196.0	One shot perforation, rifle projectile
9-1/4	6.0	6.5	1-1/4	0.75	No	252.0	-	273.0	Rifle projectile
9-1/4	7.8	7.2	1-1/4	0.75	Yes	-	414.0	266.0	One shot perforation, rifle projectile
10	14.5	10.6	1-1/4	0.75	No	237.0	-	262.0	Rifle projectile
10-1/2	14.0	12.2	1-1/4	0.75	Yes	291.0	370.0	257.0	Rifle projectile
11-1/4	19.0	8.2	1-1/4	0.75	Yes	-	411.0	327.0	One shot perforation, rifle projectile
15-1/2	19.0	9.3	1-1/4	0.75	No	402.0	-	567.0	Rifle projectile
15-3/4	7.0	13.8	1-1/4	0.75	No	430.0	-	609.0	Rifle projectile

* The impact velocity, v_1, is the maximum value experienced by the test slab for which perforation did not occur.

† v_c = impact velocity required for perforation. Theoretical values of v_c calculated for compression ratio, $\sigma = 1.0$, and the following values of Young's modulus:

0 ft/sec ≤ v_1 ≤ 25.0 ft/sec — E = 273,000 psi (from experimental data)

200 ft/sec ≤ v_1 ≤ 500 ft/sec — E = 179,000 psi (from Tabata[14])

value in the latter. In this case, the "go" was obtained in a "one-shot" test series (see Remarks, Table 8) and, thus, could be significantly higher than the actual critical value at incipient perforation.

In the high impact velocity tests (v_i> 200.0 ft/sec), theoretical* critical impact velocities fulfill "necessary" conditions for the 9-1/4-in., 10-in., 15-1/2-in., and 15-3/4-in. slabs in the "no-go" case, and for the 8-1/2-in., 9-1/4-in., and 11-1/4-in., slabs in the "go" case. For the 10-1/2-in. slab, the theoretical value of 257.0 ft/sec violates the "no-go" experimental value of 291.0 ft/sec by 11.7%.

Qualitative results obtained from low impact velocity tests confirmed previous results[6] by demonstrating the blunt penetrator's advantage in the perforation process. However, in the high impact velocity tests, imprecise control of projectile velocities made the collection of meaningful results for comparison purposes difficult. The data obtained on the relative high impact velocity performance of conical and blunt penetrators were deemed insufficient to draw any rigorous conclusions.

Tests on a 2-3/4-in. slab with the 5/8-in. and 1-1/4-in. diameter conical penetrators resulted in a lower critical impact velocity for the smaller diameter penetrator in agreement with results of the first study[6] and predictions of the present theory.

A discussion of penetration behavior observed in the laboratory tests is not included because, in this regard, better results were obtained from the field work on Arctic sea ice. However, data from penetration experiments on laboratory sea ice are plotted in Fig. 20. The data points

---

* The value of axial compression ratio employed in the theoretical calculations for both high and low impact velocity tests on laboratory sea ice and Arctic sea ice was $\alpha = 1.0$. It was not possible to obtain experimentally measured values for this quantity, as in the tests on styrofoam, because the cylindrical-conical shear plugs were not recovered intact.

for both conical and blunt penetrators are represented well by straight lines that were fitted using the method of least squares. At equivalent impact velocities, penetration produced by the conical penetrator is nearly double that of the blunt penetrator.

The most important results obtained in the tests on styrofoam slabs are presented in Figs. 25 and 26 where critical impact velocity, v_c, and shear penetration depth, z_c, versus slab thickness are plotted, respectively. In the plots, data points represent experimental results obtained in tests with 5/8-in. and 1-1/4-in. diameter blunt penetrators (Table D3). The curves denote the threshold boundaries for perforation predicted by the theory. It was possible to obtain these curves because the mechanical properties of the styrofoam were uniform over the range of slabs tested. Thus, for a given projectile and slab, critical impact velocity was only a function of thickness. In Fig. 25, curves are given for the two values of compression ratio α (α = 0.5, 0.7) that were most representative of the cylindrical-conical shear plug geometries produced in the experiments. These curves encompass the experimental data and show good agreement in predicting both trend and absolute magnitudes of the results. In the theory, calculation of z_c is independent of α; thus, a single curve is sufficient to represent the data in Fig. 26. Here, the agreement between theory and experiment is also good.

Data from the high impact velocity tests on a 10-in. styrofoam slab are not included in the plots. In this case, a cylindrical-conical shear plug was not produced; instead, the ogival-conical plug shown in Fig. 28(a) was obtained. Calculations based on the analysis of Appendix A for a cylindrical shear plug yield a theoretical critical impact velocity for this slab of 205 ft/sec. The experimental value was between 216 ft/sec and 291 ft/sec (Table D3).

For the tests on styrofoam, theoretical values of cylindrical-conical shear plug cone angle, φ, are in the range, $33^0 \leq \varphi \leq 35^0$. This calculation agrees with the experimental results (e.g., Fig. 3).

A cursory analysis of oscillographic traces showing deceleration-time response indicated that the sequence of events in the cylindrical-conical shear plug formation process was consistent with the assumptions

of the theory. For example, oscillogram (a) in Fig. 31 shows that the resisting force experienced by the blunt penetrator develops an initial, almost linear, increase with time corresponding to elastic compression of the slab material during the shear penetration phase of perforation. Next, a dwell period of constant resisting force occurs followed by a period of exponential decay as the cylindrical-conical shear plug is expelled from the slab into the underlying seawater.

Oscillogram (b) was recorded during an impact test on a sea ice slab characterized by relatively high salinity content (19.6 ppm) and a large skeleton layer. Because shear strength of this ice was exceptionally low, perforation was realized by the expulsion of a cylindrical shear plug[6]. In this case, no dwell period was recorded. Oscillogram (c), recorded during the perforation of a laboratory sea ice slab, exhibits the same characteristics as oscillogram (a) for the styrofoam slab. The relatively large amplitude half-cycle oscillation prior to the peak value does not correspond to any stress wave arrival time, either in the projectile or from the ice. The small wiggles just prior to impact were caused by the microswitch contacts. Oscillogram (d), recorded in a test where penetration but not perforation occurred, does not depict the appreciable dwell period and half-cycle oscillation that were recorded in the perforation process. Deceleration up to the peak value is followed by an exponential decay.

Field Tests

The experimental results summarized in Table 6 are plotted in Fig. 24. As before, data points represent the results of test series on Arctic sea ice covers of different temperatures and salinities; therefore, it was not possible to plot a unique perforation threshold boundary. Again, the data are plotted with respect to t/D for convenience only. Although the number of experiments was limited, the results suggest that an empirical perforation threshold boundary could represent the trend of data.

The critical impact velocities obtained from the present theory* are compared with experimental values in Table 9. The agreement between theory and experiment for two disparate projectile weights (0.75 lb and 41.5 lb) and two penetrator diameters (1-1/4 in. and 6 in.) is satisfactory. For example, theoretical values for the 8-in., 11-1/4-in., 11-3/8-in., 13-in., 16-1/4-in., and 17-in. sea ice covers satisfy "necessary" conditions being above the "no-go" values obtained experimentally. Although theoretical values for the 9-3/4-in. and 10-3/4-in. sea ice covers are above the experimental "go" values, they are in error by only 18% and 14.5%, respectively. In the case of the 16-in. and 16-1/4-in. sea ice covers, theoretical values of critical impact velocity are intermediate to the experimental "no-go" and "go" values and on an average basis in error by a maximum of 13.3%. This last result is encouraging because it indicates agreement between theory and experiment in a test where projectile weight and diameter (e.g., 41.5 lb and 6 in.) were in the size range of small weapons system equipment.

Although the number of tests performed on Arctic sea ice was limited, none of the results conflicted with trends of behavior established in the experiments on laboratory sea ice. As before, the conical penetrator produced greater penetration depths but was of lesser efficiency than the blunt penetrator in perforation. For example, in Test Series F (Table 6), experiments with 1-1/4-in. blunt and conical penetrators at corresponding impact velocities of 409 ft/sec and 406 ft/sec on the same sea ice cover (t = 13 in.) produced penetrations of 4 in. and 7 in., respectively; however, even through the penetration produced by the conical projectile was much greater than the blunt projectile penetration and represented 54% of the ice thickness, perforation did not occur. Similarly, in Test Series E, impact with the blunt and conical penetrators at velocities of 433 ft/sec and 469 ft/sec produced penetrations of 4-3/4 in. and 7-5/8 in. in an 11-1/4-in. thick ice sheet. Here, the

---

* In the theoretical calculations, sea ice basic strength values of 202 psi ($0\,^{\circ}C < T \leq -8\,^{\circ}C$) and 270 psi ($-8\,^{\circ}C < T < -23\,^{\circ}C$) were employed to establish absolute scale values on the Assur diagram.

Table 9

COMPARISON OF THEORETICAL AND EXPERIMENTAL RESULTS:
ARCTIC SEA ICE TEST SERIES, BLUNT PENETRATOR

Ice Thickness (in.)	Temperature (°F)	Salinity (ppm)	Penetrator Diameter (in.)	Projectile Weight (lb)	Perforation	Experiment v_1* (ft/sec)	Experiment v_c† (ft/sec)	Theory v_c† (ft/sec)	Remarks
8	15.5	12.1	1-1/4	0.75	No	262.0	-	345.0	Rifle projectile
9-3/4	14.0	12.4	1-1/4	0.75	Yes	332.0	444.0	523.0	Rifle projectile
10-3/4	14.5	13.8	1-1/4	0.75	Yes	465.0	494.0	565.0	Rifle projectile
11-1/4	24.5	14.0	1-1/4	0.75	No	433.0	-	639.0	Rifle projectile
11-3/8	26.0	14.0	1-1/4	0.75	No	417.0	-	625.0	Rifle projectile
13	24.0	10.3	1-1/4	0.75	No	409.0	-	822.0	Rifle projectile
15-3/4	32.0	-	1-1/4	0.75	No	-	-	-	Slush and seawater cover 3-in. deep, rifle projectile
16	17.0	10.6	6	41.5	Yes	-	124.0	105.0	One shot perforation, Navy 1 Pdr projectile
16-1/4	16.5	10.6	6	41.5	No	100.0	-	110.0	Navy 1 Pdr projectile
17	15.5	9.4	6	41.5	No	96.5	-	124.0	Navy 1 Pdr projectile

* The impact velocity, v_1, is the maximum value experienced by the test slab for which perforation did not occur.

† v_c = impact velocity required for perforation. Theoretical values of v_c calculated for compression ratio, $\alpha = 1.0$, and the following value of Young's modulus:

$200 \text{ ft/sec} \leq v_1 \leq 500 \text{ ft/sec}$

$E = 238{,}000$ psi (from Tabata[14])

conical penetrator did not produce perforation even though it passed through 68% of the ice thickness. However, tests with a blunt penetrator on laboratory sea ice produced perforation in every instance where the penetration exceeded 50% of the ice thickness.

Results obtained in Test Series D1 and D2 (Table 6) performed at inclined incidence and normal incidence, respectively, showed that equivalent penetration depths were obtained at an "inclined" impact velocity that was approximately 10% greater than the "normal" impact velocity. This result was expected because results of Ref. 6 indicated that both the penetration and perforation processes were less efficient at inclined incidence.

A plot of data collected in tests with the 6-in. diameter blunt projectile (Fig. 22) shows that the relationship between penetration depth and impact velocity may be represented by a smooth curve* which is asymptotic to the critical impact velocity ordinate. That is, infinite penetration (perforation) can be predicted when the results of penetration tests are extrapolated to a limiting value. Results of Test Series B obtained with the 1-1/4-in. diameter penetrator are in accord with this observation.

Petrographic structure of the Arctic sea ice (Test Series H) in the horizontal and vertical planes is shown in Figs. 18 and 19, respectively. In Fig. 18, grain size variation with depth is clearly evident. Specifically, cross sections in the top and bottom layers of the sea ice contain large crystals (e.g., crystal density, 0.4 - 0.8/cm^2) characteristic of coarse-grain sea ice.** The middle cross section at a depth of 5.5 in. contains relatively small close-ordered crystals (e.g., crystal

---

* The curve is approximately linear for the first three data points, confirming the penetration results in Figs. 20 and 21. The nonlinear trend, introduced by the fourth data point, becomes apparent at impact velocities close to the critical value.

** Large grain size and small crystal densities were not observed by Dykins[13] in the sea ice top layer; however, his tank-produced test specimens were frozen under the idealized conditions of still water and the absence of snow.

density, 7 - 9/cm^2) found usually in fine-grain sea ice. For none of the cross sections was it possible to obtain total light extinction at any setting of the cross-polaroid screens; therefore, preferred orientation of the crystal c-axes was not indicated.

Subgrain structure is well-defined in cross sections taken from top and bottom layers of the sea ice. In particular, the cross section at a depth of 13.5 in. shows the typical sea ice laminar grain composition (dendrites) of fresh ice platelets separated by brine inclusions containing foreign impurities rejected in the freezing process. Sea ice structure in the vertical plane (Fig. 19) indicates the corresponding grain size variation with depth noted in the series of horizontal cross sections. Here, crystals in the top layer have characteristic columnar, elongated shapes in the vertical direction.

APPLICATION AND LIMITATIONS OF THEORY

The usefulness of the theory can be demonstrated best by analyzing some illustrative problems in which curves plotting critical impact velocity versus sheet thickness for Arctic sea ice are determined. For this purpose, four air-dropped projectiles have been considered as typical (Table 10). These projectiles were assumed to be blunt-nosed and impact at normal incidence was implied by use of the theory. To gain better fundamental insight, the sea ice mechanical strength properties, tensile rupture stress σ_{φ}, shear yield stress τ_0, and dynamic compression modulus k, were chosen as independent variables in lieu of temperature and salinity. Two basic problems were treated.

TABLE 10

CHARACTERISTIC PROJECTILE DATA

Projectile	Weight (lb)	Diameter (in.)	Terminal Velocity (ft/sec)
AN-SSQ-26 Sonobuoy	18.0	4.875	--
250GP-ANM57A1 Bomb	239.0	10.750	985
Mark 46 Torpedo	550.0	12.750	--
1600 AP-ANMK1 Bomb	1523.0	14.000	1212

First, perforation threshold boundaries for each of the projectiles were calculated from the theory employing typical experimental data[8,11,14] to characterize the strength of Arctic annual sea ice in the temperature range $-8^{\circ}C \leq T \leq -23^{\circ}C$. The values chosen for the mechanical properties were:

$\sigma_{\varphi} = 200$ psi $\quad \tau_0 = 110$ psi $\quad E = 240{,}000$ psi

and ice of this description was designated "standard Arctic sea ice". Results of these calculations are presented in Fig. 44.

Second, a projectile having the same weight and diameter as the Mark 46 Torpedo was chosen and perforation threshold boundaries were determined for ranges of mechanical property values that encompass most of the data reported in Arctic references. Results of these calculations are presented in Figs. 45 through 49.

The plot of Fig. 44 indicates that the 239-lb bomb and the 1523-lb bomb can perforate "standard Arctic sea ice" thicknesses of 7-1/4 ft and 15-1/4 ft at respective terminal velocities of 985 ft/sec and 1212 ft/sec. Unfortunately, terminal velocities of the Sonobuoy and Mark 46 Torpedo were not readily available at this writing. However, if a reasonable terminal velocity of 400 ft/sec is chosen for the Sonobuoy, the plot shows that perforation will occur for any sea ice cover less than 2 ft in thickness. Similar considerations in the case of the Mark 46 Torpedo reveal that for a free-fall, no-drag, air drop from a height of 200 ft (v_1 = 113.5 ft/sec), perforation at normal incidence will occur for a sea ice cover up to 3 ft in thickness.

Perforation threshold boundaries plotted in Fig. 45 show that, for a 6-ft thick ice cover, a 3-fold variation in typical values of sea ice tensile strength ($100 \leq \sigma_\varphi \leq 300$ psi) results in a 2.5-fold variation in critical impact velocity. Thus, an accurate determination of σ_φ is of primary importance in the perforation problem. However, this result does not apply for sea ice shear strength, τ_0, because Fig. 46 demonstrates that critical impact velocity is insensitive to changes in τ_0 up to a thickness of approximately 10 ft. Figure 47 shows that an 11.8-fold variation in Young's modulus ($85 \times 10^3 \leq E \leq 1000 \times 10^3$ psi) results in a 2.2-fold variation in critical impact velocity; thus, the accurate determination of E is of secondary importance. It is interesting to note that the curves in Fig. 47 exhibit crossover intersection points at certain thicknesses so that at a given thickness below the crossover value critical impact velocity varies inversely with Young's modulus and at thicknesses greater than the crossover value it varies directly with Young's modulus.

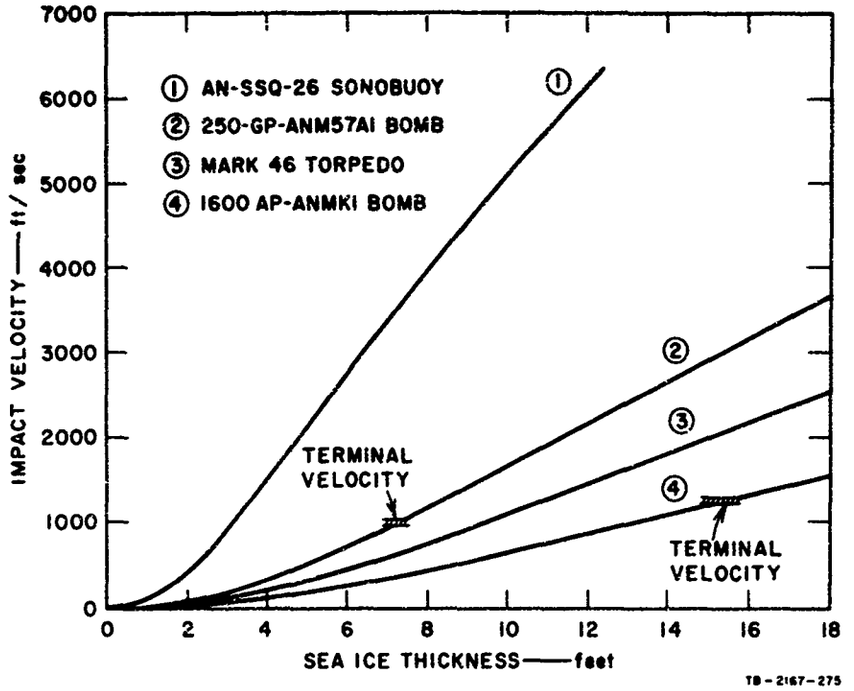

FIG. 44 PERFORATION THRESHOLD BOUNDARIES FOR VARIOUS PROJECTILES: "STANDARD ARCTIC SEA ICE"
σ_ϕ = 200 psi
τ_o = 110 psi
E = 240,000 psi

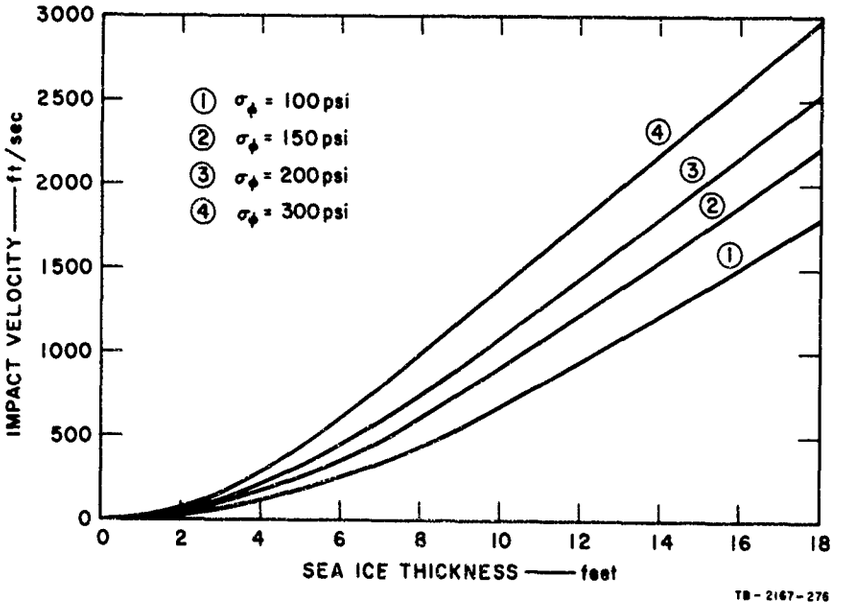

FIG. 45 PERFORATION THRESHOLD BOUNDARIES FOR VARIOUS SEA ICE TENSILE STRENGTHS
τ_o = 110 psi
E = 240,000 psi
m_1 = 550.0 lb
D = 12.750 in.

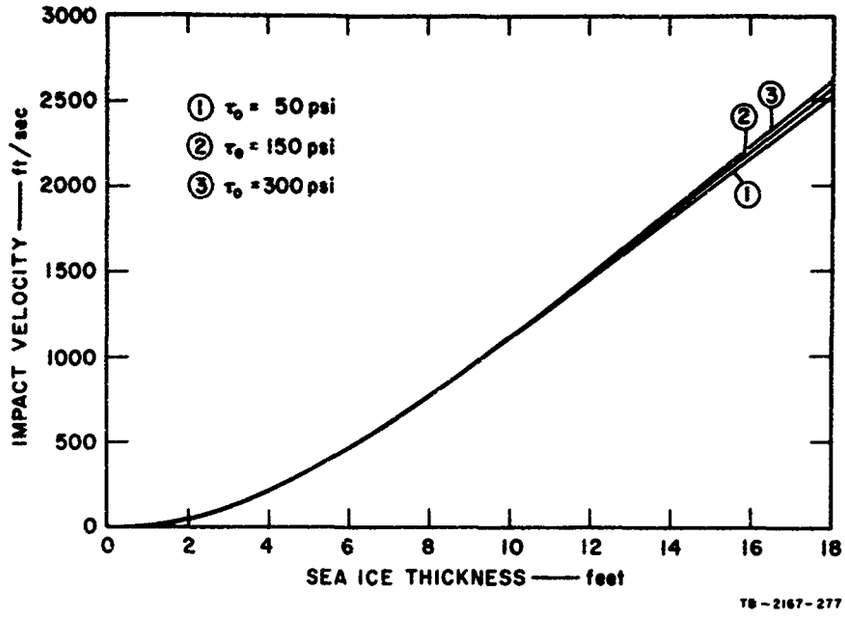

FIG. 46 PERFORATION THRESHOLD BOUNDARIES FOR VARIOUS SEA ICE SHEAR STRENGTHS

σ_ϕ = 200 psi m_1 = 550.0 lb
E = 240,000 psi D = 12.750 in.

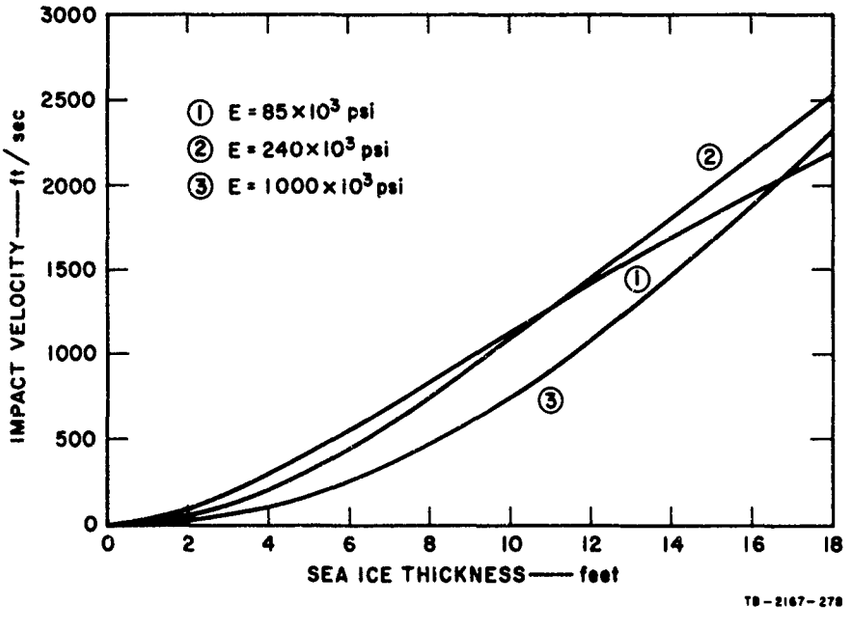

FIG. 47 PERFORATION THRESHOLD BOUNDARIES FOR VARIOUS SEA ICE ELASTIC MODULI

σ_ϕ = 200 psi m_1 = 550.0 lb
τ_o = 110 psi D = 12.750 in.

The variation of critical impact velocity with sea ice thickness for different projectile diameters is plotted in Fig. 48.* An important feature is that these curves also exhibit crossover points indicating that optimum choices of projectile diameter can be related to specific ice thicknesses. For example, in the ice thickness range 0 through 3 ft, use of a 6-in. diameter projectile results in lower values of impact velocity for perforation than with a 2-in. diameter projectile while the converse is true for ice thicknesses greater than 3 ft.

The data contained in Fig. 48 are replotted in Fig. 49 to show the variation of critical impact velocity with projectile diameter for different sea ice thicknesses. In this plot, the theory indicates that, for perforation, certain projectile diameters should be avoided because they lie in a range where higher impact velocities are required than for diameters that are outside the range. For example, in the perforation of a 6-ft thick sea ice cover, projectile diameters between 2 in. and 24 in. would be relatively inefficient. **

With regard to limitations, the present theory only treats perforation of a sea ice cover subjected to impact of a blunt penetrator at normal incidence. When the sea ice mechanical strength properties, σ_{φ}, τ_0, and E are used as input variables in the computer program, there are no restrictions on values of the other independent variables. † However, in practical calculations, values of the dependent variable, v_c (i.e., critical impact velocity), are limited by the terminal velocity of the projectile.

---

* The theoretical curves have been cut-off below ratios of $t/D = 1$. For these ice thickness, penetrator diameter ratios, the perforation problem involves plate bending effects and, in this case, the present theory is not applicable.

** Qualitative observations made in the experiments on styrofoam test slabs indicated that perforation was obtained most readily at slab thickness-penetrator diameter ratios (t/D) close to $t/D = 2$. These results are not at variance with the theoretical predictions. In this regard, it would be useful to perform impact tests on styrofoam test slabs using a wide range of different penetrator diameters to either verify or disprove this interesting aspect of the theory.

† With the exception that implicit in the present theory is the premise that perforation occurs when a cylindrical-conical shear plug is expelled from the ice cover. Thus, the theory is not applicable for low t/D values ($t/D < 1.0$) where the ice behaves as a plate.

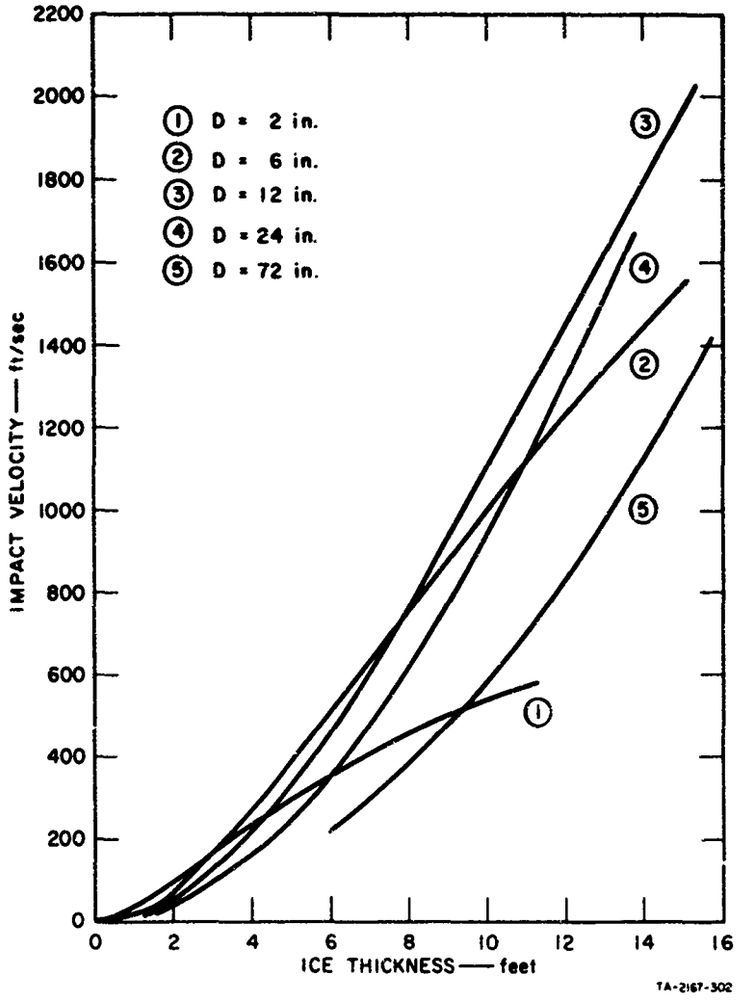

FIG. 48 PERFORATION THRESHOLD BOUNDARIES FOR VARIOUS PROJECTILE DIAMETERS: "STANDARD ARCTIC SEA ICE" σ_ϕ = 200 psi; τ_o = 110 psi; E = 240,000 psi

When the Assur theory is used to relate mechanical strength to sea ice temperature and salinity content, the restrictions on ranges of variables that can be used for computer program inputs are the following:

if	$\lvert T \rvert > -9.5^\circ C$	then	$2 \leq S \leq 20$ ppm
	$-4.3^\circ C < T \leq -9.5^\circ C$		$2 \leq S \leq 10$ ppm
	$-2.0^\circ C < T \leq -4.3^\circ C$		$2 \leq S \leq 5$ ppm

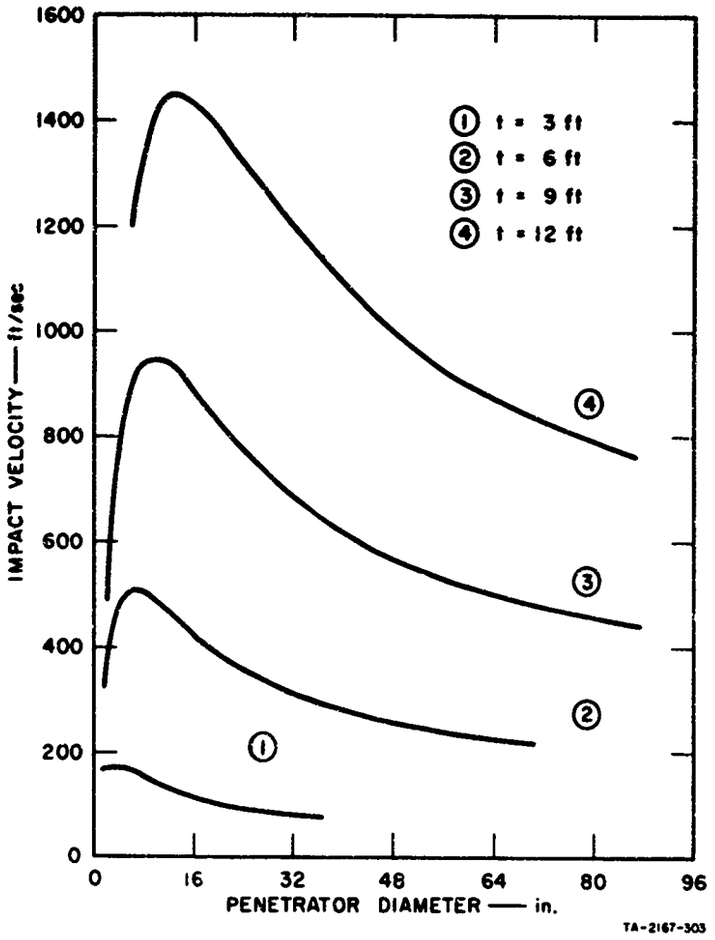

FIG. 49 PERFORATION THRESHOLD BOUNDARIES FOR VARIOUS SEA ICE THICKNESSES: "STANDARD ARCTIC SEA ICE" σ_ϕ = 200 psi; r_o = 110 psi; E = 240,000 psi

The present computer program does not duplicate the Assur curves (Fig. 43) in the region where increased strength due to the precipitation of solid $NaCl2H_2O$ salts occurs (i.e., $|T| > -22.9^oC$). Instead, the linear curves in the region, $-8.2^oC \leq T \leq -22.9^oC$, are simply extended into the region, $|T| > -22.9^oC$. This modification to the Assur diagram means that the computer program is not valid for perennial or Polar sea ice.

RECOMMENDED FUTURE RESEARCH

Future research in the mechanics of sea ice penetration should be pursued in two general areas. First, a greater theoretical effort should be undertaken to gain better fundamental understanding of the perforation process, especially at the relatively higher impact velocities that are characteristic of freely falling projectiles. Second, attention should be directed toward the design and development of projectiles and ancillary hardware to be used specifically for the perforation of an Arctic sea ice cover. A subsidiary task should be the continuation of Arctic field tests over a more extended range of the problem variables. It is recommended that perforation tests on laboratory sea ice be discontinued. These experiments have already furnished a significant amount of basic information and it is believed that their usefulness has been exhausted.

To date, analysis of this problem has relied on concepts of rigid body dynamics and a work-energy formulation to obtain the critical impact velocity. The theory is not capable of predicting internal stress states, regions of plastic flow, or dynamic effects related to the propagation of shock waves in the sea ice. These phenomena increase in importance with impact velocity and a knowledge of their consequences at military ordnance velocities is essential to the proper design of sea ice-piercing projectiles. Results obtained in the present styrofoam tests concerning internal zones of plastic deformation and the formation of conical-ogival plugs, and the pioneering studies of Dr. S. Hanagud[29,30] (Stanford Research Institute) concerning high pressure stress wave propagation in snow and ice are important first contributions to this task.

In addition, Arctic field tests have shown that the presence of an overlying snow cover can influence strongly the penetration capability of a projectile. Theoretical analysis of this aspect of the penetration problem should be tractable and must be attempted. Some attention should be devoted to including the nonhomogeneous and nonisotropic properties of sea ice in future calculations.

Unfortunately, time has not permitted an analysis of the cratering phenomenon observed in high velocity impact tests on both laboratory and Arctic sea ice. It is important to ascertain the quantity of available impact energy dissipated in the formation of craters because this fraction does not contribute necessarily to the efficiency of the perforation process. A complete theoretical and experimental investigation of this problem can lead to better projectile nose designs that avoid losses due to cratering.

Experimentally, future Arctic study should include further tests with gun-powered, large diameter, large mass projectiles on thicker sea ice covers than were tested heretofore. In some of the field tests, deceleration force-time histories should be recorded during the penetration process.* From these data, a mathematical formulation of critical yield stress functions, including strain rate effects, can provide more exact mathematical model relationships. The results of the present Arctic tests were extremely encouraging and additional field study should be most fruitful. Consideration should be given to conducting tests with airdropped projectiles. For this purpose, the cooperation of the University of Alaska and use of their field test station on Kotzebue Sound, Alaska, has been suggested (Dr. H. Peyton). This location is within reasonable distance of the U.S. Naval Air Station, Kodiak, Alaska.

Investigations concerning the dynamic material properties of sea ice should be undertaken. Although a wide body of literature treating the static, creep, and viscoelastic properties of ice is available, little or no data are published on the corresponding properties characteristic of rapid loading and/or impact loading.** These latter cases, which introduce inertia effects to the problem, can result in material property

---

* Technical experience in the use of projectile-mounted accelerometers has been acquired in this investigation.

** It was only at the conclusion of this investigation that the author learned of the work by H. Napadansky[31] in this field.

values differ significantly from currently employed static data. Well-established experimental and theoretical techniques for the determination of dynamic criteria have been pioneered in the metal, glass, and ceramic technologies and should be applicable to ice studies.

Finally, an investigation similar to the present one should be carried out on the mechanics of penetration of fresh ice. Antisubmarine warfare activity in bodies of water such as the Gulf of St. Lawrence would involve tactical operations in regions where fresh ice is predominant.

APPENDIX A

ANALYSIS OF ICE PERFORATION PROCESS THAT PRODUCES A CYLINDRICAL SHEAR PLUG

APPENDIX A

ANALYSIS OF ICE PERFORATION PROCESS THAT PRODUCES A CYLINDRICAL SHEAR PLUG

In the initial penetration study[6], impact tests on sea ice produced cylindrical shear plugs when perforation occurred. This result was due to the relatively high salinity content and thick skeleton layer characteristic of test slabs manufactured in a closed container. Ice in this condition evidenced large brine content and low shear strength and thus exhibited a propensity to fail entirely in shear.

The data collected in Ref. 6 were plotted on the basis of the mathematical model (Fig. A-1) and analysis outlined in this Appendix. Laws of conservation of momentum and energy and assumptions underlying the classical theory of impact* were employed in the theoretical analysis.

Conservation of momentum and mechanical energy yield, respectively,

$$m_1 v_1 = (m_1 + m_2)\, v_2 \tag{A1}$$

$$1/2\ (m_1 + m_2)\, v_2^2 = \int_0^t \tau_{rz}(\xi, \dot{\xi})\, \pi\, D\, (t-\xi)\, d\xi \tag{A2}$$

Equation A2 relates the amount of kinetic energy imparted to the projectile-plug combination immediately after impact, and the work done in expelling the shear plug from the slab. For incipient perforation, the penetrator exit velocity is set equal to zero.

---

* Transient stresses, contact deformations, and vibrations of the colliding bodies are neglected as are hydrodynamic drag forces, buoyant body forces, and sliding friction forces on the penetrator. Also, in agreement with experimental observations, it is assumed that impact is plastic (no rebound) and that the slab remains motionless during shear plug ejection.

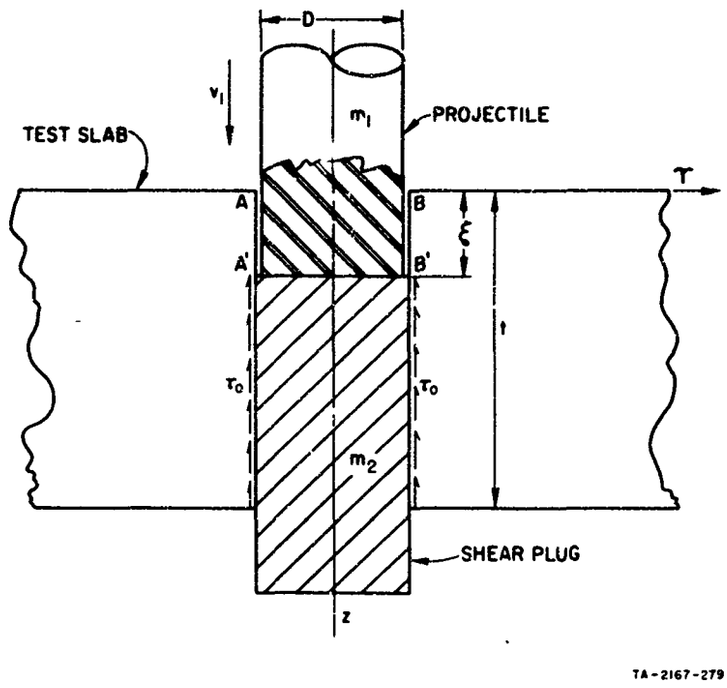

FIG. A-1 SKETCH OF MATHEMATICAL MODEL FOR CYLINDRICAL SHEAR PLUG

It is assumed that the sea ice exhibits rigid-plastic material behavior; then, the shear stress function, $\tau_{rz}(\xi,\dot{\xi})$, can be represented by the shear yield stress value, τ_o. Using this result, performing the integration in Eq. A2, and substituting for v_2 from Eq. A1, there results

$$1/2 \frac{m_1^2 v_1^2}{m_1 + m_2} = \tau_o \frac{\pi Dt^2}{2} \tag{A3}$$

but

$$1/2 \frac{m_1^2 v_1^2}{m_1 + m_2} = 1/2 \frac{m_1 v_1^2}{1 + \frac{m_2}{m_1}} \tag{A4}$$

and for quantities typical of the experimental program

$$\frac{m_2}{m_1} \ll 1 \tag{A5}$$

so that

$$1/2\ m_1 v_1^2 = \tau_0 \frac{\pi D t^2}{2} \qquad (A6)$$

Equation A6 expresses the requisite kinetic energy for perforation of a sea ice slab having a known shear yield stress. The data obtained in the experiments of Ref. 6 were plotted according to this formula and are given in Fig. A-2. Here, the data squares representing tests in which perforation did not occur are filled. An empirical curve was passed through data points obtained at incipient perforation and, thus,

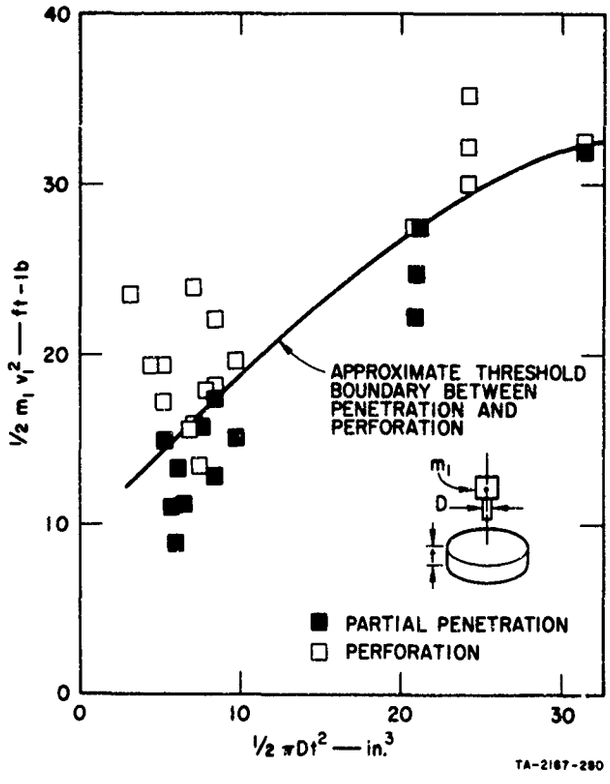

FIG. A-2 PLOT OF TEST RESULTS OBTAINED WITH BLUNT PENETRATORS, FROM REF. 6

represents an experimental threshold boundary for complete penetration. With minor exceptions, the impact tests that produced perforation lie above the curve. A theoretical threshold boundary was not plotted because values of shear strength were not obtained in the initial study[6].

APPENDIX B

CALCULATION OF PENETRATOR MAXIMUM PENETRATION AND PEAK DECELERATION FORCES DUE TO IMPACT ON SEA ICE

APPENDIX B

CALCULATION OF PENETRATOR MAXIMUM PENETRATION AND PEAK DECELERATION FORCES DUE TO IMPACT ON SEA ICE

The peak deceleration force experienced by a rigid, cylindrical blunt penetrator upon impact with sea ice is analyzed. Simplifications are introduced by the following assumptions:

- The sea ice has sufficient thickness to be considered as a halfspace, and exhibits elastic-plastic material behavior (Fig. B-1)
- The inertia of the medium is neglected and only the static stiffness is employed
- The law of conservation of mechanical energy is valid for sea ice and friction losses and other dissipative effects are neglected
- The static values of material properties can be used
- Cratering due to impact does not occur.

From the conservation law (Appendix A)

$$1/2\ m_1 v_1^2 = \int_0^{\xi_y} P \cdot d\xi + \int_{\xi_y}^{\xi_{max}} P_y \cdot d\xi \qquad \text{(B-1)}$$

where: m_1 and v_1 are the mass and impact velocity of the penetrator, P and ξ are the resisting force and displacement in the vertical direction (Fig. B-2), and the subscripts y and max refer to yield and maximum values of the quantities, respectively. The relationship between P and ξ for the indentation of a rigid cylindrical flat plug in an elastic halfspace* was determined first by Boussinesq and is given in Bycroft[32]

---

* The indentation relationship for a rigid cylindrical cone (conical nose projectile) in an elastic halfspace can be found in Ref. 33.

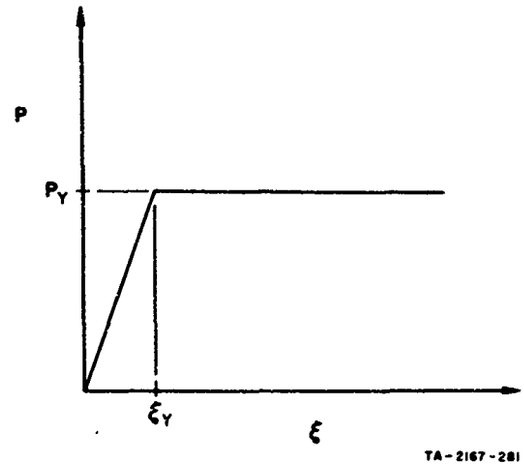

FIG. B-1 LOAD-DISPLACEMENT CURVE

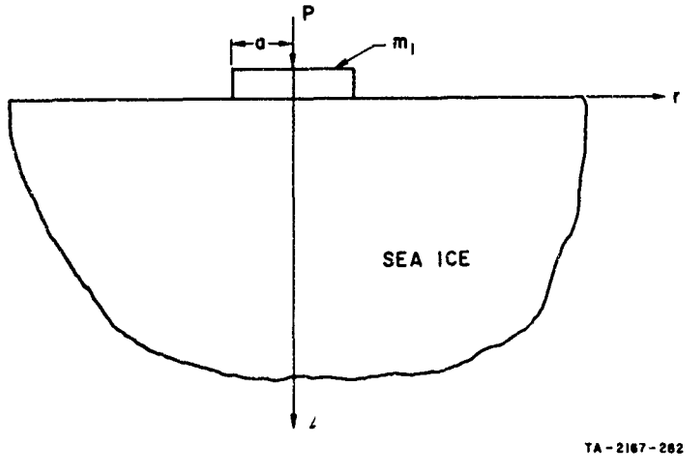

FIG. B-2 SKETCH OF RIGID CYLINDRICAL PLUG INDENTATION PROBLEM

as

$$P = \frac{2aE}{1-\nu^2}\,\xi \tag{B-2}$$

where E and ν are Young's modulus and Poisson's ratio, respectively, for sea ice. Thus, at the yield point

$$\xi_y = P_y \frac{1-\nu^2}{2aE} \tag{B-3}$$

Substituting Eqs. B-2 and B-3 in Eq. B-1 and performing the integration yields

$$1/2\ m_1 v_1^2 = \frac{1}{2}\frac{1-\nu^2}{2aE} P_y^2 + P_y \left(\xi_{max} - P_y \frac{1-\nu^2}{2aE}\right) \tag{B-4}$$

or

$$1/2\ m_1 v_1^2 = P_y\,\xi_{max} - \frac{1}{2} P_y^2 \frac{1-\nu^2}{2aE} \tag{B-5}$$

and finally

$$\xi_{max} = \frac{1}{2P_y}\left(m_1 v_1^2 + \frac{1-\nu^2}{2aE} P_y^2\right) \tag{B-6}$$

where ξ_{max} is the total penetration of the rigid plug (projectile).

Maximum deceleration experienced by a plug in sea ice that exhibits an elastic-plastic retarding force (Fig. B-1) is given simply by Newton's law of motion

$$\left.\frac{d^2\xi}{dt^2}\right|_{max} = \frac{P_y}{m_1} \tag{B-7}$$

Using this relationship, numerical calculations were made with data that were characteristic of the low impact velocity tests:

m_1 = 0.301 slugs (9.688 lb)

a = 0.625 in.

$$P_y = 616 \text{ lb}$$
$$E = 27.3 \times 10^4 \text{ psi}$$
$$\nu = 0.33$$

The value of P_y was obtained from static loading machine tests on the penetration resistance of laboratory sea ice to a 1-1/4-in. diameter blunt penetrator[6], values of E and ν were taken from experimental data obtained in the low impact velocity tests (Table B-1) and Pounder[7], respectively. The deceleration obtained from Eq. B-7 was 63.8 g. This result was low when compared to the experimental values given in Table B-1.

Table B-1

SUMMARY OF EXPERIMENTAL RESULTS OBTAINED FROM DECELERATION VERSUS TIME RESPONSES (OSCILLOGRAMS): LABORATORY SEA ICE TEST SLAB, 1-1/4 INCH DIAMETER BLUNT PENETRATOR

Test Slab	Impact No.	Peak Deceleration (g)	T* (msec)	v_1† (ft/sec)	Perforation	E** (psi)
E	1	181	0.85	18.65	Yes	26.7×10^4
	2	176	0.90	15.85	Yes	28.9
	3	184	0.96	14.20	Yes	31.5
	4	155	1.25	12.95	Yes	22.4
	5	100	3.08	11.89	Yes	6.4
	6	155	1.65	10.45	No	21.1
	7	130	1.75	10.45	No	16.7

* T = time after impact at which peak deceleration occurred

† v_1 = impact velocity

** E = dynamic Young's modulus, calculated from initial slope of deceleration versus time response

However, the simple calculation of deceleration from Newton's law does not consider effects due to sea ice inertia. When the dynamic equations of motion for a halfspace are employed[32], it can be shown that neglecting the inertia terms yields lower values of deceleration than those obtained in a more rigorous treatment of the problem. This phenomenon manifests itself when the relatively lower-valued static yield load is employed in the calculations in lieu of the more appropriate dynamic yield load.

APPENDIX C

CONTROL TEST FOR DYNAMIC FORCE RECORDING SYSTEM

APPENDIX C

CONTROL TEST FOR DYNAMIC FORCE RECORDING SYSTEM

A control test was devised to verify that the penetrator-mounted accelerometer provided an accurate indication of deceleration forces due to impact. The accelerometer was provided with a manufacturer's certificate of calibration; however, because the data acquisition system included an electronic filter with a 3-kc cutoff and the installation of the accelerometer in the penetrator posed some difficulty, it seemed advisable to check the instrumentation system output by an independent control test. For this purpose, Hexcel* blocks were subjected to low velocity impact; the deceleration forces were recorded (Fig. 8) and also calculated from a knowledge of Hexcel properties and observed crushing distances.

An appropriate Hexcel honeycomb core was chosen after preliminary calculations and 3 x $\frac{3}{4}$ x $\frac{3}{4}$-in. sample blocks of this material were compressed in a Baldwin testing machine. The static crushing loads, P_s, and a typical load versus displacement plot obtained from these tests are shown in Table C-1 and Fig. C-1, respectively. The values observed for P_s confirmed the original Hexcel selection. Next, Hexcel blocks of similar size were subjected to impact loading produced by the freely falling projectile. From the oscillographic traces (Fig. C-2), two negative accelerations were noted: a_1, the average maximum value and a_2, the peak value. The impact velocity, v_1, and crushing distance, H, were recorded also.

---

* Hexcel is a lightweight foil honeycomb core material used in sandwich construction and exhibits high energy absorption on impact under nearly constant crushing load.

Table C-1

COMPARISON BETWEEN CALCULATED AND OBSERVED VALUES
OF DECELERATION FOR ACCELEROMETER CONTROL TEST

TEST	v_1	H	P_s	P_d	a_c	a_1	a_2
	ft/sec	(in.)	(lb)	(lb)	(g)	(g)	(g)
1	17.4	0.430	1058	1270	130	185	204
2	17.2	0.450	1080	1185	122	197	218
3	15.7	0.386	1130	1150	118	175	215
4	17.2	0.408	1100	1310	134	175	195
5	15.8	0.426	1020	1060	109	160	215

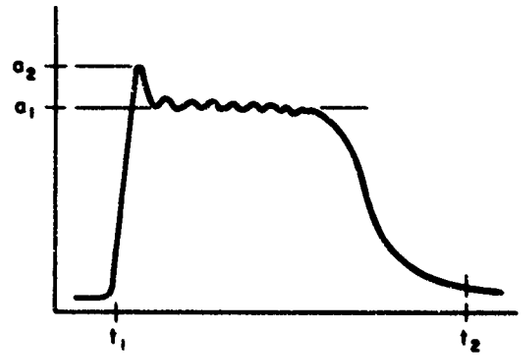

TA-2167-296

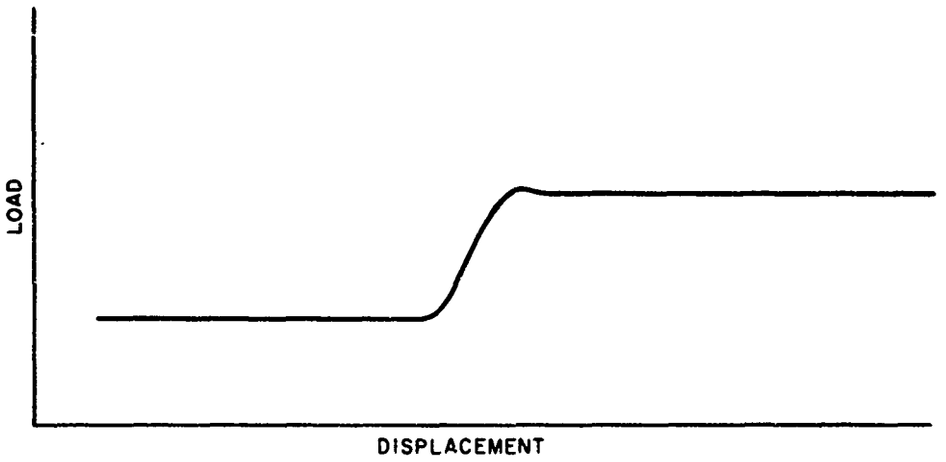

FIG. C-1 AXIAL COMPRESSIVE LOAD vs AXIAL DISPLACEMENT: STATIC TEST

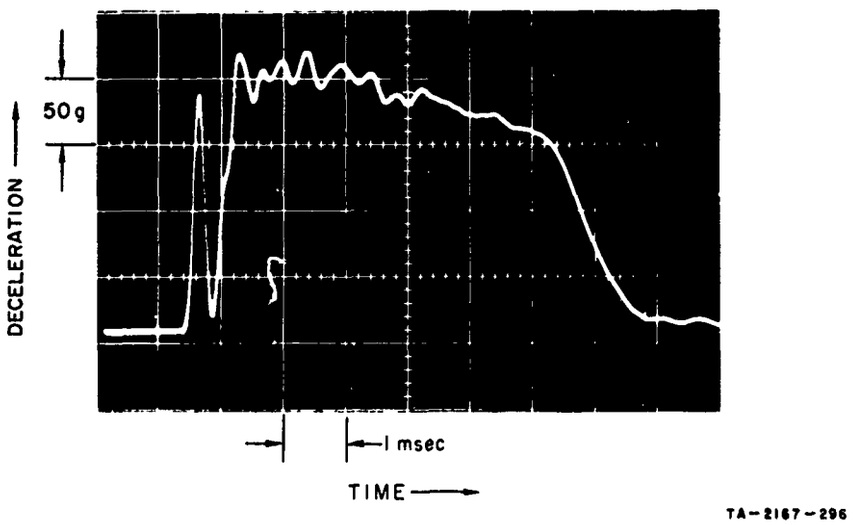

FIG. C-2 AXIAL DECELERATION vs TIME: DYNAMIC TEST

The dynamic crushing load, P_D, was evaluated from the conservation equation relating available kinetic energy at impact to the work done in crushing the block. That is,

$$1/2\ m_1 v_1^2 = P_D H \qquad \text{(C-1)}$$

The acceleration, a_c, was calculated from the law of motion for the projectile, i.e.,

$$P_D - m_1 g = m_1 a_c \qquad \text{(C-2)}$$

It was assumed that impact was plastic (no rebound), that acceleration was constant during crushing, and that the mass of Hexcel being crushed was negligibly small.

The calculated values of acceleration, a_c, compare moderately well with those observed, a_1, (Table C-1). Thus, the accelerations obtained from the oscillographic traces were employed as standard values throughout the test program since the independent control test verified that they were reasonable.

APPENDIX D

EXPERIMENTAL DATA: LABORATORY TESTS AND ARCTIC FIELD TESTS

Table D-1

EXPERIMENTAL DATA: LABORATORY SEA ICE TEST SLABS

Test Slab	Impact No.	Ice Thickness (in.)	Penetrator Profile	Penetrator Diameter (in.)	v_1* (ft/sec)	$1/2\ m_1 v_1^2$ † (ft-lb)	Perforation	Penetration (in.)	Remarks
A	1	6-3/4	Blunt	1-1/4	11.7	20.6	No	3/16	1/4 in., mushy top layer
	2				11.6	20.3	No	5/16	
	3				-	-	No	3/8	
	4				11.3	19.3	No	3/8	
	5		Conical		11.4	19.5	No	1-1/16	
	6				11.7	20.6	No	15/16	
	7				11.6	20.3	No	1	
	8				14.6	32.1	No	1-3/16	
	9				-	-	No	-	Double impact
	10				13.7	28.3	No	1-1/8	
	11		Blunt		13.7	28.3	No	5/16	
B	1	5	Blunt	5/8	-	-	No	7/8	1/8 in., mushy top surface
	2				13.0	24.0	No	3/4	
	3				12.2	21.1	Yes	-	Weak delay
	4				13.2	24.7	No	11/16	
	5				13.4	25.4	No	3/4	
	6		Conical		13.7	26.6	No	1-3/8	
	7				13.8	27.0	No	1-1/2	
	8				13.5	25.9	No	19/16	
	9		Blunt		14.7	30.7	Yes	-	Hilt penetration
	10				13.9	27.5	Yes	-	Strong delay
	11		Conical		13.6	26.2	No	1-13/16	
	12				13.8	27.0	Yes	-	Hilt penetration
	13				13.6	26.2	No	1-3/8	
	15		Blunt		11.9	20.1	No	5/8	
	16				12.5	22.2	No	5/8	
	17				11.8	19.8	Yes	-	Hilt penetration

* v_1 = impact velocity

† m_1 = projectile mass

Table D-1

EXPERIMENTAL DATA: LABORATORY SEA ICE TEST SLABS (continued)

Test Slab	Impact No.	Ice Thickness (in.)	Penetrator Profile	Penetrator Diameter (in.)	v_1* (ft/sec)	$1/2\ m_1 v_1^2$ † (ft-lb)	Perforation	Penetration (in.)	Remarks
C	1	4-1/4	Blunt	1-1/4	-	-	No	1/4	
	2				-	-	Yes	-	
	3				8.2	10.2	No	7/8	
	4				8.2	10.2	No	5/16	
	7		Conical		8.9	12.0	No	1-3/8	
	8				10.5	16.7	No	1-3/8	
	9				9.2	12.8	No	15/16	
	10		Blunt		9.3	13.1	No	3/8	
	11				9.2	12.8	No	9/16	
	12				11.4	19.7	Yes	-	
	13				9.3	13.1	Yes	-	Strong delay
	14				11.4	19.7	No	1/2	
	15				11.[illegible]	19.4	Yes	-	Hilt penetration
D	1	4-1/8	Blunt	1-1/4	16.[illegible]	40.7	No	1/2	
	2				15.4	35.8	No	3/8	
	3				14.3	30.9	Yes	-	Double impact
	4				15.8	37.7	No	1-3/8	Double impact
	5				14.7	32.5	Yes	-	Double impact
E	1	3-3/8	Blunt	1-1/4	10.2	15.8	Yes	-	
	2				8.9	12.0	Yes	-	Hilt penetration
	3				8.6	11.2	Yes	-	Hilt penetration
	4				9.1	12.6	Yes		Weak delay
	5				8.4	10.7	Yes	-	Strong delay
	6				2.4	0.87	No	-	
	7				2.4	0.87	No	-	
	8				2.4	0.87	Yes	-	Strong delay
	9				2.4	0.87	Yes	-	Strong delay
	10				2.4	0.87	No	-	

* v_1 = impact velocity

† m_1 = projectile mass

Table D-1

EXPERIMENTAL DATA: LABORATORY SEA ICE TEST SLABS (continued)

Test Slab	Impact No.	Ice Thickness (in.)	Penetrator Profile	Penetrator Diameter (in.)	v_1* (ft/sec)	1/2 $m_1 v_1^2$ † (ft-lb)	Perforation	Penetration (in.)	Remarks
F	1	2-3/4	Conical	1-1/4	6.5	6.40	No	-	
	2				7.7	8.90	Yes	-	Hilt penetration
	3				8.9	12.00	Yes	-	Strong delay
	4				7.7	8.90	Yes	-	Hilt penetration
	5				6.2	5.80	No	-	
	6				7.0	7.40	No	-	
	7				7.0	7.40	Yes	-	Strong delay
	8				7.1	7.60	No	-	
	9			5/8	6.1	5.25	Yes	-	Hilt penetration
	10				6.2	5.45	Yes	-	Hilt penetration
	11				7.1	7.15	Yes	-	Weak delay
	12				6.5	5.98	Yes	-	
	13				5.5	4.27	No	-	
	14				5.5	4.27	No	-	
	15				5.5	4.27	Yes	-	Strong delay
	16				5.5	4.27	No	-	
	17				5.6	4.27	No	-	
	18				6.3	5.62	Yes	-	Hilt penetration
	19				6.2	5.45	No	-	
	20				6.2	5.45	No	-	
	21				6.2	5.45	Yes	-	Hilt penetration
G	1	10	Blunt	1-1/4	61.0	43.2	No	1/4	Perforation not obtained,
	2				102.0	121.0	No	3/8	cratering was evident,
	3				199.0	462.0	No	2-1/8	craters not measured.
	4				237.0	655.0	No	2-7/8	
H	1	10-3/4	Blunt	1-1/4	414.0	2000.0	Yes	-	Perforation due to shear,
	2				252.0	740.0	No	5-5/8	conical plug with small
	3				226.0	592.0	No	-	cone angle.

* v_1 = impact velocity

† m_1 = projectile mass

Table D-1

EXPERIMENTAL DATA: LABORATORY SEA ICE TEST SLABS (concluded)

Test Slab	Impact No.	Ice Thickness (in.)	Penetrator Profile	Penetrator Diameter (in.)	v_1* (ft/sec)	$1/2\ m_1 v_1^2$ † (ft-lb)	Perforation	Penetration (in.)	Remarks
I	1	11-1/2	Conical	1-1/4	428.0	1960.0	Yes	-	7-1/2 x 6-3/4 in. crater
	2		Blunt		411.0	1970.0	Yes	-	4 x 3-1/4 in. crater
J	1	15-1/2	Blunt	1-1/4	258.0	775.0	No	3-7/16	3-1/2 x 3 in. crater.
	2				402.0	1880.0	No	7-1/16	Projectile produced a
	3		Conical		436.0	2035.0	No	12-1/16	crater containing ice fragments and pulverized snow.
K	1	8-1/2	Blunt	1-1/4	324.0	1225.00	Yes	-	
L	1	10-1/2	Blunt	1-1/4	243.0	687.0	No	2-3/4	3-1/2 x 3 in. crater.
	2				244.0	694.0	No	3-3/4	4 x 4 in. crater.
	3				292.0	990.0	No	4-3/4	4 x 5 in. crater, well
	4				370.0	1590.0	Yes	-	defined cylindrical shear penetration.
M	1	9-3/4	Conical	1-1/4	273.0	798.0	No	5-1/8	4-1/4 x 5-1/2 in. crater, no shear.
	2				305.0	995.0	Yes	-	
	3				303.0	980.0	Yes	-	
N	1	15-3/4	Blunt	1-1/4	331.0	1275.0	No	4-1/4	4-1/2 x 4-1/8 in. crater.
	2				389.0	1760.0	No	5-1/4	6 x 6-1/2 in. crater.
	3				408.0	1940.0	No	6-3/8	
	4				430.0	2150.0	No	7-5/8	

* v_i = impact velocity

† m_i = projectile mass

Table D-2

EXPERIMENTAL DATA: ARCTIC SEA ICE

Test Series	Impact No.	Ice Thickness (in.)	Penetrator Profile	Penetrator Diameter (in.)	v_1* (ft/sec)	1/2 $m_1 v_1^2$† (ft-lb)	Perforation	Penetration (in.)	Remarks
A	1	8	Blunt	1-1/4	262.0	798.0	No	2-3/4	4-1/2" x 3" crater
B	1	10-3/4	Blunt	1-1/4	371.0	1600.0	No	3-7/8	5-1/4" x 4-3/4" crater
	2				418.0	2030.0	No	5-1/8	6" x 5-1/8" crater
	3				465.0	2520.0	No	7	8" x 7-1/4" crater
	4				494.0	2840.0	Yes		7" x 6" crater
C	1	9-3/4	Blunt	1-1/4	119.0	165.0	No	1-7/8	2-1/2" x 2" crater
	2				332.0	1285.0	No	3-1/2	4-1/2" x 4-1/2" crater
	3				444.0	2295.0	Yes		8" x -- crater
D	1	11-3/8	Blunt	1-1/4	380.0	1820.0	No	4-5/8	6" x 4-5/8" crater
	2		Conical		308.0	1195.0	No	5-7/8	5-8" x 5-7/8" crater
	**3		Blunt		280.0	989.0	No	3-3/4	3" x 3-3/4" crater
	**4				417.0	2190.0	No	4-5/8	5" x 4-5/8" crater
	**5				415.0	2170.0	No	4-7/8	6-1/2" x 4-7/8" crater
E	1	11-1/4	Blunt	1-1/4	419.0	2210.0	No	5	7" x 5" crater
	2				433.0	2360.0	No	4-3/4	7" x 4-3/4" crater
	3				422.0	2240.0	No	4-7/8	8" x 4-7/8" crater
	4		Conical		469.0	2770.0	No	7-5/8	8" x 7-5/8" crater
F	1	13	Blunt	1-1/4	409.0	2110.0	No	4	8" x 4-5/8" crater
	2		Conical		406.0	2080.0	No	7	10" x 6-7/8" crater
G	1	15-3/4	Blunt	6	--	--	No	3/4	
	2				--	--	No	3	2" overlying sea water, no cracks, no fissures, shear penetration observed clearly.

* v_1 = impact velocity

† m_1 = projectile mass

** Tests at inclined incidence, $\alpha = 17.3^0$.

Table D-2

EXPERIMENTAL DATA: ARCTIC SEA ICE (concluded)

Test Series	Impact No.	Ice Thickness (in.)	Penetrator Profile	Penetrator Diameter (in.)	v_1 * (ft/sec)	$1/2\ m_1 v_1^2$ † (ft-lb)	Perforation	Penetration (in.)	Remarks
H	1	16	Blunt	6	124.0	9890.0	Yes		Cylindrical-conical plug observed, unable to remove plug thru sea ice, 11-1/2" x 2" crater.
I	1	16-1/4	Blunt	6	53.2	1820.0	No	1/2	10-1/2" x 1-3/4" crater
	2				79.5	4070.0	No	1-3/8	8-1/2"-10-1/2 x 2" crater
	3				100.0	6440.0	No	2-3/4	11" x 2-1/2" crater
	4				84.5	4600.0	No	1-3/4	12" x 2-3/8" crater
J	1	16	Blunt	6	96.5	5990.0	No	1-3/4	10" x 2-1/4" crater
	2				--	--	--	--	Gun jammed
	3				--	--	--	--	Gun jammed

* v_1 = impact velocity

\+ m_1 = projectile mass

Table D-3

EXPERIMENTAL DATA: STYROFOAM TEST SLABS

Test Slab	Impact No.	Styrofoam Thickness (in.)	Styrofoam Type	Penetrator Profile	Penetrator Diameter (in.)	v_1* (ft/sec)	z_c† (in.)	$1/2m_1v_1^2$** (ft-lb)	t/D‡	Perforation	Penetration (in.)	Remarks
1-I	1	1	FR	Blunt	5/8	3.47		1.70	1.6	Yes		
1-III	1	1	FR	Blunt	5/8	1.83		0.475	1.6	No	1/16	
	2					2.59		0.948	1.6	No	3/16	
	3					2.95		1.23	1.6	No	1/4	
	4					3.47		1.70	1.6	Yes		Hilt penetration
	5					3.47		1.70	1.6	Yes		Strong delay
	6					4.02		2.28	1.6	Yes		Hilt penetration
1-IV	1	1	FR	Blunt	1-1/4	4.63		3.22	.8	Yes		Slab Split up in Segments
1-V	1	1	FR	Blunt	1-1/4	2.52		0.958	0.8	No		
	2					4.63		3.22	0.8	Yes		Slab Split up in Segments
1.5-I	1	1-1/2	FR	Blunt	5/8	2.32		0.760	2.4	No	1/8	
	2					3.06		1.33	2.4	No	1/4	
	3					3.38		1.60	2.4	No	5/16	
	4					3.66		1.90	2.4	No	1/4	
	5					4.02		2.28	2.4	No	9/16	
	6					4.33	1-1/8	2.66	2.4	Yes		Hilt penetration
1.5-II	1	1-1/2	FR	Blunt	1-1/4	4.41		2.93	1.2	No	1/16	
	2					4.81		3.48	1.2	Yes		Slab Split up in Segments
2-I	1	2	FR	Blunt	1-1/4	--		--	1.6	No	9/16	
	2					--		--	1.6	No	15/16	
	3					9.86		14.6	1.6	Yes		
	4					9.86		14.6	1.6	Yes		Weak delay

* v_1 = impact velocity

\+ z_c = length of cylindrical shear yield surface at critical impact velocity

** m_i = projectile mass

‡ t/D = ratio, styrofoam thickness to penetrator diameter

Table D-3

EXPERIMENTAL DATA: STYROFOAM TEST SLABS (continued)

Test Slab	Impact No.	Styrofoam Thickness (in.)	Styrofoam Type	Penetrator Profile	Penetrator Diameter (in.)	v_i* (ft/sec)	z_c† (in.)	$1/2m_iv_i^2$** (ft-lb)	t/D‡	Perforation	Penetration (in.)	Remarks
2-II	1	2	FR	Blunt	1-1/4	9.86		14.6	1.6	Yes		Slab Split up in Segments
2-IV	6	2	FR	Blunt	1-1/4	6.65		6.66	1.6	No		
	7					6.65		6.66	1.6	No		
	1					8.10		9.89	1.6	No		
	2					9.40	1-1/4	13.3	1.6	Yes		
	3					9.40		13.3	1.6	No		
	4					9.40		13.3	1.6	No		
	5					10.8	1-5/16	17.4	1.6	Yes		Hilt penetration
2-V	2	2	FR	Blunt	5/8	4.77		3.09	3.2	No		
	3					4.77		4.77	3.2	No		
	1					5.74		5.74	3.2	Yes		Strong delay
	4					6.42		6.42	3.2	Yes		Strong delay
	5					7.33		7.33	3.2	Yes		Hilt penetration
	6					11.3		8.94	3.2	Yes		Weak delay
3-II	1	3	FR	Blunt	1-1/4	7.42		8.28	2.4	No		
	2					8.59		11.1	2.4	No		
	3					9.93		14.8	2.4	No		
	4					11.3		19.2	2.4	No		
	5					12.1		22.0	2.4	No		
	6					13.2		26.1	2.4	Yes		Strong delay
	7					13.2	2-7/8	26.1	2.4	Yes		Hilt penetration
	8					14.4	2-1/2	31.3	2.4	Yes		Hilt penetration
3-III	6	3	FR	Blunt	5/8	5.43		4.17	4.8	No		
	4					6.45		5.88	4.8	No		
	5					6.45		5.88	4.8	No		

* v_i = impact velocity

\+ z_c = length of cylindrical shear yield surface at critical impact velocity

** m_i = projectile mass

‡ t/D = ratio, styrofoam thickness to penetrator diameter

Table D-3

EXPERIMENTAL DATA: STYROFOAM TEST SLABS (concluded)

Test Slab	Impact No.	Styrofoam Thickness (in.)	Styrofoam Type	Penetrator Profile	Penetrator Diameter (in.)	v_1* (ft/sec)	z_c+ (in.)	1/2 $m_1 v_1^2$** (ft-lb)	t/D‡	Perforation	Penetration (in.)	Remarks
3-III	3	3	FR	Blunt	5/8	7.77	2-15/16	8.53	4.8	Yes		Strong delay
	1					8.66	2-7/8	10.6	4.8	Yes		
	2					8.66	2-7/8	10.6	4.8	Yes		
	7					10.4	2-13/16	15.4	4.8	Yes		Hilt penetration
4-I	1	4	FR	Blunt	1-1/4	8.89		11.9	2.4	No		
	2					11.8		21.1	2.4	No		
	3					14.4		31.1	2.4	No		
	4					16.7		41.2	2.4	No		
	5					17.8		47.4	2.4	No		
	6					19.8		59.3	2.4	No		
4-II	9	4	FR	Blunt	5/8	10.0		14.1	6.4	No		
	8					11.3		17.9	6.4	No		
	7					13.1		24.2	6.4	No		
	6					15.3	3-7/8	33.4	6.4	Yes		Hilt penetration
	5					17.2	3-1/2	41.7	6.4	Yes		Hilt penetration
	4					18.7	3-1/2	49.7	6.4	Yes		Weak delay
	1				1-1/4	19.8	3-1/2	59.3	2.4	No		
	2				1-1/4	19.8	3-1/2	59.3	2.4	Yes		Hilt penetration
	3				5/8	19.8	3-7/8	55.8	6.4	Yes		Weak delay
10-I	1	10	BB	Blunt	1-1/4	58.0		39.2	8	No	3-5/8	
	3					97.2		110.0	8	No	6-3/4	
	4					135.5		216.0	8	Yes		Partial expulsion
	5					157.5		291.0	8	Yes		Clean perforation
	2					199.5		466.0	8	Yes		

* v_1 = impact velocity

\+ z_c = length of cylindrical shear yield surface at critical impact velocity

** m_1 = projectile mass

‡ t/D = ratio, styrofoam thickness to penetrator diameter

APPENDIX E

COMPUTER PROGRAM

Appendix E

COMPUTER PROGRAM

The program was written in Algol 60 for the Burroughs B5500 digital computer machine and calculates:*

- Critical impact velocity, $V_1(v_c)$
- Critical impact energy, MV2 $(1/2m_1v_c^2)$
- Thickness-diameter ratio, T2A(t/D)

from the following inputs:

- Projectile weight, $M(m_1g)$, and radius, A(D/2)
- Sea ice thickness, T(t)
- Sea ice tensile strength, SIGMAH (σ_φ), shear strength, TAU (τ_0) and compression modulus, K = AA/T ($k = E/t$)
- Compression ratio, ALPHA (α).

Moreover, based on the Assur theory for the relative strength of sea ice, a subroutine was developed and programmed to relate sea ice tensile strength, σ_σ, to

- Sea ice temperature, T(T), and salinity content, SAL(S).

The subroutine fits the Assur diagram curves (Fig. 43) by 4th order polynomial expressions in the temperature range, $0^oC < T \leq -23^oC$ $(-10^oF \leq T \leq +32^oF)$. To obtain σ_φ for arbitrary given values of T and S, an ordinate is erected at T to intersect the family of four salinity curves; then, a four-point interpolation procedure is used to calculate σ_φ at S.

In the present program, τ_0 is calculated from σ_φ $(\tau_0 = \sigma_\varphi/2)$ and k is obtained from a characteristic value of E $(k = E/t)$.

---

* Quantities; V_1, MV2, etc., are machine variables, and quantities in parentheses, v_c, t/D, etc., are theory variables.

```
BEGIN
     REAL LOW, MID, UP, PHIL, PHIR, V1, DIFF1,DIFF2,DIFF3, Z2, Z1, ABF,
AA,ALFA,  KK1,KK2,KK3,C2,   S, C, S2, Y1, Y2, Y3, K1, K2, K3, ABY, FBAR,
                    I, T, M, K, A, TAU, SIGMA, CON, CONS, EPS, PHI, ETA;
REAL MV2, T2A;
INTEGER TAUJ;
     LABEL LAB1, LAB2, REED, FIN, DOWN;
     INTEGER J, L;
     FILE CRVAHE(2,10);
     FILE OUT PRINT 4(2,15);
FORMAT FMR(/"EITHER THERE IS NONE OR MORE THAN ONE ROOT IN THE INTERVAL
(",F6.3,",",F6.3,"), Y1=",E12.5,"Y2=",E12.5/),
       FMZ(/"ZC IS NOT IN THE INTERVAL[0.0,T],ZC=",E12.5/),
       FMT1(/"ZC1 AND ZC2 DO NOT INTERSECT IN THE INTERVAL [2.0,100.0],D
IFF1=",E12.5,"DIFF2=",E12.5/),
       FMT4("AFTER 100 ITERATIONS ZC1 AND ZC2 DID NOT CONVERGE"/
"I=",F5.1,X2,"ZC2-ZC1=",E12.5,X2,"ZC2=",E12.5,X2,"ZC1=",E12.5,X2,"PHI=",
E12.5,X2,"V1=",E12.5),
FMT3(///"M=",F7.3,"  A=",F7.3,"  TAU=",F7.3,"  T=",F7.3,
    "  SIGMAH=",F7.3,"  SIGMAV=",F7.3,
    "  SAL=",F5.2,"  TEMP=",F5.2,"  ALFA=",F5.2,
               //"  T","       ZC","       PHI","         V1",X9,"K/T",
X7,"T2A",X7,"MV2",X7,"K"),
FMT2(F5.2,7F10.2);
REAL SIGMAH,SIGMAV;
REAL X, TEMP, SAL, Y;
INTEGER HORVER;
FORMAT FSAL1("ERROR"/,"TEMPERATURE IS OUT OF RANGE"/),
FSAL5("Y1234",4E20.8/),
       FSAL4("TEMP=",E20.8,"SAL=",E20.8,"SIGMA=",E20.8/),
       FSAL2("ERROR"/,"SALINITY IS OUT OF RANGE"),
  FSAL3("ERROR"/,"SPECIFIED SALINITY AND TEMPERATURE DO NOT INTERSEC");
REAL PROCEDURE W1(X);
     VALUE X ; REAL X ;
   BEGIN W1←4.25014978+(1.03140271+(-0.0968482243+(3.98192990-3
            -5.62788391Q-5 ×X)×X)×X)×X  END PROCEDURE W1 ;
REAL PROCEDURE W2(X);
     VALUE X ; REAL X ;
   BEGIN W2←2.94850092+(0.93067281+(-0.0712832277+(2.64380797Q-3
            -3.58522651Q-5 ×X)×X)×X)×X  END PROCEDURE W2 ;
REAL PROCEDURE W3(X);
     VALUE X ; REAL X ;
   BEGIN W3←2.41510297+(0.594029968+(-0.02658944442+4.829075860-4×X)×X)×X
                                        END PROCEDURE W3 ;
REAL PROCEDURE W4(X);
     VALUE X ; REAL X ;
   BEGIN W4←-3.8375808+(1.36678625 +(-0.0668767776+1.173017730-3×X)×X)×X
                                        END PROCEDURE W4 ;
PROCEDURE SALINITY(TEMP,SAL,HORVER,Y);
     VALUE TEMP, SAL , HORVER;
     REAL  TEMP, SAL, Y ;
INTEGER HORVER;
  BEGIN  LABEL   ADJUST, QUIT, ERR ;
         REAL X1,X2,X3,X4,X34,X12,YONE,YTWO,YTHREE,YFOUR;
REAL CONH,CONV;
X1←3.0+7.0×(SAL-2.0)/18.0;
X2←29.0-X1;
X3←TEMP-X1;
X4←1.3×X3/X2;
X12←0.9×X3/X2;
CONH←27.0;
CONV←22.0-X12;
```

```
     IF TEMP ≥ 30.0 OR TEMP ≤ 2.0 THEN BEGIN WRITE(PRINT,FSAL1);
                                   GO TO QUIT END;
     IF SAL > 20.0 OR SAL < 2.0 THEN   BEGIN WRITE(PRINT,FSAL2);
                                   GO TO QUIT END;
IF SAL=20.0 THEN BEGIN IF TEMP>12.5 THEN BEGIN Y←W4(TEMP);
                                                GO TO ADJUST END;
                       IF TEMP>9.5 THEN BEGIN Y←1.92307×TEMP-18.269165;
                                                GO TO ADJUST END;
                                                GO TO ERR END;
IF SAL=10.0 THEN BEGIN IF TEMP>5.7 THEN BEGIN Y←W3(TEMP);
                                                GO TO ADJUST END;
                       IF TEMP>4.3 THEN BEGIN Y←3.57142×TEMP-15.357106;
                                                GO TO ADJUST END;
                                                GO TO ERR END;
IF SAL=5.0 THEN BEGIN  IF TEMP>2.7 THEN BEGIN Y←W2(TEMP);
                                                GO TO ADJUST END;
                       IF TEMP>2.0 THEN BEGIN Y←7.1428×TEMP-14.2856;
                                                GO TO ADJUST END;
                                                GO TO ERR END;
IF SAL=2.0 THEN BEGIN  IF TEMP>1.2 THEN BEGIN Y←W1(TEMP);
                                                GO TO ADJUST END;
                                                GO TO ERR END;
          X1 ← SAL - 2.0 ;              YONE  ← W1(TEMP) ;
          X2 ← SAL - 5.0 ;              YTWO  ← W2(TEMP) ;
          X3 ← SAL - 10.0;              YTHREE← W3(TEMP) ;
          X4 ← SAL - 20.0;              YFOUR ← W4(TEMP) ;
          X34←X3×X4 ;
          X12←X1×X2 ;
     IF TEMP > 12.1 THEN BEGIN Y←-YONE×X2×X34/432.0+YTWO×X1×X34/225.0
          -YTHREE×X12×X4/400.0 + YFOUR×X12×X3/2700.0;GO TO ADJUST END;
     IF TEMP > 9.5 THEN BEGIN  YFOUR←1.92307×TEMP-18.269165;
                               Y←-YONE×X2×X34/432.0+YTWO×X1×X34/225.0
          -YTHREE×X12×X4/400.0 + YFOUR×X12×X3/2700.0;GO TO ADJUST END;
     IF TEMP > 5.7 THEN BEGIN IF SAL > 10.0 THEN GO TO ERR;
                               Y←YONE×X2×X3/24.0-YTWO×X1×X3/15.0
                                 +YTHREE×X12/40.0; GO TO ADJUST END ;
     IF TEMP > 4.3 THEN BEGIN IF SAL>10.0 THEN GO TO ERR ;
                                    YTHREE←3.57142×TEMP-15.357106;
                               Y←YONE×X2×X3/24.0-YTWO×X1×X3/15.0
                                 +YTHREE×X12/40.0; GO TO ADJUST END ;
     IF TEMP > 2.7 THEN BEGIN IF SAL>5.0 THEN GO TO ERR ;
                               Y←-(YONE×X2-YTWO×X1)/3; GO TO ADJUST END;
               IF SAL > 5.0 THEN GO TO ERR ;   YTWO←7.1428×TEMP-14.2856;
                               Y←-(YONE×X2-YTWO×X1)/3.0;
ADJUST: IF HORVER=2        THEN BEGIN IF TEMP>23.0 THEN Y←Y+1.0;
                  Y←CONV×Y;  GO TO QUIT END;
                  Y←CONH×Y;  GO TO QUIT;
ERR: WRITE(PRINT,FSAL3); GO TO FIN;
QUIT; END PROCEDUR SALINITY ;
PROCEDURE ROOT;
      BEGIN     LABEL L1;
                                          PHIL←0.2 ; PHIR← 1.0 ;
                  S←SIN(PHIL); C←COS(PHIL); S2←S×S; C2←C×C;
                  Y1←2.0×(S2×S-ETA×C×(2.0×C2-1.0))/(S2×C2×C);
          S←SIN(PHIR); C←COS(PHIR); S2←S×S;   C2←C×C;
                  Y3←2.0×(S2×S-ETA×C×(2.0×C2-1.0))/(S2×C2×C);
        KK1←SIGN(Y1); KK3←SIGN(Y3);
             IF KK1=KK3 THEN BEGIN WRITE(PRINT,FMR,PHIL,PHIR,Y1,Y3);
                                     GO TO DOWN END;
L1;       PHI←0.5×(PHIR-PHIL)+PHIL;
          S←SIN(PHI); C←COS(PHI); S2←S×S;   C2←C×C;
                  Y2←2.0×(S2×S-ETA×C×(2.0×C2-1.0))/(S2×C2×C);
          ABY←ABS(Y2);
             IF ABY>EPS AND PHIR-PHIL>EPS THEN BEGIN KK2←Y2/ABY;
             IF KK1=KK2 THEN BEGIN      PHIL←PHI; Y1←Y2; GO TO L1 END;
                           KK3←KK2; PHIR←PHI; Y3←Y2; GO TO L1 END;
```

```
          END;
PROCEDURE ZCEE(VEE,DIFF);
     VALUE VEE;
     REAL VEE,DIFF;
      BEGIN          Z1←     CON×VEE;
                IF (Z1<0) OR (Z1>T) THEN BEGIN WRITE(PRINT,FMZ,Z1);
                                                GO TO DOWN END;
                     ETA← A/(T-Z1);
                     ROOT;
                     S←SIN(PHI);  C←COS(PHI);
                     FBAR←(S+2.0×ETA×C)/(S×C×C);
SIGMA← SIGMAH;
Z2←SIGMA×FBAR/(ETA×ETA×K);DIFF←Z2-Z1;
          END;
                      L←0;
REED:READ(CRVAHE,/,SAL,TEMP) [FIN];
      SALINITY(TEMP,SAL,1,SIGMAH);
TAU←0.5×SIGMAH;    SIGMAV←0.0;
READ(CRVAHE,/,M,A,T) [FIN];
FOR ALFA←0.7 STEP 0.1 UNTIL 1.0 DO BEGIN
                IF L=4 THEN BEGIN WRITE(PRINT[PAGE]);  L←0 END;
WRITE(PRINT,FMT3,M,A,TAU,T,SIGMAH,SIGMAV,SAL,TEMP,ALFA); L←L+1;
T2A←0.5×T/A;
FOR AA←50000,100000,142260, 238000,273000 DO BEGIN K←AA/T;
    CON←SQRT(M×12.0/(ALFA×32.2×3.1415927×A×(2.0×TAU+ALFA×A×K)));
          I←0.0;  EPS←0.0000001;
          UP←T/CON-0.5; LOW←0.1; MID←0.5×(UP-LOW);
          ZCEE(LOW,DIFF1);
          ZCEE(MID,DIFF2);
          ZCEE(UP ,DIFF3);
          K1←DIFF1/ABS(DIFF1);  K3←DIFF3/ABS(DIFF3); ABF←ABS(DIFF2);
               IF K1=K3 THEN BEGIN WRITE(PRINT,FMT1,DIFF1,DIFF3);
                                                    GO TO DOWN END;
LAB2:     I←I+1.0;
          K2←DIFF2/ABF;
               IF K1=K2  THEN BEGIN LOW←MID; DIFF1←DIFF2;
                                                      GO TO LAB1 END;
          K3←K2; UP←MID; DIFF3←DIFF2;
LAB1:     MID←0.5×(UP-LOW)+LOW;
          ZCEE(MID,DIFF2);
          ABF←ABS(DIFF2);
               IF ABF≤EPS OR UP-LOW≤EPS THEN BEGIN PHI←57.2958×PHI;
MV2←M×MID×MID/64.4;
WRITE(PRINT,FMT2,T,Z2,PHI,MID,K,T2A,MV2,AA);
                                                      GO TO DOWN END;
               IF I<100.0 THEN GO TO LAB2;
          WRITE(PRINT,FMT4,I,DIFF2,Z2,Z1,PHI,MID);
DOWN:END  END;
      GO TO REED;
FIN: END.
```

REFERENCES

1. "Ice and Snow," edited by W. D. Kingery, (M.I.T. Press, Cambridge, Mass., 1963).

2. Wilson, D. P., "The Arctic, a Selective Bibliography," NSL Technical Memo No. 904.3-03-64 (1964).

3. "Proceedings of the International Conference on the Physics of Ice and Snow," edited by Z. Yosida, Hokkaido University, Sapporo, Japan, (August 1966).

4. Benert, R., "Penetration of Shaped Charges into Frozen Ground," CRREL TR-130, U.S. Army Materiel Command, Hanover, N.H. (November 1963).

5. Charest, J., P. Duler, and J. Rinehart, "Mechanics of Penetration of Piles into Permafrost," CRREL TR-122, U.S. Army Materiel Command, Hanover, N.H. (September 1965).

6. Ross, Bernard, "Penetration Studies of Ice with Application to Arctic and Subarctic Warfare," for Submarine Arctic Warfare and Scientific Program, Contract Nonr-2332(00), Stanford Research Institute, Menlo Park, California (November 1965).

7. Pounder, E. R., "The Physics of Ice," (Pergamon Press, Oxford, England, 1965), p. 11-29, 86-113.

8. Assur, A., "The Composition of Sea Ice and Its Tensile Strength," Arctic Sea Ice, Pub. No. 598 of the National Academy of Sciences-National Research Council, Washington, D. C. (1958).

9. Weeks, W. F., "The Structure of Sea Ice: A Progress Report," Arctic Sea Ice Conference Proceedings, NAS-NRC Pub. No. 598 (1958).

10. Butkovich, T. R., "Strength Studies of Sea Ice," U.S. Army SIPRE Research Report No. 20 (1956).

11. Pounder, E. R. and E. M. Little, "Some Physical Properties of Sea Ice," I, Canadian Jour. of Physics, 37, 443 (1959).

12. Voitkovskii, K. F., "The Mechanical Properties of Ice," Trans, AMS-T-R-391, American Meteorol. Soc., U.S. Dept. of Commerce (1960).

13. Dykins, J. E., "Ice Engineering-Tensile and Bending Properties of Sea Ice Grown in a Confined System," Tech. Rpt., R415, U.S. Naval Civil Engineering Laboratory, Port Huenome, California (January 1966).

14. Tabata, T., "The Flexural Strength of Small Sea Ice Beams," to appear in Proc. Int'l. Conf. on the Physics of Ice and Snow, Hokkaido University, Sapporo, Japan (August 1966).

15. Bailey, J. T., S. Evans, and G. de Q. Robin, "Radio Echo Sounding of Polar Ice Sheets," Nature, 204, 4957, 420-421 (October 31, 1964).

16. Evans, S., and G. de Q. Robin, "Glacier Depth Sounding from the Air," Nature, 210, 5039, 883-885 (May 28, 1966).

17. Bilello, M. A., "Sea Ice Temperature Curves for Slidre Fjord, Canada," Personal Communication, CRREL, U.S. Army Materiel Command, Hanover, N.H. (April 1965).

18. Livingston, C. W., "Bomb Penetration Tests, Fort Churchill, Canada," U.S. Army SIPRE Tech. Rpt. 71 (September 1960).

19. Goldsmith, W., "Impact," (Edw. Arnold, Ltd., London, 1960).

20. Goldsmith, W., T. W. Liu, and S. Chulay, "Plate Impact and Perforation by Projectiles," Experimental Mechanics, 5, 12 (December 1965).

21. Florence, A. L., and A. E. Gorum, "Interaction of Projectiles and Composite Armor," Proc. of 2nd Symposium on Light Weight Armor Materials, Mellon Institute, Pittsburgh, Pa. (May 1966).

22. Tetelman, A. S., and E. J. McEvily, "Fracture of Structural Materials," (John Wiley and Sons, Inc., New York, 1967).

23. Zebel, N. R., "Containment of Fragments from Runaway Reactor," SRI Tech. Rpt. No. 1, Poulter Laboratories, Contract No. AT(04-3)-115 for the U.S. Atomic Energy Commission (April 1958).

24. Hill, R., "The Mathematical Theory of Plasticity," (Oxford Press, England, 1950), p. 256.

25. Zubov, N. N., "L'dy Arktiki (Arctic Ice)," (Izd. Glavesmorputi, Moscow, 1945).

26. Tsurikov, V. L., "The Problem of Ice Strength, " Severnyi Morskoi Put, 16, 45-74 (1939).

27. Anderson, D. L., "A Model for Determining Sea Ice Properties," Arctic Sea Ice, Washington, NAS-NRC Pub. No. 598 (1958).

28. Anderson, D. L., and W. F. Weeks, "A Theoretical Analysis of Sea Ice Strength," Amer. Geophys. Union. Trans., 39, 4 (1958).

29. Hanagud, S., "Finite Amplitude Spherical Waves in a Locking-Relaxing Solid," Invited Research Lecture, Proc. 5th U.S. Nat'l Cong. of Appl. Mech., p. 63-77 (1966).

30. Hanagud, S., "Snow as a Locking Material-High Pressure Properties of Snow," to appear in the Proc. of the Int'l. Conf. on the Physics of Ice and Snow, Hokkaido University, Sapporo, Japan (August 1966).

31. Napadansky, H., "Dynamic Response of Snow to High Rates of Loading," CRREL TR-119, U.S. Army Materiel Command, Hanover, N. H. (1964).

32. Bycroft, G. N., "Forced Vibrations of a Rigid Circular Plate on a Semi-Infinite Elastic Space," Trans. Roy. Soc. London, Series A, 248, 327-368 (January 1956).

33. Sneddon, I. N., "Fourier Transforms," (McGraw-Hill, Inc., New York, 1951) p. 462-468.

UNCLASSIFIED

Security Classification

DOCUMENT CONTROL DATA - R & D

(Security classification of title, body of abstract and indexing annotation must be entered when the overall report is classified)

1. ORIGINATING ACTIVITY (Corporate author)	2a. REPORT SECURITY CLASSIFICATION
Stanford Research Institute 333 Ravenswood Avenue Menlo Park, California 94025	UNCLASSIFIED 2b. GROUP

3. REPORT TITLE

PENETRATION STUDIES OF ICE WITH APPLICATION TO ARCTIC AND SUBARCTIC WARFARE—PHASE II STUDY

4. DESCRIPTIVE NOTES (Type of report and inclusive dates)

Final Report

5. AUTHOR(S) (First name, middle initial, last name)

Ross, Bernard

6. REPORT DATE	7a. TOTAL NO. OF PAGES	7b. NO. OF REFS
May 1967	168	33

8a. CONTRACT OR GRANT NO.	9a. ORIGINATOR'S REPORT NUMBER(S)
Nonr-2332(00) b. PROJECT NO. RF 018-02 c. RF 018-02-06 d. NR 274-008	NWRC-3072 9b. OTHER REPORT NO(S) (Any other numbers that may be assigned this report)

10. DISTRIBUTION STATEMENT

This document is subject to special export controls and each transmittal to foreign governments or foreign nationals may be made only with prior approval of the Office of Naval Research (Code 462).

11. SUPPLEMENTARY NOTES	12. SPONSORING MILITARY ACTIVITY
	NOL, White Oak, Maryland

13 ABSTRACT

Impact tests with freely falling and explosively powered projectiles were performed on laboratory sea ice test slabs made from frozen seawater at Stanford Research Institute, and on Arctic sea ice *in situ* at Point Barrow, Alaska. In the experiments, particular attention was devoted to studying the mechanisms of penetration and perforation. Ranges of values investigated for the basic parameters were: impact velocity, 8-20 ft/sec and 50-494 ft/sec; projectile weights, 0.75, 9.69, and 41.5 lb; penetrator diameters, 5/8 in., 1-1/4 in., and 6 in.; penetrator profiles, blunt and conical; sea ice thickness, 3-3/8 - 17 in.; sea ice temperature, +7°F - +32°F, and sea ice salinity, 7.2 - 17.1 ppm. All tests were carried out at normal incidence except for one sequence on Arctic sea ice in which the angle of incidence was 17.3° from vertical.

Results of the tests indicate that a cylindrical, blunt-end penetrator was more effective in perforation than a corresponding penetrator with a conical end. The blunt penetrator, impacting at normal incidence, perforated both laboratory sea ice and Arctic sea ice by expelling a cylindrical-conical shear plug from the test specimen. For this behavior, a mathematical model was constructed and a theoretical analysis developed from which the minimum impact velocity for perforation (critical velocity) was obtained. The critical velocity was found to be a function of projectile mass and diameter, and sea ice thickness, shear strength, tensile strength, and elastic modulus. The theory did not consider effects due to cratering.

Sea ice mechanical properties were related to temperature and salinity content by the Assur theory, and a digital computer program was written to represent these strength relationships. In addition, the present theory was programmed so that, for a given projectile and sea ice cover, critical impact velocity could be determined directly from temperature and salinity content in the range of temperature, +32°F through -10°F (0°C through -23°C), and salinity, 2 ppm through 20 ppm. Agreement between predictions of the theory and a limited number of experimental results was good.

Finally it was recommended that future investigations in this problem focus on a better theoretical understanding of the mechanics of penetration and the development of projectiles to be used specifically for perforation of Arctic sea ice.

DD FORM 1 NOV 68 1473 (PAGE 1)

S/N 0101-807-6801

UNCLASSIFIED

Security Classification

14. KEY WORDS	LINK A		LINK B		LINK C	
	ROLE	WT	ROLE	WT	ROLE	WT
Arctic ice						
Laboratory ice						
Penetration						
Perforation						
Projectile						
Impact velocity						